REPORT DOCUMENTATION PAGE

Form Approved
OMB No. 0704-0188

1. AGENCY USE ONLY (Leave blank)	2. REPORT DATE	3. REPORT TYPE AND DATES COVERED
	November 1989	Final Report

4. TITLE AND SUBTITLE

Cable Stayed Static Linear Analysis for the Captain William Moore Creek Bridge

5. FUNDING NUMBERS

HPR 88-7

6. AUTHOR(S)

J. Leroy Hulsey
David K. Delaney

7. PERFORMING ORGANIZATION NAME(S) AND ADDRESS(ES)

University of Alaska Fairbanks
Institute of Northern Engineering
539 Duckering Building
Fairbanks, AK 99775-0660

8. PERFORMING ORGANIZATION REPORT NUMBER

INE 88.44

9. SPONSORING/MONITORING AGENCY NAME(S) AND ADDRESS(ES)

State of Alaska
Department of Transportation and Public Facilities
Statewide Research M/S 2554
2301 Peger Road
Fairbanks, Alaska 99709-5316

10. SPONSORING/MONITORING AGENCY REPORT NUMBER

FHWA AK-RD-90-08A

11. SUPPLEMENTARY NOTES

Conducted in cooperation with the U.S. Department of Transportation, Federal Highway Administration

12a. DISTRIBUTION/AVAILABILITY STATEMENT

12b. DISTRIBUTION CODE

13. ABSTRACT (Maximum 200 words)

A 300-ft cable-stayed bridge, located on the highway between Skagway, Alaska and Carcross, Canada, is used to carry loaded ore trucks that weigh approximately 160,000 lbs and normal light traffic that consists of campers, buses, and automobiles. The bridge is a two-lane structure with a laminated timber deck supported by transverse floor beams spanning two stiffened ASTM A588 steel box girders. The box girders have 20-, 30-, 123-, and 127-foot span lengths.

The bridge was instrumented to evaluate the static live-load performance when subjected to a loaded ore truck. Experimental strains and deflections were recorded and compared with a static elastic two-dimensional finite element model. The 2-D model provided satisfactory results with symmetric loads.

14. SUBJECT TERMS

Keywords: bridges, loads, load tests, testing, finite element analysis, instrumentation

15. NUMBER OF PAGES

16. PRICE CODE

17. SECURITY CLASSIFICATION OF REPORT	18. SECURITY CLASSIFICATION OF THIS PAGE	19. SECURITY CLASSIFICATION OF ABSTRACT	20. LIMITATION OF ABSTRACT
Unclassified	Unclassified	Unclassified	UL

CABLE-STAYED STATIC LINEAR ANALYSIS
for the
CAPTAIN WILLIAM MOORE CREEK BRIDGE

Final Report

J. Leroy Hulsey
Associate Professor of Civil Engineering
David K. Delaney
Graduate Assistant, Dept. of Civil Engineering
UNIVERSITY OF ALASKA FAIRBANKS
INSTITUTE OF NORTHERN ENGINEERING

November 1989

Prepared for

State of Alaska
Department of Transportation and Public Facilities
Statewide Research M/S 2554
2301 Peger Road
Fairbanks, Alaska 99709-5316

In cooperation with

U.S. Department of Transportation
Federal Highway Administration

Report No. FHWA AK-RD-90-08A

TABLE OF CONTENTS

LIST OF FIGURES

LIST OF TABLES

ACKNOWLEDGMENTS

The authors would like to thank the Alaska Department of Transportation and the Federal Highway Administration for providing the research funds to investigate the static behavior of the Captain William Moore Creek Bridge near Skagway Alaska.

Special thanks are due to Mr. Richard W. Briggs, Electronic Technician with the Alaska Department of Transportation for his contributions during this effort.

ABSTRACT

The Captain William Moore Creek Bridge is an unusual 300-ft cable-stayed bridge located on the highway between Skagway, Alaska and Carcross, British Columbia. The bridge has a laminated timber deck supported by transverse floor beams that span between two stiffened ASTM A588 steel box girders. The box girders have span lengths of 30, 123, 127, and 20 ft.

This bridge was originally designed in 1974 to carry AASHTO HS20-44 highway loads and was strengthened in 1986 to carry B-Train trucks hauling ore that, when loaded, weigh approximately 160,000 lbs.

In the summer of 1988, this bridge was instrumented with strain gages on the box girders, pylons, and an upstation column abutment support. In addition, environmental sensors were installed to monitor solar radiation, wind speed, air temperature, and the temperature distribution through a box girder.

The bridge was subjected to a static Snooper truck (used as the control load) and static B-Train loads at predetermined locations. Experimental top-of-girder deflections and girder, pylon, and left upstation column abutment support strains resulting from the test loads were measured. They were then compared with analytical results from a static, two-dimensional, finite element model. Girder strains were obtained at the inner surface of the top and bottom flanges. Pylon strains were recorded near the support bases.

1. INTRODUCTION

1.1 Purpose of Analytical Study

Generally, when an experimental study is implemented, it is used to develop an understanding of the behavior of some part or parts of a structure that cannot be evaluated by available analytical techniques. However, unless the structure is extremely simple and load conditions are well defined, experimental results alone will typically not explain the overall behavior of a structure.

However, it should be noted that instrumentation and a subsequent testing program are the only accurate means available to characterize materials. Further, if the tests are well defined, experimental results will provide strains and displacements for a known load condition. Experimental results are limited by the number of load conditions, the location of the instruments, and the accuracy of the tests. An analysis, however, will provide an understanding of the behavior provided the geometry is accurate, the boundary conditions are valid, and the load transfer is representative.

Thus, when possible, it is desirable to combine a theoretical analysis with an experimental verification. It was therefore the purpose of this study to:

a) Develop a simple two-dimensional finite element prediction model of the Captain William Moore Creek Bridge,

b) Identify significant assumptions affecting the validity of the two-dimensional analytical model, and

c) Assess the effects of the boundary conditions and material properties by a comparison of the experimental results with the theory.

1.2 Analysis History

Cable-stayed bridges are based on the idea that high-strength cables can be used instead of piers to support bridge girders and thus provide for long free spans. This provides a complex system with a high degree of indeterminacy combined with limited nonlinear elastic cable behavior.

Cable-stayed bridge nonlinearity may be produced by three sources: large displacements, bending moment-axial force interaction, and cable drape producing a catenary cable shape (1).

Numerous analytical methods have been proposed by previous investigators. Some of these methods only account for linear behavior, where others have attempted to account for nonlinear effects of the system. The following paragraphs provide a review of the work presented to date by other investigators.

B.E. Lazar (2) suggested a two-dimensional planar analysis based on a stiffness approach to analyze the behavior of cable-stayed bridges, while M.C. Tang (3) developed a modulus reduction method (or transfer-matrix method) to evaluate the behavior of a cable-stayed bridge. Both of these authors suggested an iterative linear elastic analysis procedure for predicting nonlinear behavior of cable-stayed bridges.

Y.C. Loo and S. Srivanich (4) proposed a method based on the use of an equivalent planar system analysis to determine cable forces and a three-dimensional finite strip analysis to study main stiffening girders. Depending on the technique used to find cable forces, this method provided the opportunity to describe nonlinear cable behavior. The method is only applicable to bridges with single-plane cable arrangements in combination with a single or multiple cell box girder.

M. Como, et al. (5) examined the static behavior of long-span cable-stayed bridges with cables in a fan arrangement scheme. The study focused on the prevailing truss behavior of the bridge through the use of a continuous model and basic statics equations. This method was used since the physical behavior of the fan-shaped scheme is similar to that of a truss. That is, the main state of stress is axial in the stays and girder. Girder bending was considered to be a secondary concern. This analysis provided a "truss solution" for the cable elements of the bridge and local bending effects for the girder.

C. Crawford and P. Loris (6) presented a three-dimensional finite element model composed of beam, truss, and cable elements to describe the Brooklyn Bridge. The bridge is a combination suspension and cable-stayed system. The finite element model consisted of approximately 6,000 nodes and 23,000 elements and was used to analyze various rehabilitation strategies.

H. Nakai, et al. (7) developed an analytical method for analyzing the elasto-plastic and finite displacement behavior of a cable-stayed bridge from construction to completion. The method was based on the use of a three-dimensional model that consisted of a straight box girder and cable elements to determine the ultimate strength of the bridge. Cable nonlinearities and nonlinearities induced by element deformations were taken into account.

Experimental models have been employed on numerous occasions to investigate prototype behavior of cable-stayed bridges. They have also been used to confirm analytical results, analyze questionable construction phases or techniques, and predict the nonlinear performance of cable-stayed bridges (8,9,10).

R. Das (11) developed a procedure for the design of stiffening girders for a cable-stayed bridge. An iterative method to account for large displacements by the finite element method was used to explain the transfer of cable forces to the main girder. N. Gimsing (12) studied the horizontal deflection at the top of the pylons for multi-span cable-stayed bridges. It was found that, for a cable-stayed bridge with several main spans, inner cable systems cannot efficiently horizontally fix the tops of inner pylons. The results showed that, unless massive pylon cross-sections are used, unacceptable vertical deflections of the stiffening girder can occur. Two measures to limit deflections were discussed, first, a triangular pylon design and, second, a horizontal cable connecting all pylon tops.

Most available research to date is either limited in its applicability to single-plane cable configurations (two-dimensional planar systems, etc.), or involve methods developed for specific configurations such as the single or multiple cell box girder type cable-stayed bridge (4). The analytical results reported in the literature for box girder type bridges with orthotropic steel

decks have generally focused on membrane stresses and local bending moments in the steel box girder.

In addition to longitudinal and local bending of the plates that comprise a box girder, eccentric loads induce torsional bending, which must be accounted for in the analysis. Therefore, analytical methods are needed to account for the three-dimensional interaction of the nonlinear behavior of cables and effects of eccentric loading. Traditional two-dimensional plane frame or three-dimensional space frame programs do not satisfy this need.

In previous studies of cable-stayed bridges reported in the literature, the load is transferred between girders through the torsional rigidity of the deck either through the use of an orthotropic steel deck or through transverse stiffening girder diaphragms.

1.3 Captain William Moore Creek Bridge

The Captain William Moore Creek Bridge is a unique cable-stayed bridge for four reasons. First, the clear span of the structure is very short. Second, the girder-pylon bearing support interface is very unusual. Third, the load transfer between girders is obtained through floor beams connected to the main girders by web plates (shear only transfer). Fourth, the structure experiences light traffic volumes but unusually heavy loads and harsh environmental conditions.

The bridge has a timber deck supported by floor beams, which provide limited interaction between girders. The floor beams are connected to the main girder by web plates. It is assumed that the web plates transfer little-to-no moment (shear connection), consequently, a precise piece-wise investigation of the individual girders is not necessary to gain an understanding of the girder member stresses and displacements. Although cable nonlinearities may be present in the Moore Creek bridge, the girder-pylon-bearing assembly design provides unique support features. So, for the above stated reasons, a two-dimensional linear elastic finite element model (13) composed of beam and cable elements was considered an acceptable benchmark and therefore used for the analysis presented in this report.

2. EXECUTIVE SUMMARY

The Captain William Moore Creek Bridge was originally designed in 1974 to carry conventional AASHTO HS20-44 design loads. In 1986 it was strengthened to carry loaded ore trucks moving from Yukon Territory to Skagway, Alaska.

The behavior of the bridge under the influence of these unusual loads was questioned. Therefore, it was the objective of this study to experimentally evaluate the performance of the structure for the heavy ore truck (B-Train) loads.

Part 1 of the study consisted of an experimental investigation to evaluate the structural performance of the 300-ft cable-stayed bridge under static loading conditions. The study consisted of five parts: instrumentation calibration in the laboratory, field instrumentation installation, field testing, data evaluation, and presentation of results. (The experimental results are presented in a separate report.)

A two-dimensional finite element analytical comparison of the field results was also conducted and is presented herein. This was Part 2 of the study.

Two types of test loads were applied to the bridge: a preweighed Snooper truck, equivalent to an AASHTO H20-44 design load, and approximately 160,000 lb. loaded ore trucks. The axle weight distribution for each ore truck was obtained from a weight ticket. Each static test was carried out by positioning the truck's front axle on the bridge deck at a preselected location determined to produce the maximum stress in the box girder/girders.

In this study, a two-dimensional static finite element analysis was performed for both the Snooper truck and the B-Trains at three load positions marked on the bridge deck. These were Position 4 (48 ft from the downstation end), Position 9 (108 ft from the downstation end), and Position 14 (168 ft from the downstation end).

In each test, the truck to be tested was located with the front wheels centered at the appropriate load position. After a truck was in place,

strains, girder temperatures, cable deformation, ambient air temperature, wind speed, and horizontal solar radiation were recorded. When possible, top-of-girder elevations were also recorded for both unloaded and loaded conditions.

In this report, results are presented for nine Snooper truck tests, Test Series SCDOS04 and Test Series SCDOS05. These tests were limited to the same three load positions used to study the B-Trains (Load Positions 4, 9, and 14) with the truck in the left lane, bridge centerline, and right lane. Details of additional Snooper truck experimental results can be found in Part I. Special emphasis is given to the heavy ore truck (B-Train) load conditions, strain, stress and displacement results.

2.1 Maximum Strains

Strains were recorded on the inside surface of the top and bottom plate of the box girders, and on the exterior face of the pylon bases just above the stiffeners. Strains were also recorded at the downstation exterior face of the upstation left column support.

The maximum experimental strains recorded for the nine Snooper truck tests and the B-Trains at the three load are presented in Table 2.1 below. It can be

Table 2.1 Bridge Maximum Measured Strains and Stresses
(Results are in micro-strains, stress in ksi)

Item	Location(a)	Experimental		Calculated	
		Strain	Stress(b)	Strain	Stress(b)
(Snooper Truck)					
Left girder	33.25′	58	1.7	71	2.1
Right girder	33.25′	53	1.5	72	2.1
Left column	upstation	8	0.2	2	0
Left pylon	base	39	1.1	49	1.4
Right pylon	base	30	0.9	25	0.7
(B-Trains)					
Left girder	98′	224	6.5	276	8.0
Right girder	98′	207	6.0	246	7.1
Left column	upstation	26	0.8	23	0.7
Left pylon	base	134	3.9	193	5.6
Right pylon	base	103	3.0	143	4.1

a) Distances are along bridge incline from downstation end.
b) Stress is calculated from $\sigma = E\epsilon$

seen that the maximum experimental stress due to the B-Trains was 6.5 ksi. The corresponding calculated stress using the 2-D model was 8.0 ksi.

2.2 Girder Deflections

On each day of testing, prior to any tests and without traffic, top-of-girder elevations were recorded for both box girders. During testing and when possible, top-of-girder elevations were recorded for the test load cases. Girder deflections were calculated by determining the elevation differences between the loaded and unloaded state. Top-of-girder elevations for the Snooper truck loads were obtained during conditions of wind and fog. Thus, these elevations gave unreliable girder deflections. However, the maximum calculated deflection for the Snooper truck, due to the three load positions #4, #9, and #14, was 0.77 inches. The B-trains produced a maximum measured deflection of 2.76 in. The maximum deflection predicted by the finite element model for the B-trains was 3.4 in.

Axle weights of the B-Trains did not vary significantly from truck to truck and for like loading conditions, and the experimental data showed excellent repeatability, thus validating the instrumentation technique and testing procedure.

3. MATHEMATICAL MODEL

This portion of the study was conducted by preparation of a two-dimensional finite element model of the bridge structure. Because the bridge boundary conditions were not well known, and the behavior of the girder-to-pylon bearing support was not known, a parametric study was conducted to assess the effects of these conditions. It is the purpose herein to describe how these studies were accomplished.

3.1 Software Used for Analysis

Finite Element Program

The program selected for this study was the Soil Structure Interaction-Program-Nonlinear (SSIPNL) two-dimensional frame analysis computer program written by J. Leroy Hulsey while a private consultant and before joining the University of Alaska Fairbanks. The program uses the finite element method. This technique provides for a domain to be divided into a finite number of discrete elements. Element properties and structure geometry are described. Equations for each element stiffness matrix are assembled into a global banded matrix, the independent variables (loads) are assembled into a global vector, and a set of simultaneous equations are solved for the dependent variables (displacements). Final results provided by the analysis include displacements, element forces and moments, strains and stresses. Elements available in the program include:

a) 6-degree of freedom (dof) beam elements;

b) 2-dof axial (bar) elements;

c) Linear axial/rotational springs with provisions for eccentric attachment;

d) Linear flexibility matrix; and

e) Nonlinear axial springs.

The program allows use of both two-dimensional bar and beam elements within the structure, as well as the option of inserting linear axial/rotational or

nonlinear axial springs at any node in the system. Nodal point, concentrated member (element) loads, or varying distributed member loads can be handled with an exact transformation used for distributing forces to the nodes. Imposed support displacements are provided, and both member loads and/or nodal point loads may be applied as separate or combined load cases. Member loads include:

a) Concentrated loads;

b) Varying distributed loads;

c) Member temperatures; and

d) Member strains.

Post-Processor

The finite element program SSIPNL was modified to create a table of computed forces and a table of computed displacements for the elements and nodes of the model that were used to study the girders, pylon bases and upstation column of the Captain William Moore Creek Bridge.

A post-processor program was written in FORTRAN 77 to transform the computed forces into strains, sort the information, and create tables comparing the computed strains and deflections with the experimental values at the corresponding points. Strains were computed at nodes i and j from the two-dimensional linear-elastic analysis by combining axial and flexural stresses with the appropriate sign, then dividing by the modulus of elasticity for steel (29,000 ksi); see Fig. 3.1. The calculated strain at node i is given by

$$\epsilon_i = \frac{-P_i}{EA} + \frac{M_i\, y}{E\, I} \qquad (1a)$$

and at node j the calculated strain is given by

$$\epsilon_j = \frac{P_j}{EA} - \frac{M_j\, y}{E\, I} \qquad (1b)$$

where P is the axial force in the member, A is the cross-sectional area, E is the modulus of elasticity, M is the moment, y is the distance from the neutral

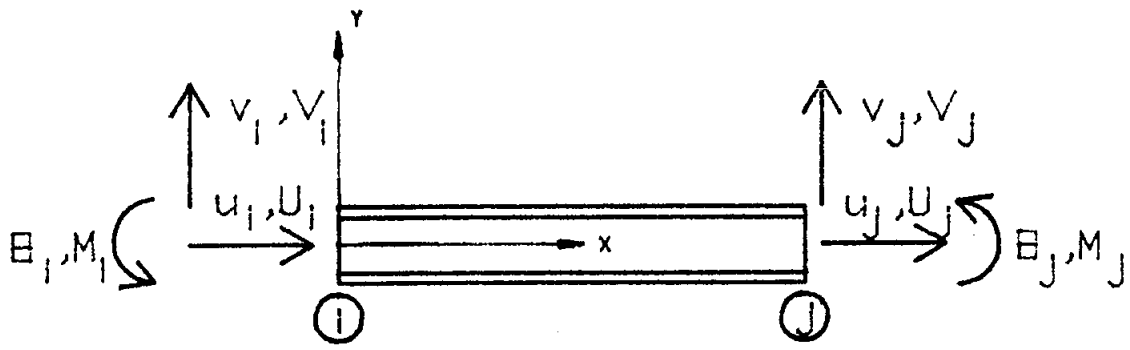

Top

$$\sigma_I = -\frac{U_I}{A} + \frac{M_I c}{I}$$

$$\sigma_J = \frac{U_J}{A} - \frac{M_J c}{I}$$

Bottom

$$\sigma_I = -\frac{U_I}{A} - \frac{M_I c}{I}$$

$$\sigma_J = \frac{U_J}{A} + \frac{M_J c}{I}$$

Beam Element

(Local Coordinates)

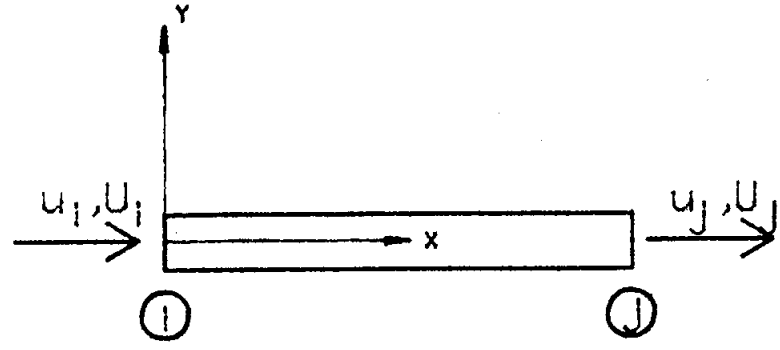

$$\sigma_I = -\sigma_J = -\frac{U_I}{A}$$

Bar Element

(Local Coordinates)

Fig. 3.1 The Beam and Bar Elements

surface (positive in local y-direction), and I is the moment of inertia of the section.

Strains were calculated for all girder elements and at nodes on the remaining portion of the structure that corresponded to strain gage locations. The results were used to develop tables of computed and measured strains at strain gage locations.

Tables of computed and measured deflections were also created for the experimental tests when deflection data were recorded. These tables provided a comparison between the calculated deflections and the monitored test deflections.

After the data were post-processed and sorted, the generated tables indicated above were used to prepare plots for visual presentation and comparison of results.

3.2 Analytical Procedure

Before instrumentation was ordered for the project, an analysis of a single box girder on the Captain William Moore Creek bridge was performed. This analysis involved developing moment influence lines for the girder and locating the Snooper truck and B-train loads along the girder to produce maximum girder stresses. Based on these results, instrumentation and data acquisition needs were prepared and sensors were ordered.

The preliminary analysis accomplished three objectives. These were to: a) define the location of the strain gages for the experimental phase of the project; b) define predetermined axle positions for each type of load; and c) provide guidance for the anticipated magnitude of experimental strains expected during the field tests. The strain magnitude results were used to design the monitoring equipment and check the field results.

After the experimental studies were conducted in the field, the researchers returned and processed the data for each sensor. In order to evaluate the bridge performance for the experimentally placed static loads, a two-

dimensional finite element model was prepared. Using this model, the field B-Train tests were simulated, and strains were calculated at each strain gage location and compared with the experimental results. This model was then modified through parametric studies to accurately represent the boundary conditions, girder pylon connection, girder-to-strut connection, and the effect of element approximations for the pylon behavior. The following section provides the reader with an insight into how these studies were conducted.

3.3 Initial Finite Element Approximation Model

A node was provided at each point of interest for the Captain William Moore Creek Bridge. For example, along the girder, nodes were placed at all changes in section, floor-beam-to-girder connections, locations of strain gages, pylon intersection, forestay cable connection points, and column and strut support connections. Figure 3.2 shows the initial node and element numbering scheme selected. Sections with node numbers not shown imply nodes were sequentially numbered within the section.

The pylon was divided into four sections. The pylon base extending from the bottom of the base plate to the beginning of the tapered section at bottom of the girder constituted one section. The upper tapered portion was divided into three sections, approximately equal in length and having section properties of the average of their end sections. At the pylon mast, the forestay and backstay cables were connected to nodes located at the intersection of their lines of action.

The girder is supported at the pylon by a curved steel plate and a 1-inch neoprene pad (see Fig. 3.3). The curved steel plate was provided to launch the girder during construction; the neoprene bearing pad was provided for support. The investigators assumed that the girder was not supported by the curved steel plate.

The first parametric studies were conducted based on the above assumption; the finite element model only accounted for the neoprene pad situated at the bottom girder flange. Axial deformations along the pad were assumed to be

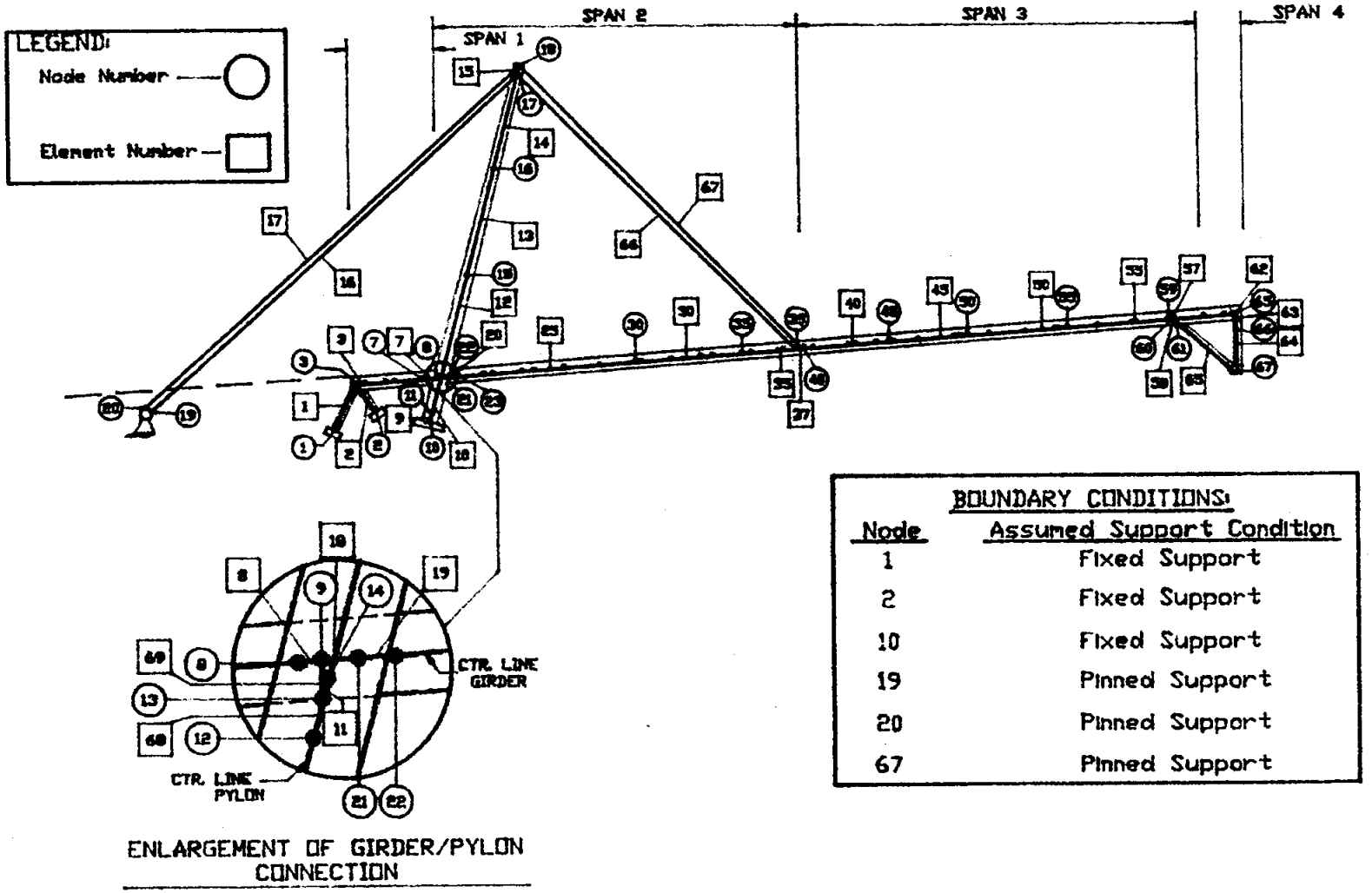

Figure 3.2 Initial Two-Dimensional Finite Element Model

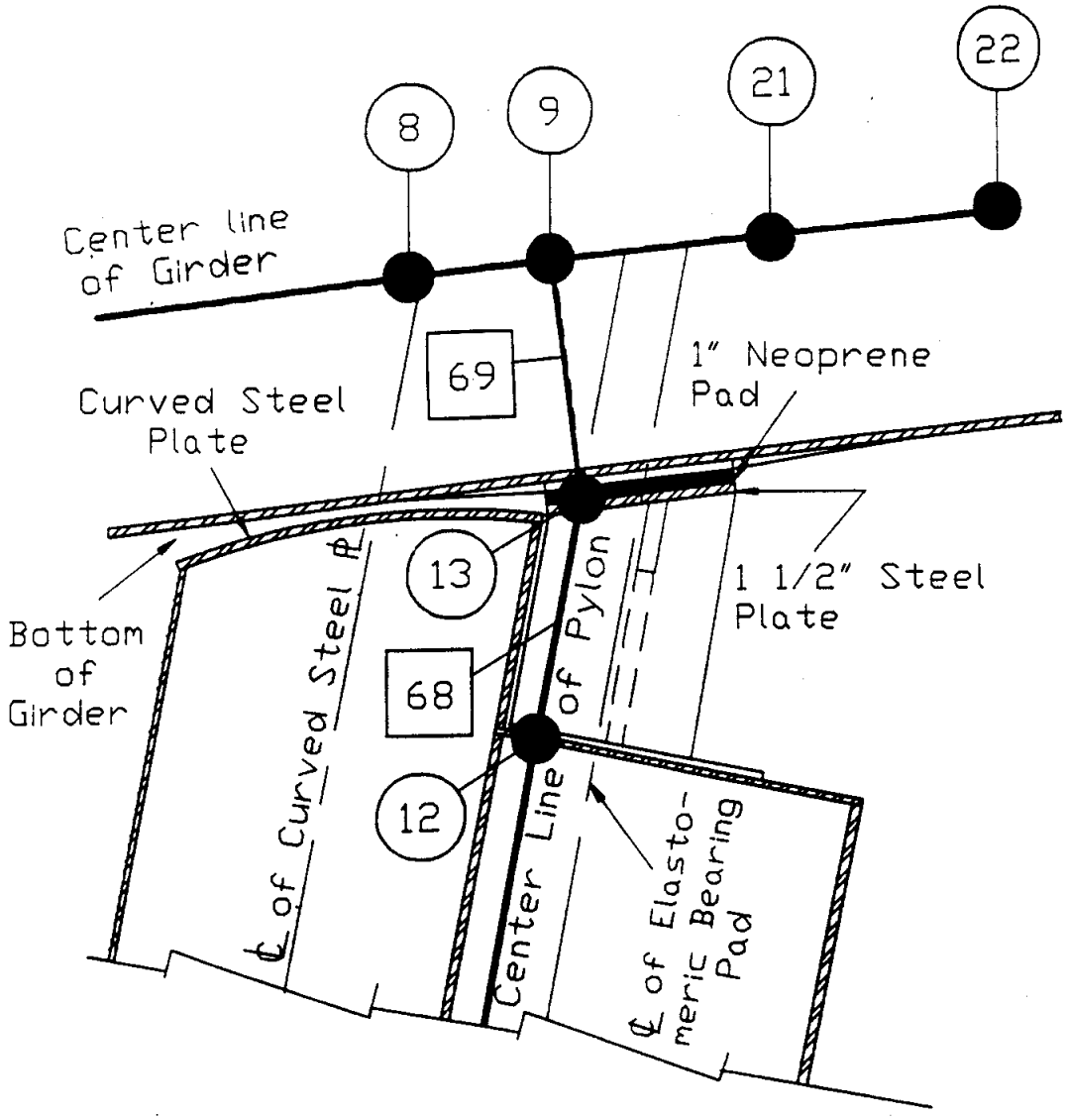

Element	Properties
68	A - Actual X-sect. I - Approx. Zero
69	A - Extremely Large I - Extremely Large

□ - Element No., ○ - Node No.

Fig. 3.3 Initial Model of Curved Steel Plate & Bearing Pad

negligible. Thus, in connecting the girder to the pylon, it was important to simulate the transfer of forces perpendicular to the girder through the bearing pad without imposing any rotational resistance on the girder by the pylon. Therefore, a node was positioned on the pylon center line at the bottom of the girder, node 13 (see Fig. 3.3). This was the actual girder-to-pylon connection point.

The bearing behavior was simulated by including a very rigid element that connected the neutral surface of the girder to the connecting point at the bottom of the girder. This rigid element was modeled with both an extremely large area (A) and moment of inertia (I). The element connecting the bottom of the girder to the pylon base (essentially modeling the elastomeric bearing pad that supports the girder at the pylon) was initially given an area (A) equal to that of the actual section of the elastomeric pad, as shown in the construction details, and a moment of inertia (I) of approximately zero. This was to allow the transfer of axial forces from the girder to the pylon base but no rotational resistance by the pylon on the girder.

The support (boundary) conditions initially selected were:

1) The downstation supports (columns at end of girder) and the pylon support were fixed.

2) The backstay cable supports, as well as the upstation column and strut supports, were pinned.

The bridge was originally designed and constructed to support AASHTO HS20-44 highway loads. Remedial work was later performed on the bridge to reinforce the box-shaped girders sufficiently to handle additional load imposed by B-Trains.

The box girder reinforcement was in the form of ASTM A588 steel cover plates on the top and bottom flanges of the girders at locations predicted to have a high probability of experiencing over-stressed conditions under B-Train loads. Figure 3.4 shows the locations of the reinforcing plates. The analysis for the remedial work was performed by Stanley Engineering Ltd. and was checked by the Bridge Design Section of the Alaska DOT&PF.

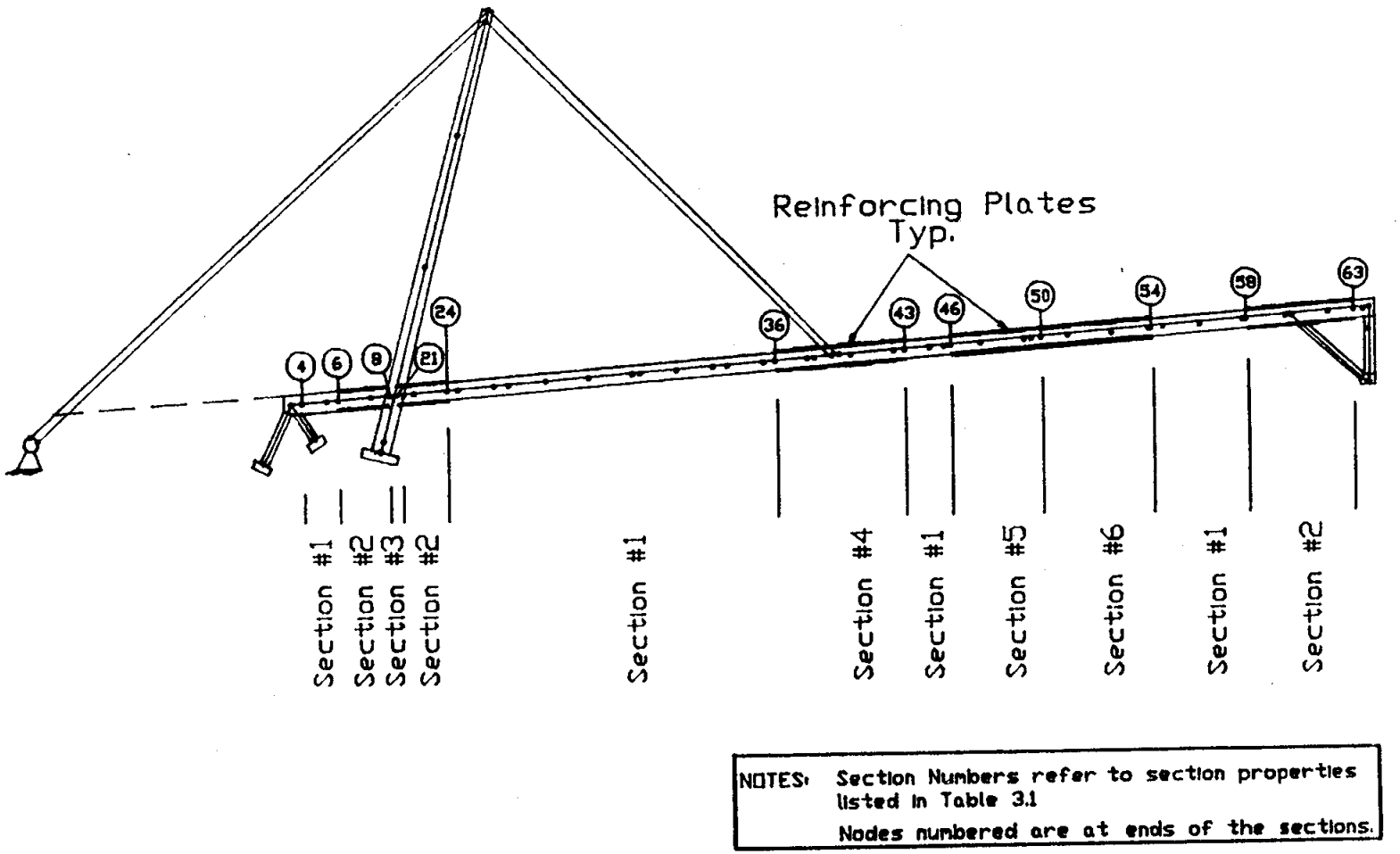

Fig. 3.4 Locations of Girder Sections

The element section properties used in this analysis included all remedial work to date. For example, the sections were based upon cross-section details used for the construction of the bridge at locations where no remedial work had been done. At places where remedial work had been done, the new section was used. Table 3.1 shows the section properties used for this study.

Table 3.1 Section Properties (2-D FEM)

Sect. No.	Plate Width W_t(a) (in)	Plate Width W_b(a) (in)	Area (in^2)	Moment of Inertia (in^4)	Section Modulus (in^3)	Description
1	N.P.	N.P.	83.1	52662.2	1726.6	Original Girder
2	29.0	29.0	126.6	94131.3	3012.2	Girder w/ Plates
3	29.0	30.63	127.8	95429.8	3025.4	Girder w/ Plates
4	N/A	N/A	115.6	83897.5	2663.4	Girder @ Cables
5	22.63	30.63	117.1	85015.3	2720.5	Girder w/ Plates
6	25.0	25.0	120.6	88411.5	2829.2	Girder w/ Plates
7	N/A	N/A	285.3	99012.4	3049.4	Girder Concrete Filled (downstation abut.)
8	N/A	N/A	5.4	N/A	N/A	Cables
9	N/A	N/A	199.2	92869.1	2855.8	Pylon Base
10	N/A	N/A	90.5	45454.4	1502.5	Pylon Base to Taper
11	N/A	N/A	86.5	38550.8	1364.6	Lowest Upper Pylon Section
12	N/A	N/A	78.5	32290.5	1331.6	Middle Upper Pylon Section
13	N/A	N/A	70.5	17536.5	866.0	Top Upper Pylon Section
14	N/A	N/A	80.6	59603.6	2483.5	Concrete Filled Column
15	N/A	N/A	27.8	31076.8	1294.9	Strut
16	N/A	N/A	2354.6	0.01	0.01	Elastomeric Bearing Pad
17	N/A	N/A	1000.0	900000.0	20000.0	Girder Center to Bottom
18	N/A	N/A	999999.0	0.01	0.01	Curved Steel Plate

Notes: (a) See Fig. 3.5
(b) See Fig. 3.4 for locations of the sections along the girders

3.4 Load Conditions

The calculated results presented in this report are based on the load conditions used for static load tests in the summer of 1988. Both the Snooper truck and B-Trains were positioned on the bridge deck at specific locations for the tests. Axle configuration and axle weights for each truck were determined for each vehicle.

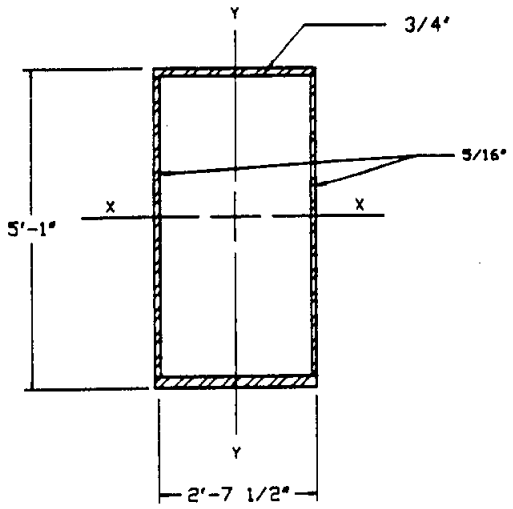

Original Girder Cross-Section

Section for Section
Property #1

(See Table 3.1)

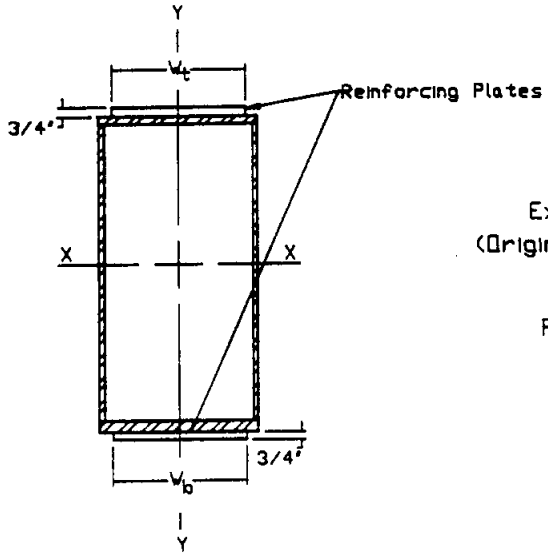

Existing Girder Cross-Section
(Original Box with Reinforcing Plates)

Section for Section
Properties #2, 3, 5, & 6

(See Table 3.1)

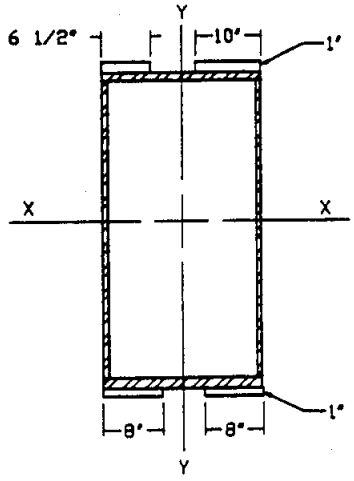

Existing Girder Cross-Section
Girder Section at Forestay Cables

Section for Section
Property #4

(See Table 3.1)

Fig. 3.5 Typical Girder Sections

Based on the above information, principles of statics were used to calculate the distribution of loads to the girders. For example, knowing the truck's longitudinal location along the bridge (by position number), the loads were distributed to the appropriate floor beam, and knowing the transverse location of the truck with respect to the left guardrail, the beam loads were distributed to the right and left girders.

The girder-distributed loads were used as input loads for the finite element program.

3.5 Parametric Studies

All studies were based on the assumption that the truck axle weights were distributed equally to the tires on each side of the truck. Based on this assumption, numerical model sensitivity studies were conducted by comparing analytical results with experimental results when the B-Train was centered on the bridge center line. These comparisons enabled the investigators to evaluate the validity of the model for the bearing supports and support condition assumptions.

The center line load case was selected to tune the model because the loading symmetry produced approximately symmetrical measured strain results. Nodal point loads generated as stated above for B-Train #204 centered on the center line of the bridge at positions #4, #9, and #14 were based on the measured positions of the B-train truck with this test run.

Tables A.1 through A.4 in Appendix A show the truck number, for the experimental tests, with their axial weights and the corresponding computed nodal point loads for the truck at each position tested. Based on a parametric study, it was determined that the following areas be investigated:

1) support (boundary) conditions,

2) pylon properties, and

3) interaction between the elastomeric bearing pad and curved steel plate which support the girder at the pylon.

Support Condition Studies

Pylon Supports. The pylon base supports were constructed on piles. It was therefore initially assumed that rotation about the pylon base was minimal and that the node at the base was fixed. The results indicated that this was a valid assumption.

Upstation End Bent. The gage located at the left side of the upstation column (gage 25, node 66) was used to compare the effect of pinned versus fixed support assumptions at the upstation column support. The pinned support assumption produced a computed strain at the base support much lower than measured. Initially, it was assumed that this indicated that the column support might have rotational resistance. The support node was then assumed fixed. The fixed support assumption produced a substantial improvement between calculated and measured at this gage, but this change produced a divergence in the comparison of strains at the gages located near the connection of the upstation strut to the girder (node 61).

The construction plans showed that the column was supported with a prestressed rock anchor but the base of the strut was not. The results of the analysis indicated that even though the two members were connected at the support by a cast concrete block, their support behavior acted independently. Therefore, an additional node (node 68) was added to the model immediately adjacent to the node previously used to describe the support. This node was used as the support node for the inclined strut (see Fig. 3.6). The strut support was then modeled as pinned and the column support node left fixed.

Downstation End Bent. The downstation end bent supports were also constructed in a manner similar to the upstation end. For example, one was constructed with a prestressed rock anchor and the other was not (see Fig. 3.6). Thus, by the same reasoning used at the upstation end, these supports were modeled with node 2 fixed and node 1 pinned.

End Bent Results. Refinements to the boundary conditions improved the results at gages located near the upstation inclined strut-to-girder connection and near the upstation column base (gages 5,6,7,8 & 25). However, a comparison

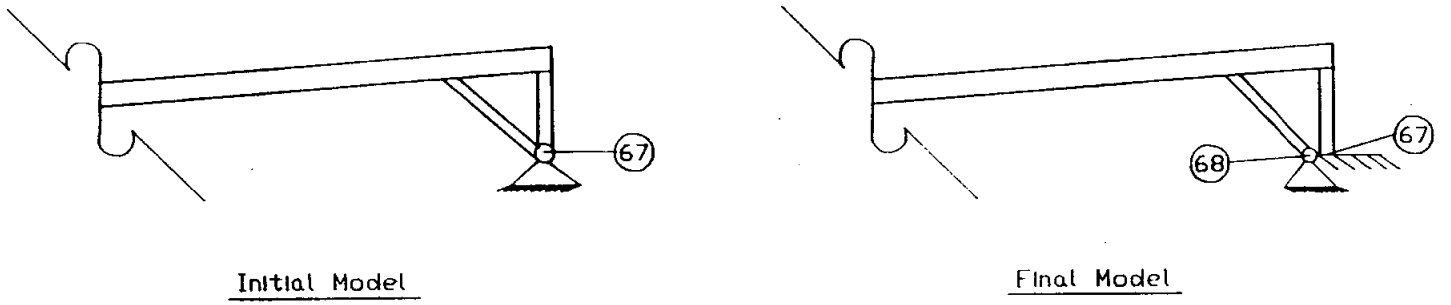

(a) Up Station

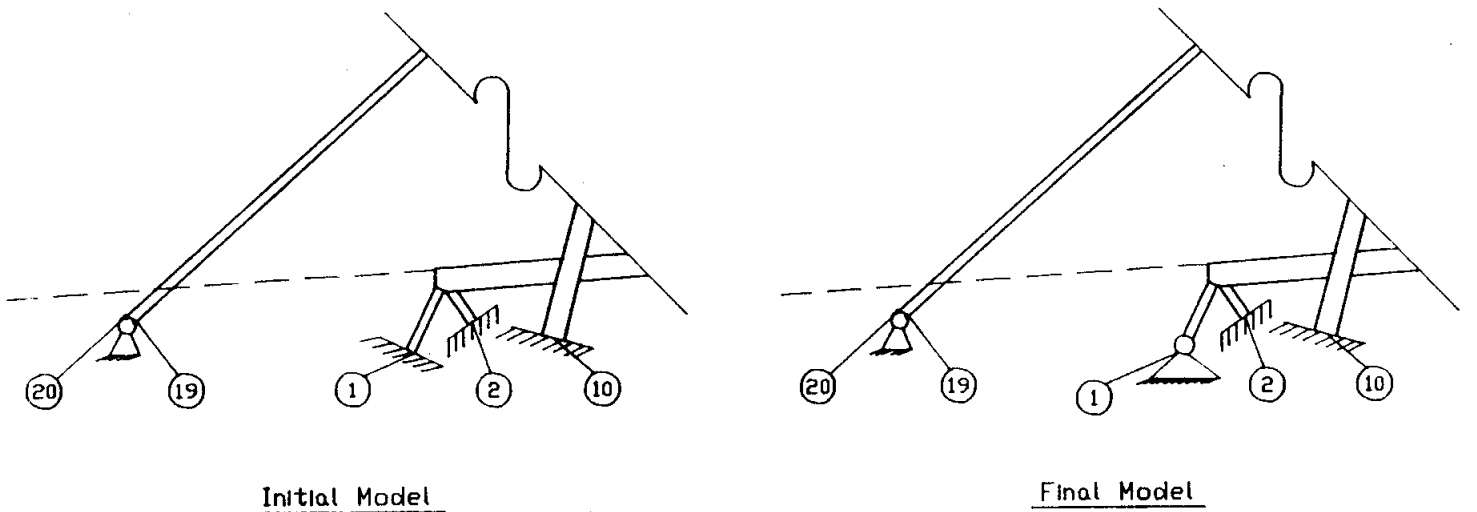

(b) Down Station

Fig. 3.6 Approximation for the Support Conditions

a) Upstation End Bent Supports
b) Downstation End Bent Supports

between experimental and calculated strains at the other gage locations remained virtually unchanged.

Pylon Section Properties Approximation Studies

The upper tapered portion of the pylon tower was approximated by three elements, each with a different constant cross section. The effects of this assumption on the results were studied in the following manner (see Fig. 3.7):

a) All three elements were given the same cross-section as the base of the taper (larger extreme section), and

b) The three elements were then given the same cross-section as the top of the taper (smaller extreme section).

The results showed very little or no change in the comparison of computed strains vs. measured strains resulting from modification to the pylon properties. Thus, the tapered section was approximated with three elements. Each element's section properties were average over the length of the element.

Girder Bearing-to-Pylon Support Parametric Studies

Each box girder for the Captain William Moore Creek Bridge was supported 30 feet from the downstation end by the pylon with a curved steel plate and a one-inch elastomeric bearing pad. The effect of this support on the behavior of the structure was initially questioned by the authors. For example, the following question was posed.

Is the girder supported by the curved steel plate, by the elastomeric bearing pad or by a combination of the two at the pylon-to-girder-connection?

Hereafter in this report, the elastomeric bearing pad will be referred to as the EBP and the curved steel plate will be referred to as the CSP. Strain gages at the base of the pylon (node #11) were used to study how the calculated transfer of forces from the girder to the pylon affected the base strains. The following procedure was used to answer the above question.

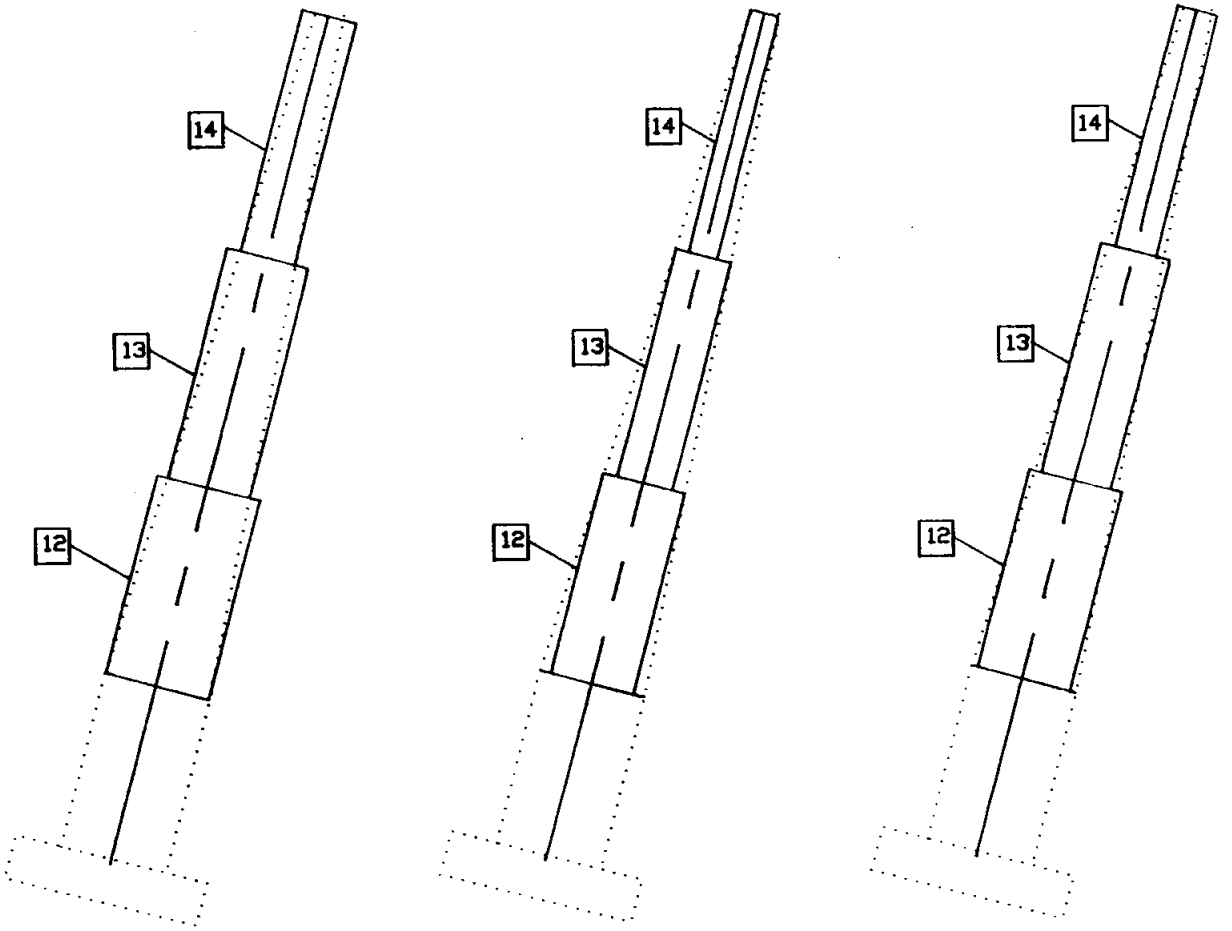

CASE 1

Constant Element Area as Pylon Area at Base of Element.

CASE 2

Constant Element Area as Pylon Area at Top of Element.

CASE USED

Constant Element Area as Average of Pylon Area at Base and Top of Element.

□ – Element Number

Fig. 3.7 Pylon Tapered Section Approximation

Model 1 (Initial Model). The engineering plans show a small gap between the CSP and the bottom flange of the girder (see Fig. 3.8). As stated earlier, it was assumed that the CSP was provided to launch the girder (as implied in the construction plans) at time of construction. Therefore, only the EBP portion of the connection was included in the initial finite element model (see Fig. 3.9). The model accounted for the EBP bearing by the use of

a) a rigid element from the girder neutral axis to the bottom flange and

b) an element between the bottom flange to the pylon center line. This element had an area equal to the actual section and a small moment of inertia to simulate free rotation.

Parametric studies for this assumption (computer runs) showed that an excess axial force and a deficient moment was transferred to the pylon base by this model.

Model 2. It was concluded that the CSP, in combination with the EBP, transferred load from the girder to the pylon. That is, a couple was induced on the pylon at this location. The model for the EBP was left the same as in the previous parametric study.

It was further concluded that, since the EBP was constructed along the center line of the pylon (line of action) and the CSP was constructed at an offset distance from this line, the eccentricity of the axial force carried by the CSP would induce additional moment to the base of the pylon. Thus, two elements were added (see Fig. 3.9). These were:

1) One (element 70) was inserted from the center of the girder to a node located at the contact point between the CSP and the girder. This element was given a large area and moment of inertia to simulate a rigid element.

2) The other (element 11) connected the bottom of the girder to the pylon to approximate the CSP behavior. This element was given an an extremely large area (since the curved steel plate represented an infinitesimal contact area) and a moment of inertia approximately equal to zero because the pylon was only resting on the plate and bearing.

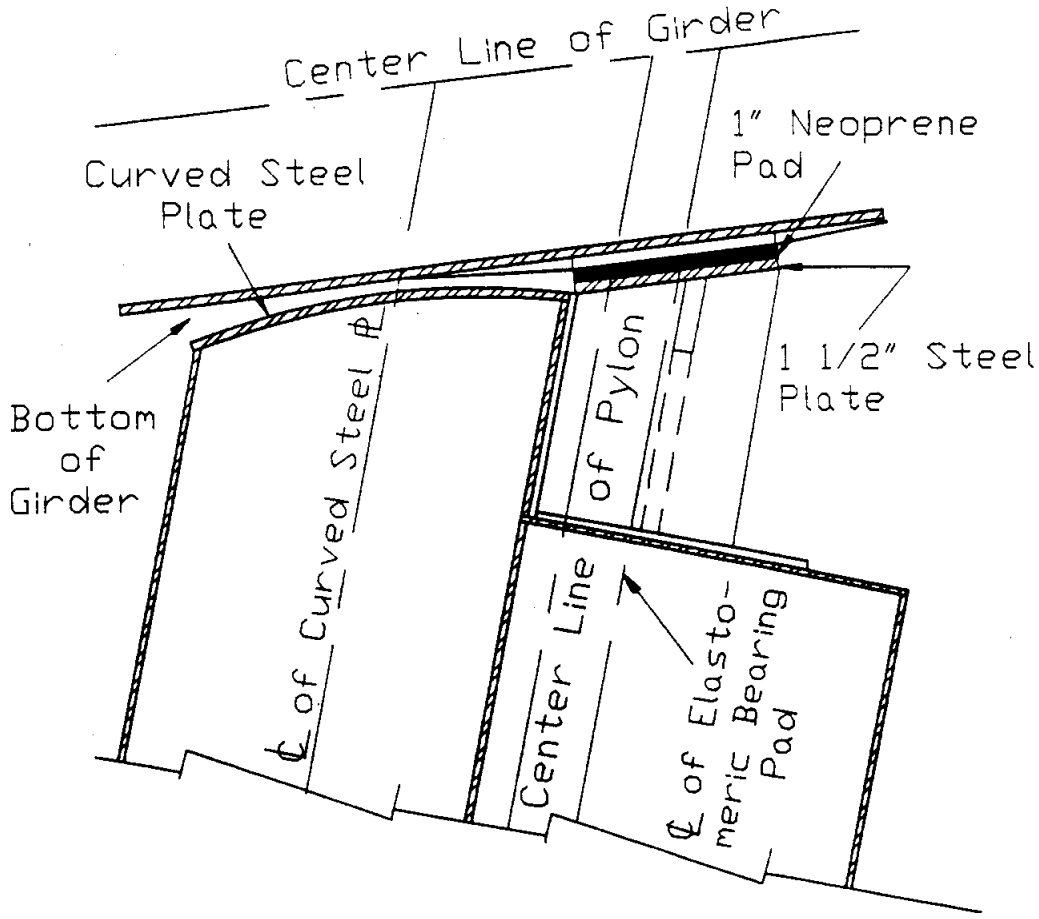

Fig. 3.8 Detail of Pylon-Girder Connection

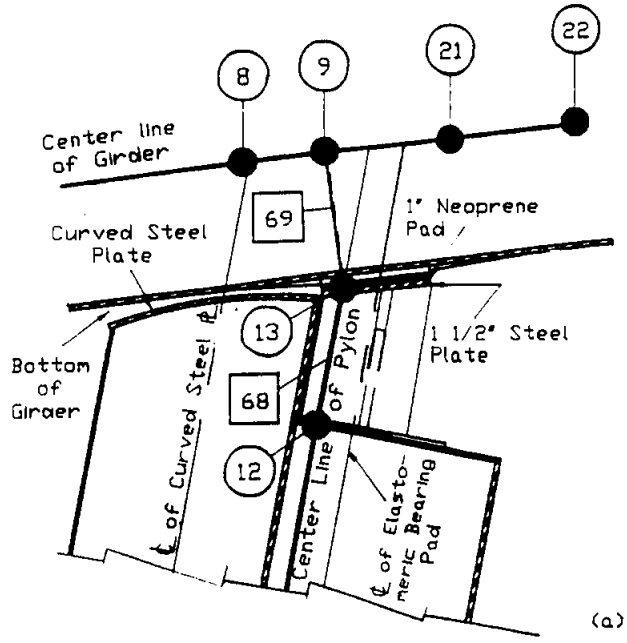

(a) Model 1

Element	Properties
68	A - Actual X-sect. I - Approx. Zero
69	A - Extremely Large I - Extremely Large

□ - Element No. ○ - Node No.

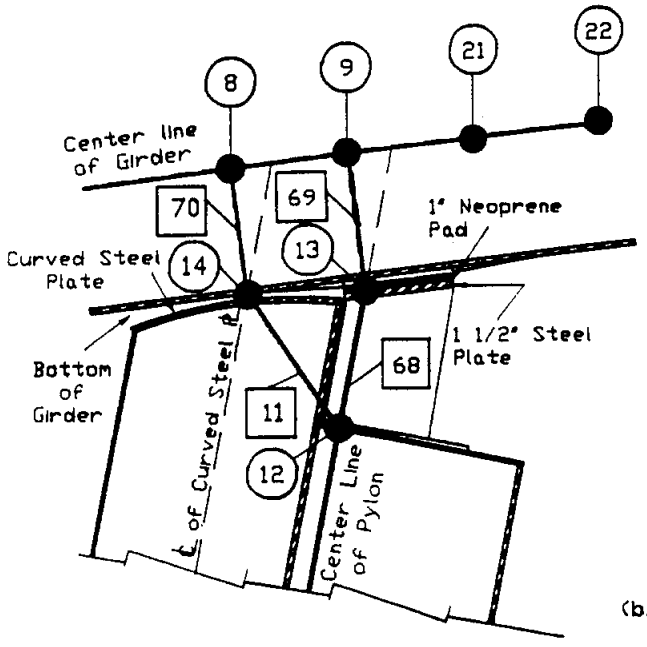

(b) Model 2

Element	Properties
11	A - Extremely Large I - Approx. Zero
68	A - Actual X-sect. I - Approx. Zero
69	A - Extremely Large I - Extremely Large
70	A - Extremely Large I - Extremely Large

Using the following parameters for elements of Model 2

Element	Properties
11	A - Extremely Large I - Approx. Zero
68	A - 1/4 Actual I - Approx. Zero E - For Neoprene
69	A - Extremely Large I - Extremely Large
70	A - Extremely Large I - Extremely Large

(c) Final Model

Fig. 3.9 Girder to Pylon Bearing Model
a) Model 1- Elements for EBP Approximation
b) Model 2- Elements for CSP & EBP Approximation
c) Final Model- Elements for CSP & EBP Approximation

The results of this study did not provide a satisfactory comparison between the measured and calculated strains.

Final Model Refinements. The properties of the element used to model the EBP were changed to incorporate the neoprene pad and the steel plate on top of the member immediately beneath the girder (see Fig. 3.9c). The deflection of each component was computed for a unit load and added together for a total deflection of the composite section. The modulus of elasticity for the neoprene was determined from literature provided by the Alaska State DOT&PF (14) to be approximately 8,200 psi. Based on the modulus of the neoprene bearing pad and with the total deflection of the composite section, an effective equivalent area was computed for the element with a modulus equal to that of the neoprene.

Because of the proximity of the EBP to the CSP, rotation of the girder about the CSP resulted in a varying amount of compression of the EBP. According to the literature (14), the modulus of neoprene increases with the amount of compression up to approximately 10% compression and then begins to approach a constant value.

The calculated finite element deflections showed that the EBP experienced a very small amount of compression. Therefore, only a small percentage of the stiffness of this element could actually be utilized. To account for this behavior, the effective area of the element was reduced to approximately one-quarter of its computed value. This approximation gave favorable results.

Results of the Parametric Study

The results of the parametric study provided the following findings:

1) The support (boundary) conditions for this structure are:

   a) that backstay cable supports, the downstation column without a prestressed rock anchor, and the upstation strut behave as pinned supports, and

   b) that the downstation column with a prestressed rock anchor, pylon base, and the upstation column behave as fixed supports.

2) Three equal-length elements, each with properties equal to the average of the section over its length, provide sufficient refinement for the tapered section of the pylon to model the overall behavior of the structure.

3) The combined influence of the elastomeric bearing pad and the curved steel plate have a significant effect on the structures behavior. The amount of influence of the EBP is primarily dependent on the amount of compression experienced by the neoprene pad when the compression is 10% or less of the total thickness.

3.6 Final Finite Element Model

Based on the parametric studies presented in section 3.5, it was concluded that the finite element model presented in Figure 3.10 will accurately describe two-dimensional behavior for the Captain William Moore Creek Bridge. The nonlinear influence of the cables was not considered in this study.

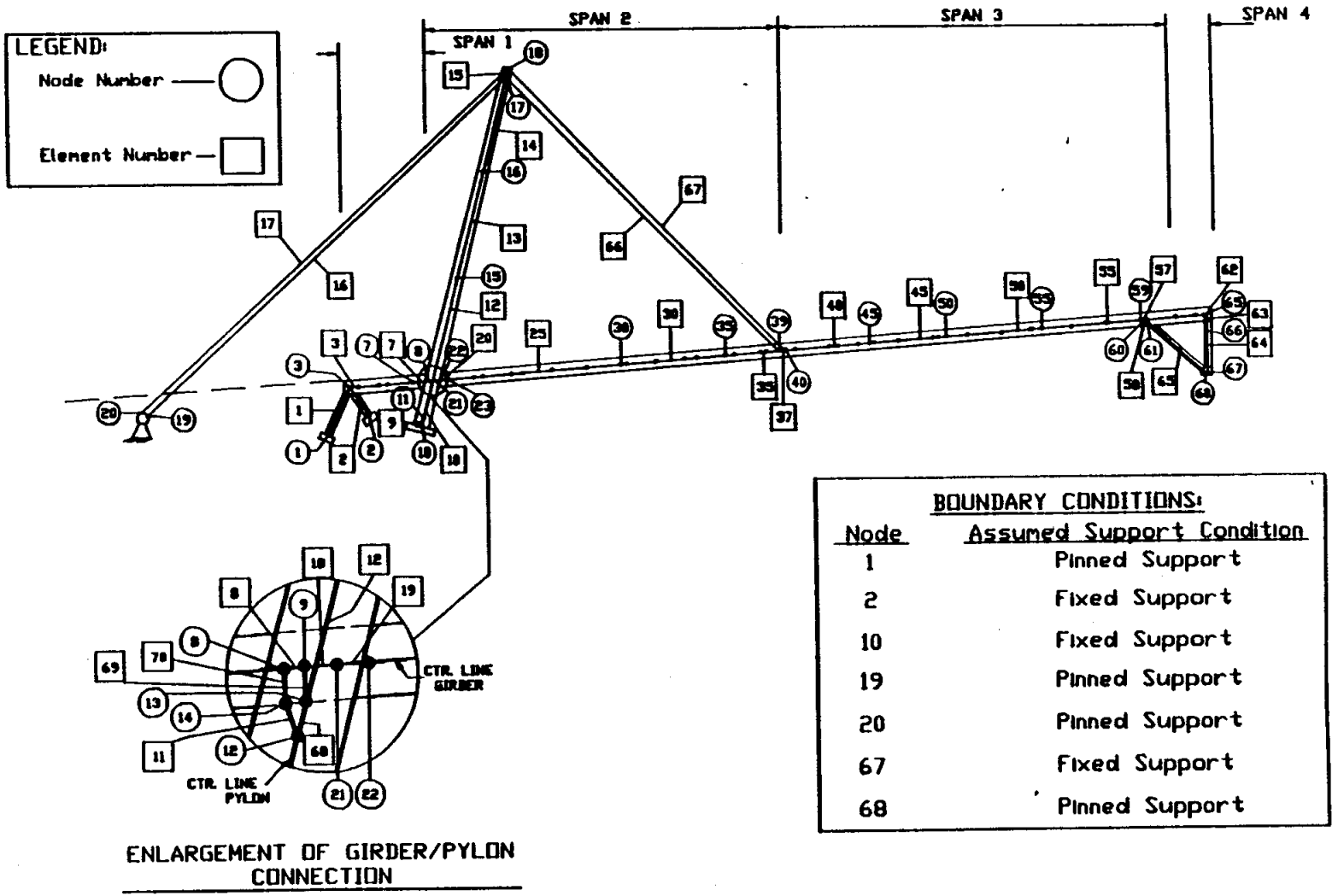

Fig. 3.10 Final Finite Element Model

4. ANALYTICAL COMPARISON

During the third week of August, 1988, the Captain William Moore Creek Bridge near Skagway, Alaska was instrumented and field tested for static loads. Static loads involved two types of trucks, a Snooper truck which used as a control vehicle and loaded ore trucks (B-Trains) (see Fig. 4.1). Detailed experimental results are presented in a separate report (Part 1 of this study).

4.1 Static Load Conditions

Snooper Truck Loads

Part of the tests consisted of subjecting the bridge to static loads using a Snooper truck. The Snooper truck had a front axle weight of 8.18 kips and duals of 15.78 kips, giving the truck a total weight of 39.74 kips.

There were a total of 106 load condition tests with the Snooper truck. The tests involved 53 cases with the truck in the left lane, 28 with the truck in the right lane and 25 with the truck on the bridge center line. The first 25 tests in the left lane were not valid. All tests were described as if the reader were looking upstation towards Whitehorse.

For the purpose of this report, only the Snooper truck tests with corresponding deflection measurements were compared analytically. These were 9 tests, test series SCDOS04 with the truck on the bridge centerline at load positions #4, #9, and #14 and test series SCDOS05. In test series SCDOS05, 3 tests were conducted with the truck the left lane and 3 with the truck in the right lane for positions #4, #9, and #14. The results due to the tests not reported herein should be examined in a later study.

B-Trains

Four B-Train trucks in a static position were tested on the bridge during this same week. Just prior to testing, a weight ticket was obtained and documented for the truck. The four trucks tested weighed between 155.07 and 157.556

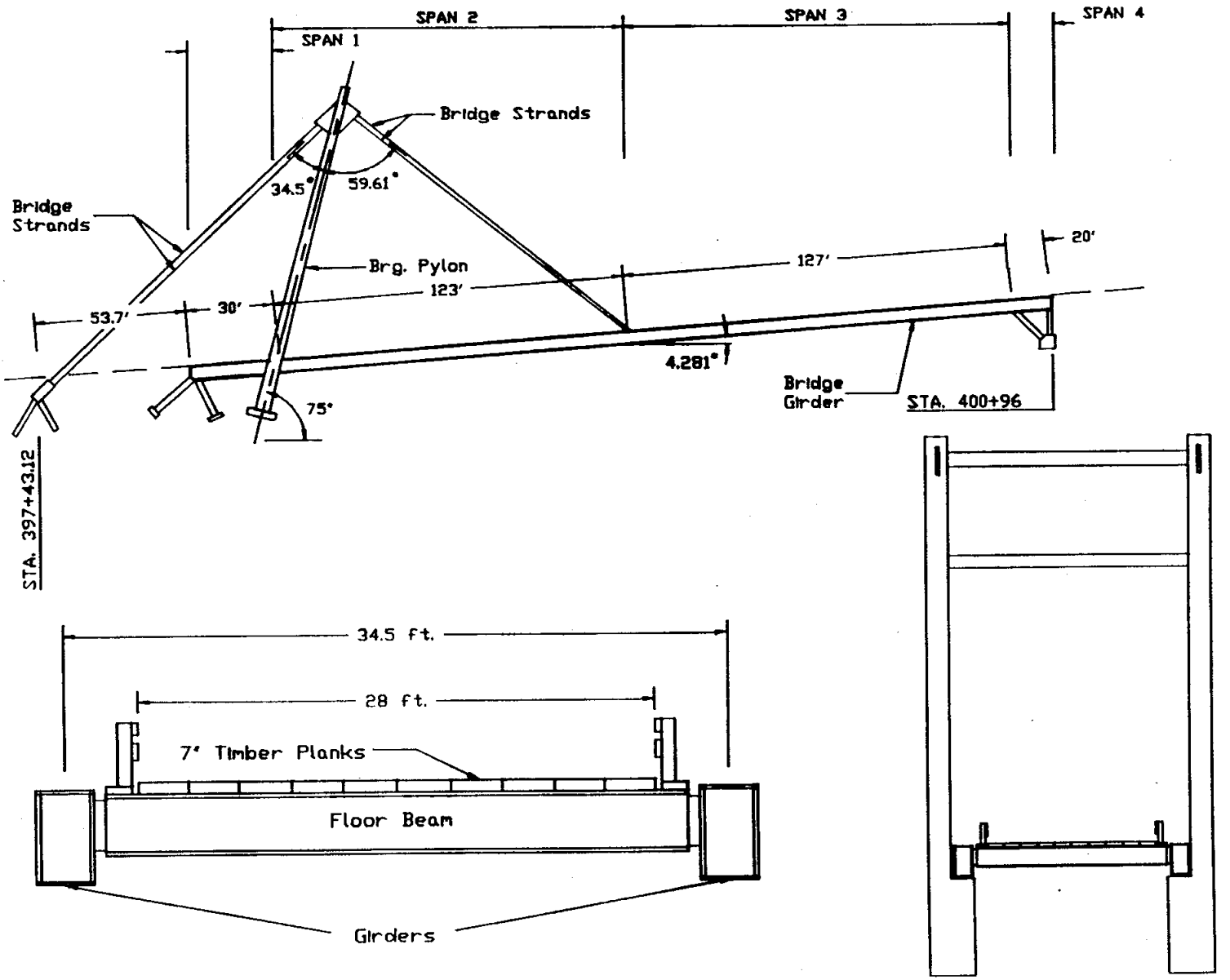

Fig. 4.1 Elevation of Captain William Moore Creek Bridge

kips. A total of 12 B-Train static load positions were tested with these trucks. Six were for loads in the left lane, three on the bridge center line, and three with a truck in the right lane.

The different load conditions were located at predetermined positions on the bridge deck to evaluate the performance of the structure. A comparison between the 2-D analysis and the experimental data is presented here for consideration.

4.2 Girder Deflections

It was the purpose of this study to analytically simulate the field test studies performed in August 1988 for the Captain William Moore Creek Bridge and to correlate the girder deflection analysis results with the experimental values.

Figure 4.2 presents the finite element model nodes that corresponded to locations where girder elevation measurements were recorded.

Snooper Truck

Studies involving the Snooper truck control loading were based on the nine tests stated previously. Because of the wind and fog effect on the top-of-girder elevation readings, measured deflections were unreliable and are not reported. The maximum calculated deflection for these tests was 0.77 inches. The calculated deflections are presented in Figs D.1 through D.9 in Appendix D.

B-Trains

Girder deflection data were recorded for the following B-Train static tests. These were: a) Test series #SLD0B08 (static, left lane, truck facing downstation, B-train, test no. 8) and b) Test series #SCD0B10 (static, center line, facing downstation, B-train, test no. 10). It was found that the girder deflections predicted by the 2-D model produced by the B-Train static loads

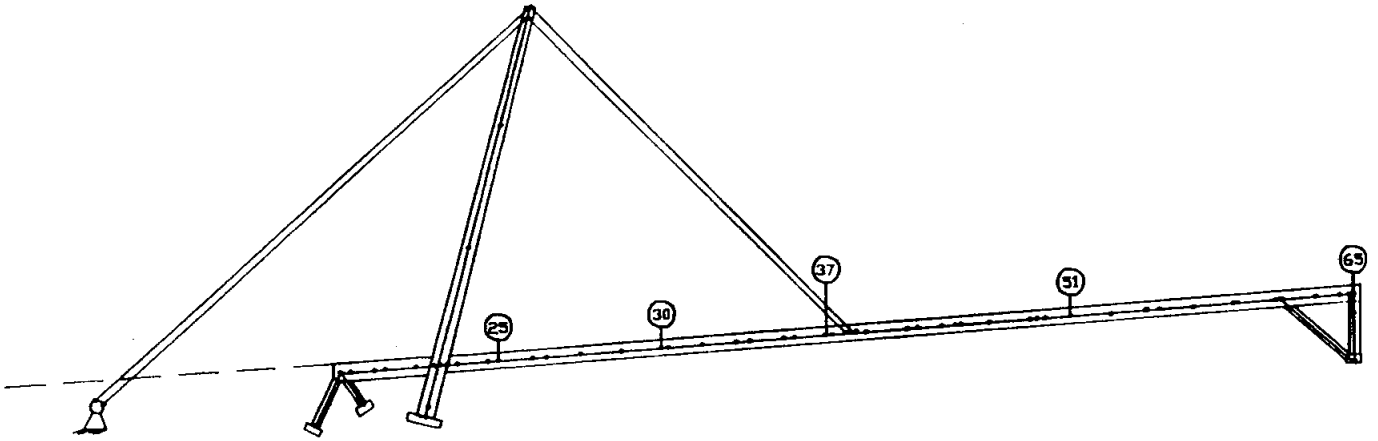

Fig. 4.2 FEM Model Showing Nodes for Deflection Study

compared well with the experimental data. The following presentation illustrates the validity of this conclusion.

Tests #SLDOB08. This series of tests was conducted with a 157.379 kip B-Train (#216) positioned in the left lane (see Appendix A, Table A.2). Figures 4.3 through 4.5 show the truck as it was positioned on the bridge and the resulting deflected shape of the bridge superstructure for each position. The magnitude

of the actual deflection was magnified by a factor of 70 for illustrative purposes.

It can be seen that the finite element model predicted larger deflections than were measured for the left girder (with the truck in the left lane this is the side with the larger portion of the load). These results implied that the bridge system is stiffer along the loaded side than the finite element model.

Conversely, for these same loads, the finite element model predicted smaller deflections for the right girder than were measured. Since the truck was in the left lane, the right side of the structure supported the smaller portion of the load. This indicated that the bridge was more flexible than the finite element model on the side opposite the load.

A detailed comparison between the calculated and measured deflections is presented in Appendix B, Tables B.1 and B.2 for test series #SLDOB08. These results illustrate that the actual bridge system does not behave in a true two-dimensional sense. Therefore three-dimensional effects due to deck torsional rigidity, pylon frame action, and cable interaction seems to influence its behavior.

Tests #SCDOB10. This series of tests was conducted with a B-Train (#204) positioned on the center line of the bridge. The B-Train weighed 157.556 kips. Figures 4.6 through 4.8 show the truck as it was placed on the bridge, with the deflected shape under the truck shown. Again, the magnitude of the actual deflection was magnified by a factor of 70 for illustrative purposes.

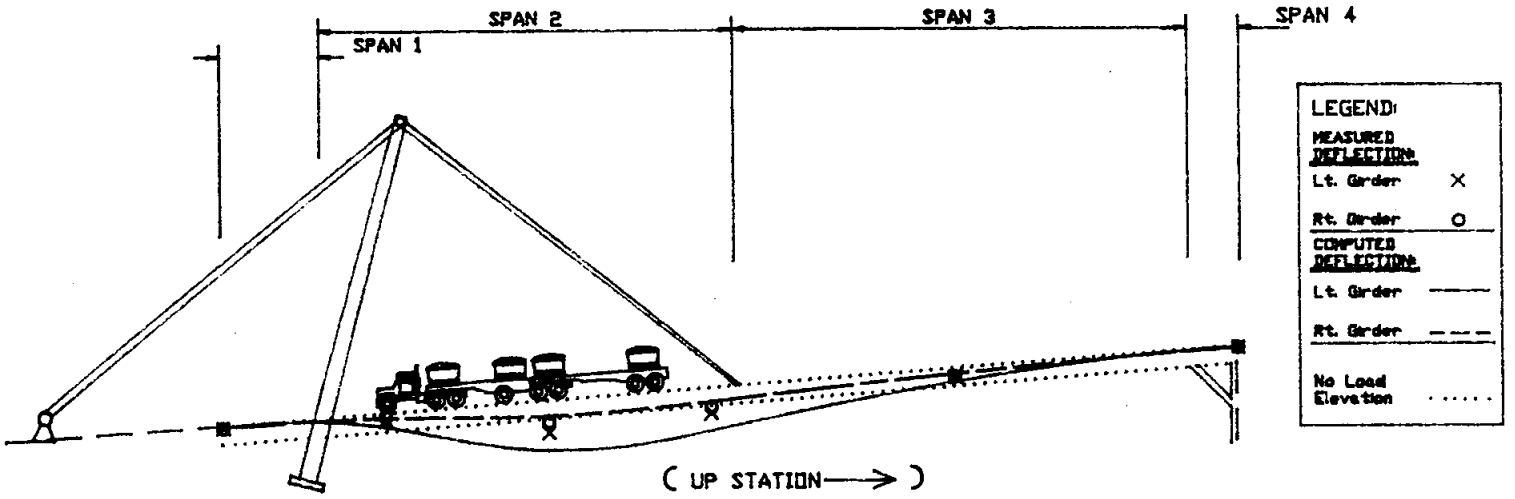

BRIDGE PROFILE WITH B-TRAIN
AT POSITION #4

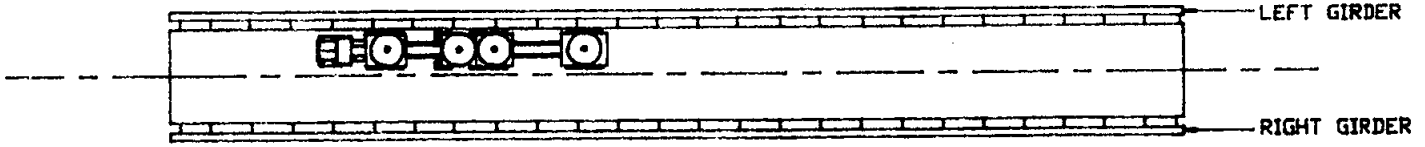

BRIDGE PLAN WITH B-TRAIN
AT POSITION #4

Fig. 4.3 Girder Deflections for B-Train #216 in Left Lane at position #4

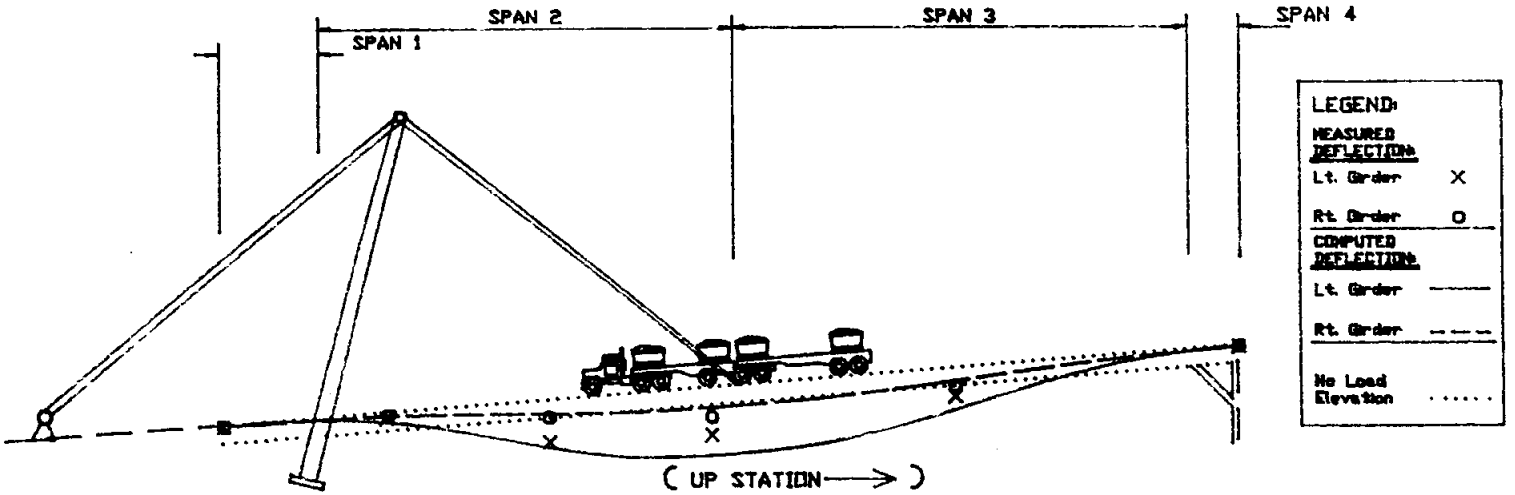

BRIDGE PROFILE WITH B-TRAIN
AT POSITION #9

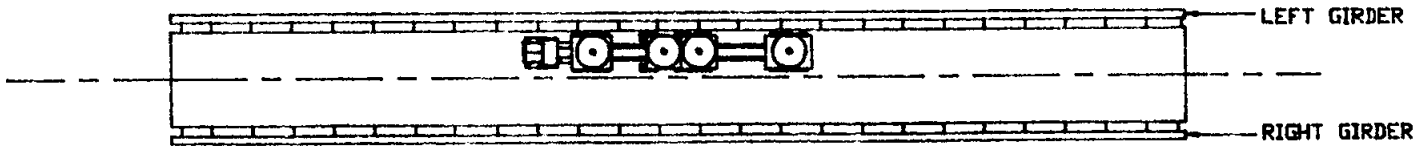

BRIDGE PLAN WITH B-TRAIN
AT POSITION #9

Fig. 4.4 Girder Deflections for B-Train #216 in Left Lane at position #9

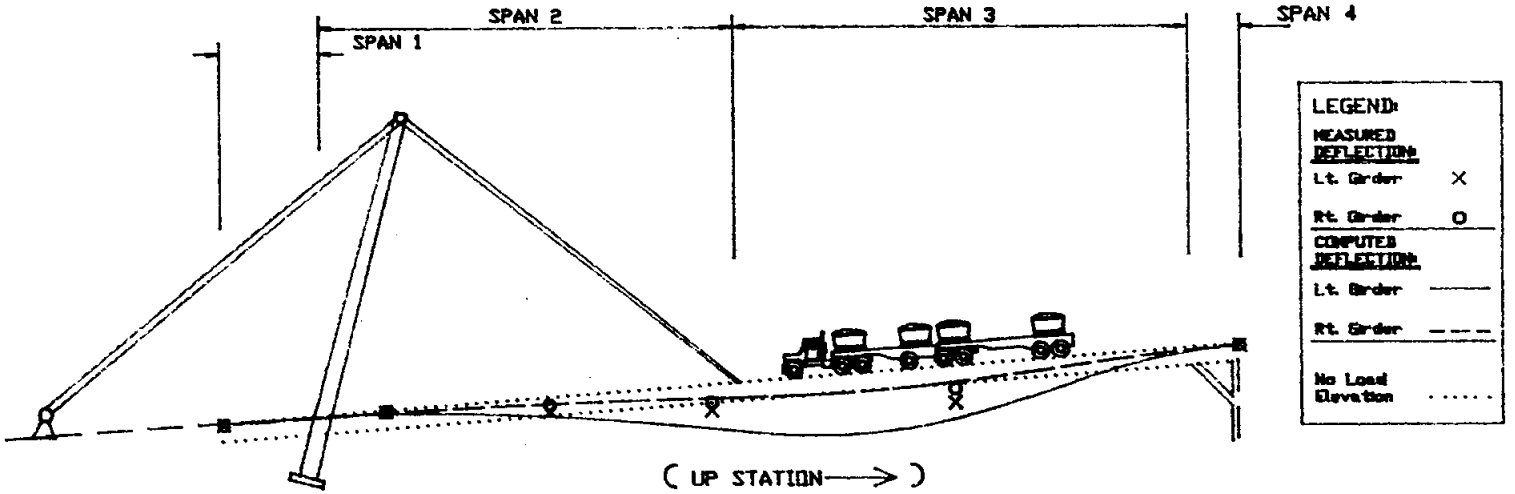

BRIDGE PROFILE WITH B-TRAIN
AT POSITION #14

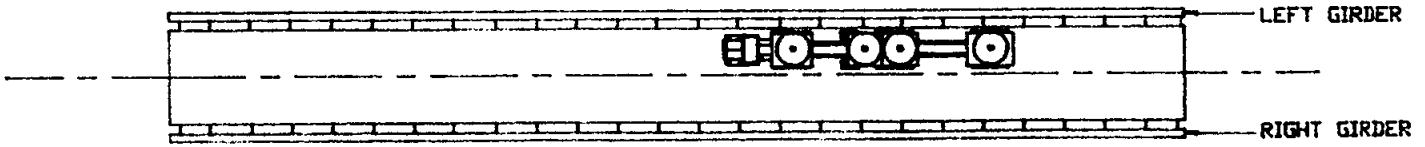

BRIDGE PLAN WITH B-TRAIN
AT POSITION #14

Fig. 4.5 Girder Deflections for B-Train #216 in Left Lane at position #14

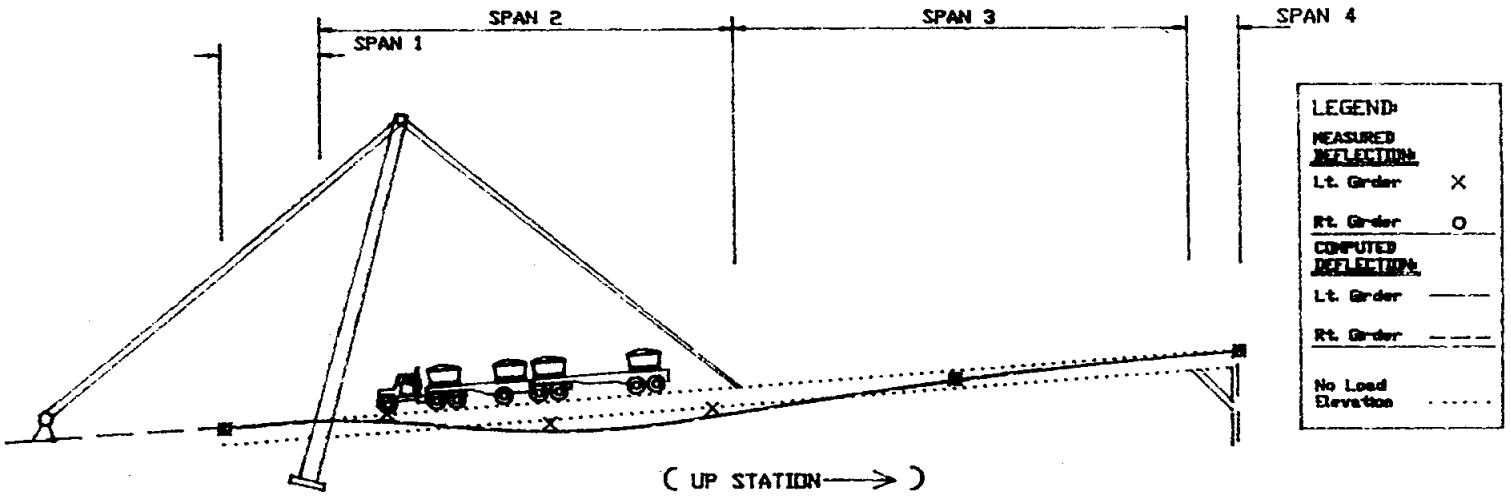

BRIDGE PROFILE WITH B-TRAIN AT POSITION #4

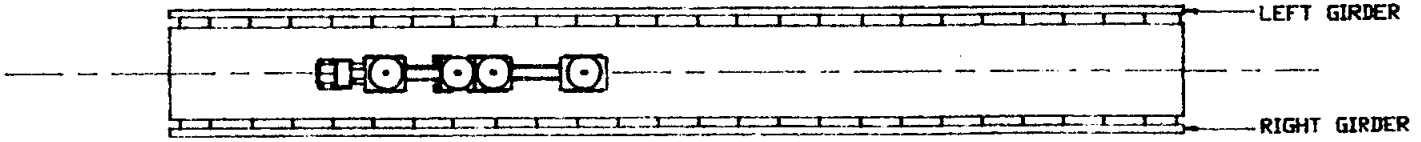

BRIDGE PLAN WITH B-TRAIN AT POSITION #4

Fig. 4.6 Girder Deflections for B-Train #204 on Center Line at position #4

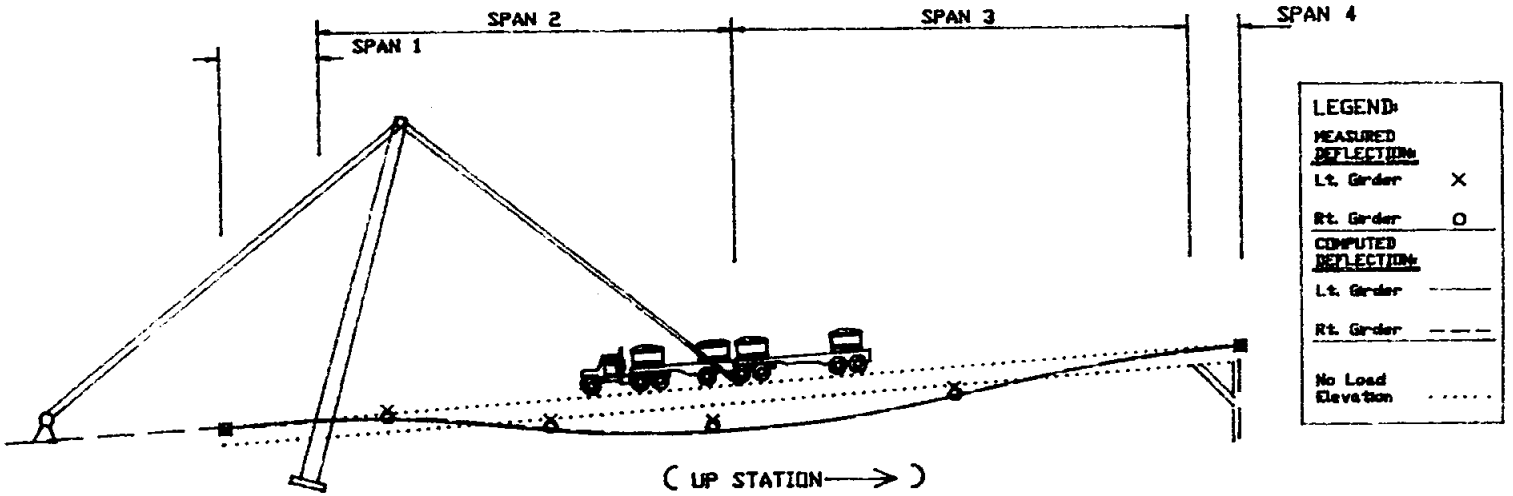

BRIDGE PROFILE WITH B-TRAIN
AT POSITION #9

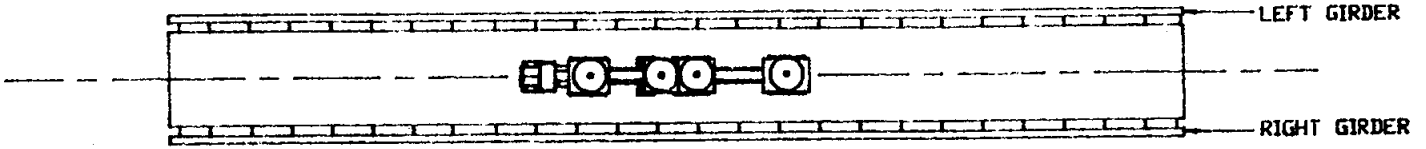

BRIDGE PLAN WITH B-TRAIN
AT POSITION #9

Fig. 4.7 Girder Deflections for B-Train #204 on Center Line at position #9

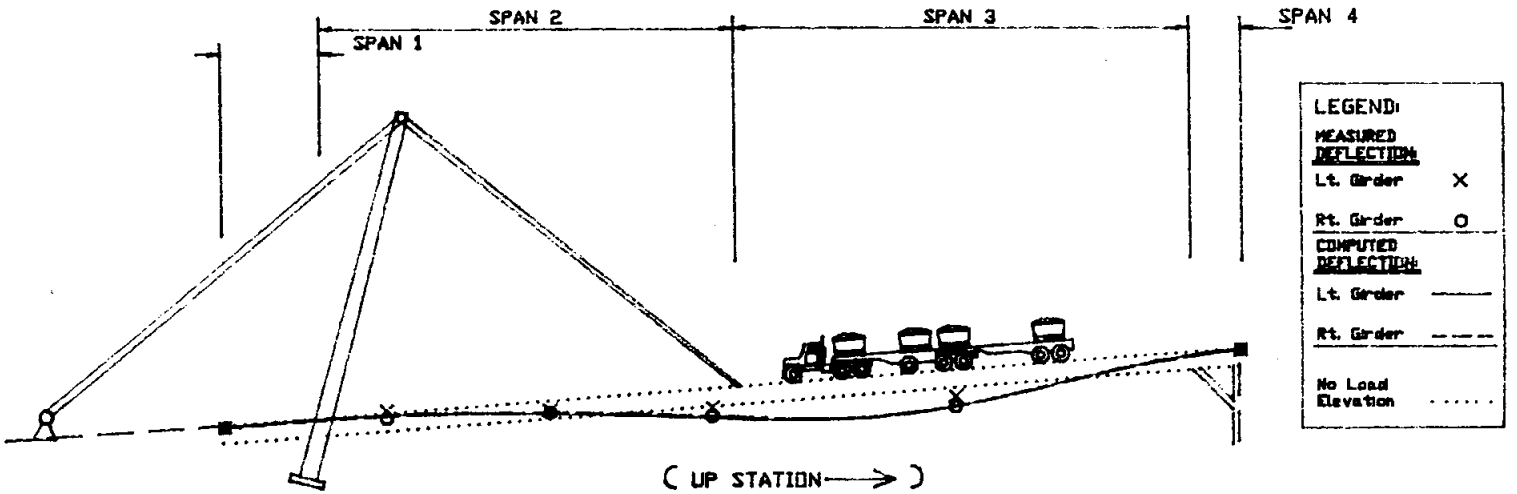

BRIDGE PROFILE WITH B-TRAIN
AT POSITION #14

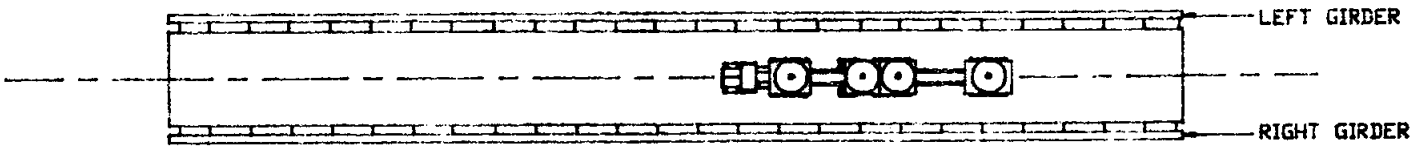

BRIDGE PLAN WITH B-TRAIN
AT POSITION #14

Fig. 4.8 Girder Deflections for B-Train #204 on Center Line at position #14

The measured girder deflections for this test series compared much better than the previous test series. For example, some of the computed values were slightly larger than measured and others were less. As stated above, the B-Train was positioned with the truck centered on the center line of the bridge and both girders were expected to support the same amount of load. Tables B.3 through B.4 in Appendix B show a detailed comparison between the calculated and measured deflections for test series #SCDOB10.

It appears that under the circumstance of symmetric loading the system can be reasonably assumed to behave as a two-dimensional system. During the field test, some measurements could not be taken on the right girder due to fog obstructing the view.

4.3 Strains and Stresses

Nodes for the finite element model were placed at all strain gage locations, changes in section, member intersections, and bearing locations. Element strains at the nodes were calculated using Eqs. 1a and 1b and were compared with experimental results. Figure 4.9 shows the finite element model nodes which correspond to gage locations. All stresses were approximated by the following relationship.

$$\sigma = E \epsilon \tag{2}$$

where E is the modulus of elasticity of the steel (29,000 ksi) and ϵ is the appropriate strain.

Snooper Truck

Experimental strains for the nine Snooper truck tests (truck on the bridge centerline, in the left lane, and right lane for positions #4, #9, and #14) were compared with a two-dimensional finite element model. A detailed comparison of these studies is presented in Appendix D, Tables D.1 through D.3. The maximum strains and stresses for the left side and right side of the bridge are presented in Tables 4.1 and 4.2, respectively.

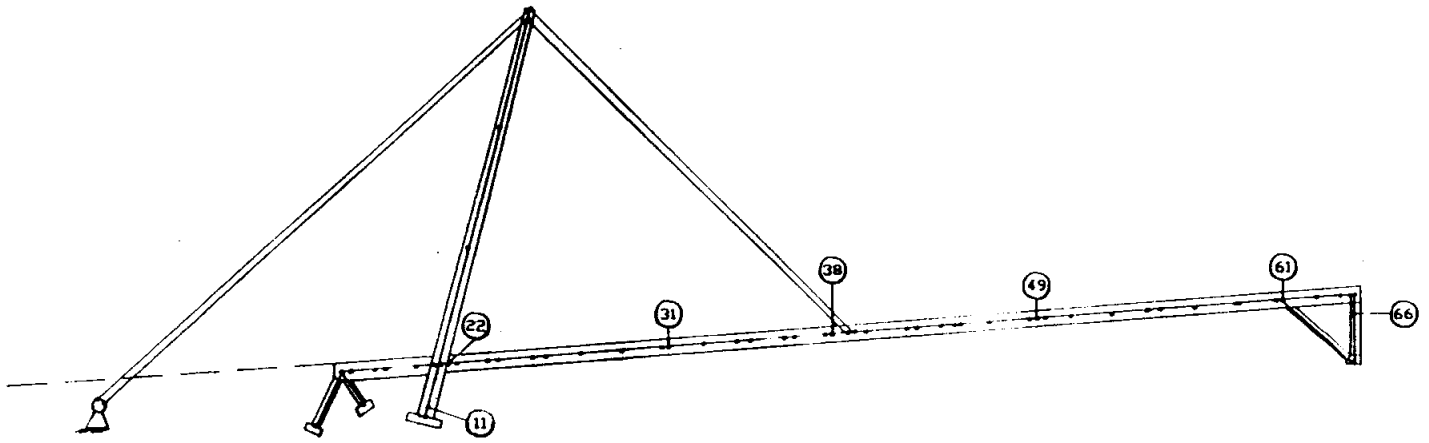

NOTES:

Nodes numbered correspond to field installed strain gage locations.

Fig. 4.9 FEM Nodes Located at Installed Strain Gage Locations

Table 4.1. Left Side Maximum Strains and Stresses Due to Snooper.

Description	Load Position	----Strains(micro)--- Measured	Calculated	---Stresses (ksi)--- Measured	Calculated
Truck on Centerline					
Top of Girder (33.25')	#9	44	44	1.3	1.3
Bot of Girder (33.25')	#9	-41	-51	-1.2	-1.5
Left Pylon (upsta face)	#9	-32	-29	-0.9	-0.8
Strut (downsta face)	#14	4	4	0.1	0.1
Truck in Left lane					
Top of Girder (98.0')	#9	-55	-71	-1.6	-2.1
Bot of Girder (33.25')	#9	-58	-71	-1.7	-2.1
Left Pylon (upsta face)	#4	-39	-49	-1.1	-1.4
Strut (downsta face)	#14	10	6	0.3	0.2
Truck in Right lane					
Top of Girder (33.25')	#9	24	26	0.7	0.8
Bot of Girder (33.25')	#9	-26	-30	-0.8	-0.9
Left Pylon (upsta face)	#4(a)	-14	-19	-0.4	-0.6
d.o.	#9(b)	-16	-17	-0.5	-0.5
Strut (downsta face)	#14	8	2	0.2	0.

(a) Location of maximum calculated strain
(b) Location of maximum measured strain

Table 4.2. Right Side Maximum Strains and Stresses Due to Snooper.

Description	Load Position	---Strains(micro)--- Measured	Calculated	--- Stresses (ksi)-- Measured	Calculated
Truck on Centerline					
Top of Girder (33.25')	#4	41	42	1.2	1.2
Bot of Girder (33.25')	#9	-41	-51	-1.2	-1.5
Right Pylon (upsta face)	#9	-30	-25	-0.9	-0.7
Truck in Left lane					
Top of Girder (98.0')	#9	-22	-30	-0.6	-0.9
Bot of Girder (33.25')	#9	-23	-30	-0.7	-0.9
Right Pylon (upsta face)	#9	-14	-15	-0.4	-0.4
Truck in Right lane					
Top of Girder (33.25')	#9	-53	-70	-1.5	-2.0
Bot of Girder (33.25')	#9	-53	-72	-1.5	-2.1
Right Pylon (upsta face)	#9	-30	-36	-0.9	-1.0

B-Trains

Tests #SLD0B06. A loaded B-Train (#207) facing downstation with a weight of 155.07 kips was positioned approximately 49 in. from the guardrail in the left lane. Experimental data were recorded when the front axle was located statically at positions #4, #9, and #14 on the bridge deck. The portion of axle loads carried by each girder was calculated for these positions and is presented in Table A.1, Appendix A. These girder loads were used in the 2-D finite element model. Note that the left girder supported the larger portion of the load.

Tables C.1a and C.1b in Appendix C provide a detailed comparison between the experimental and calculated strains for this static test series. Figures 4.10 through 4.12 show the strains along the left girder, and Figures 4.13 through 4.15 show the strains along the right side girder.

The maximum discrepancy between experimental and computed strain on the left side of the bridge occurred in the vicinity of the pylon, along the bottom of the girder, with the truck at position #4. The analysis over-predicted this strain by 89 micro-strains (see Table C.1a). On the right side of the bridge, the maximum strain difference occurred in the vicinity of the upstation strut at the bottom of the girder with the truck at position #14 (see Table C.1b). The 2-D model underpredicted the strain by 66 micro-strains.

Generally, the results show that the 2-D finite element approximation over-predicted strains on the left side of the bridge and under-predicted the strains on the right side of the bridge. This indicates that the structure behaves three dimensionally.

The maximum experimental stress was -6.3 ksi. This stress occurred at the top of the left girder, 98 feet from the downstation end. The maximum calculated stress was -8.6 ksi. This stress occurred at the bottom of the girder, 33.25 feet from the downstation end. Table 4.3 provides a summary of the maximum strains and stresses for this test series.

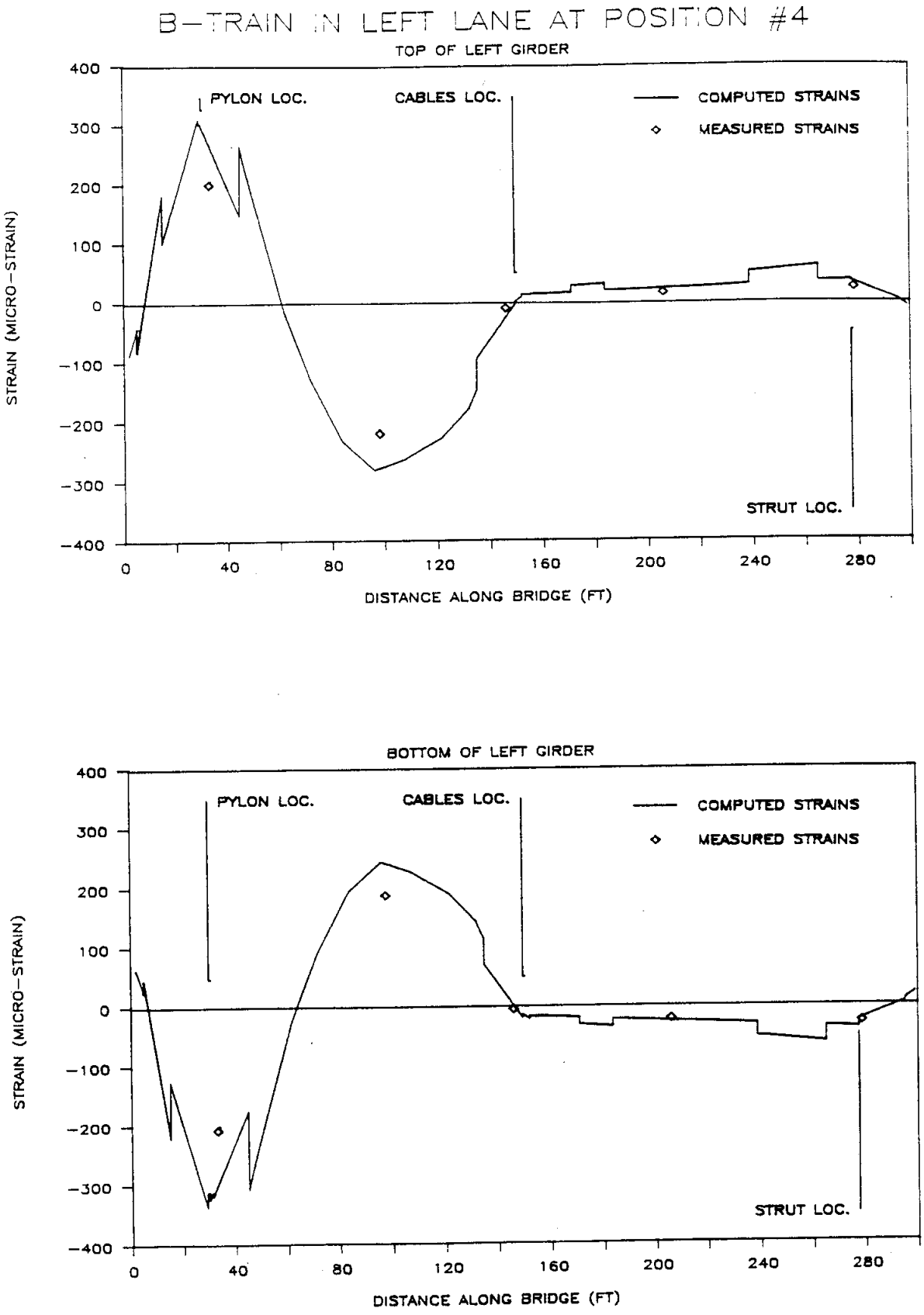

Fig. 4.10 Strain in the Left Girder for B-Train #207 in Left Lane at position #4

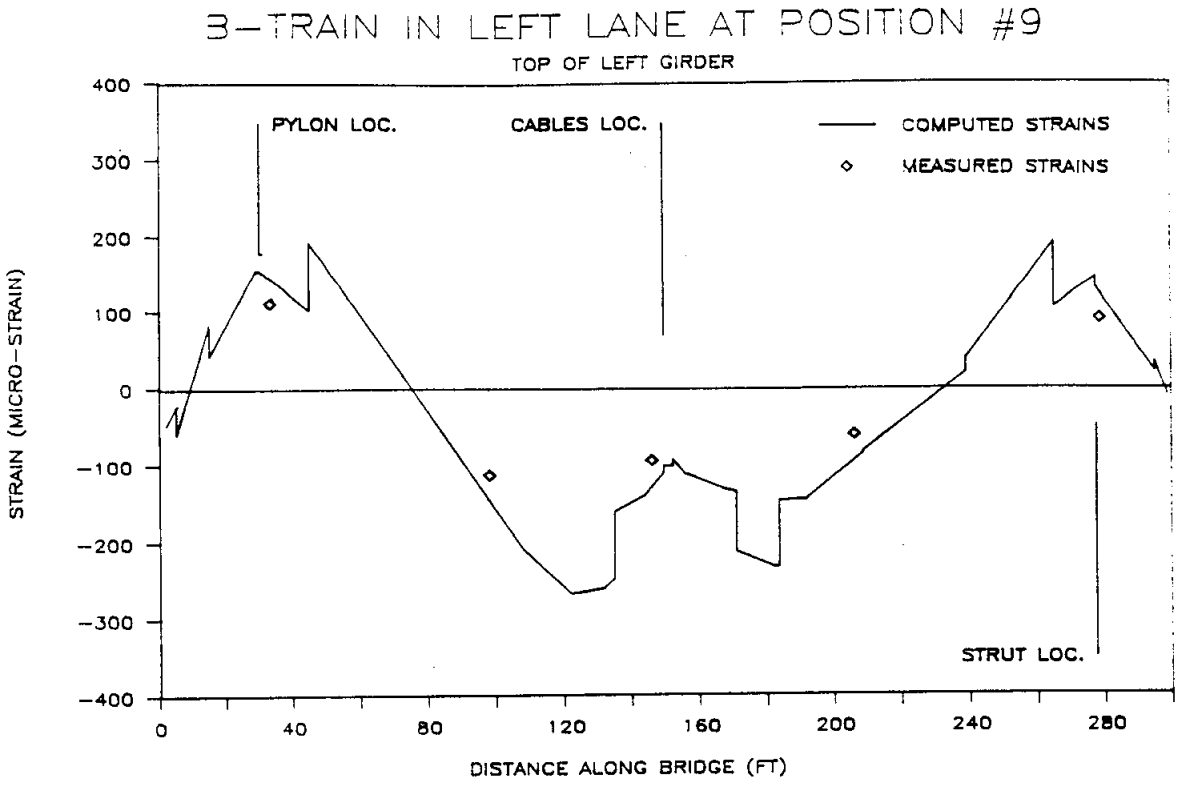

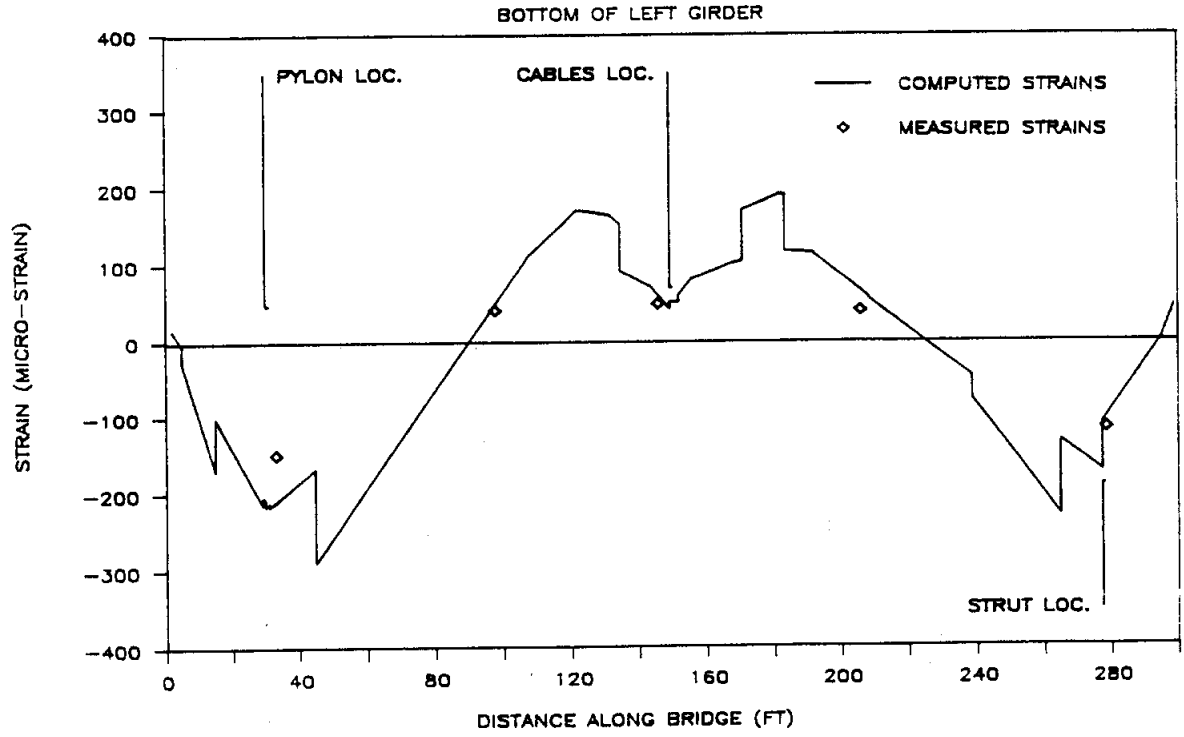

Fig. 4.11 Strain in the Left Girder for B-Train #207 in Left Lane at position #9

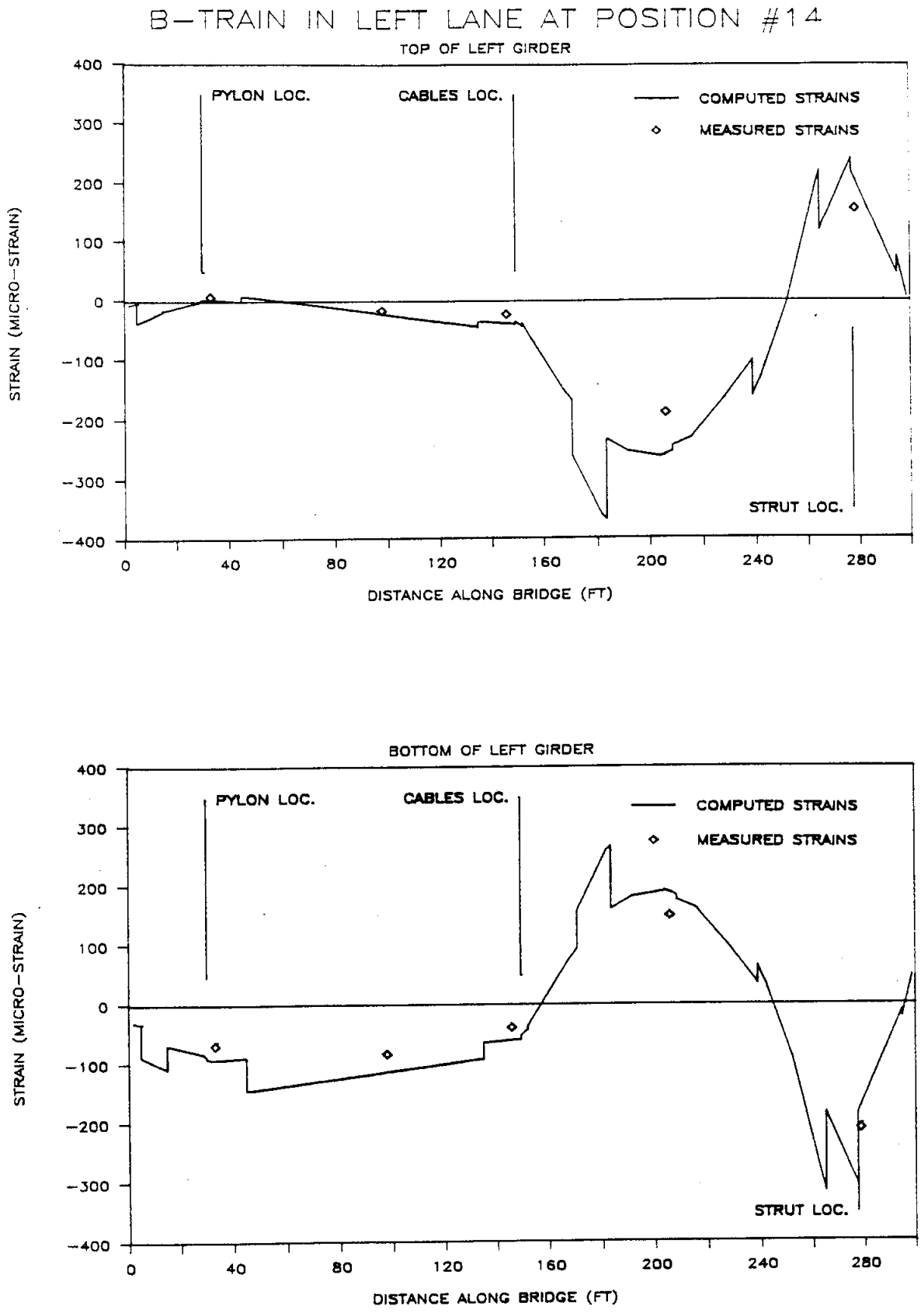

Fig. 4.12 Strain in the Left Girder for B-Train #207 in Left Lane at position #14

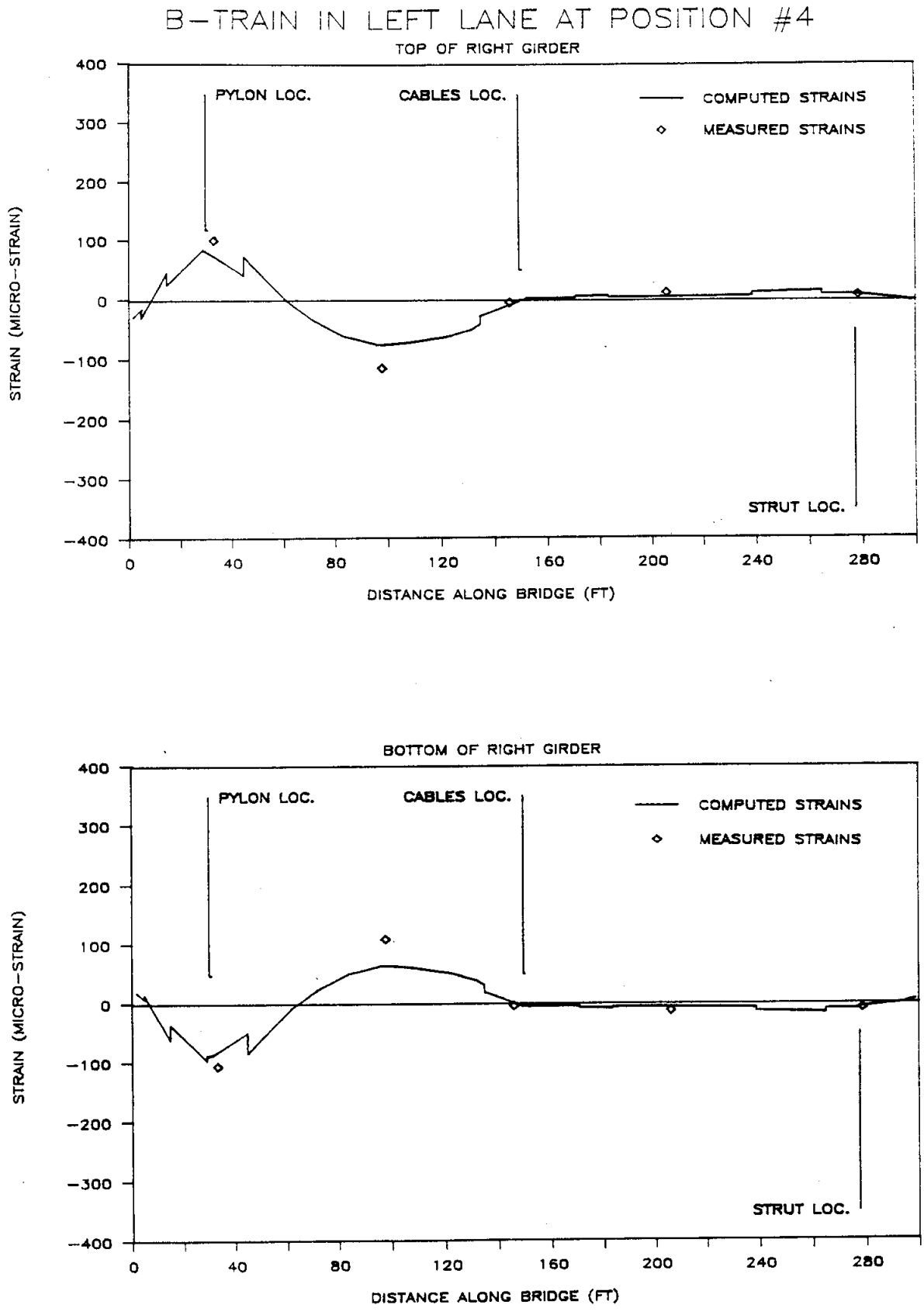

Fig. 4.13 Strain in the Right Girder for B-Train #207 in Left Lane at position #4

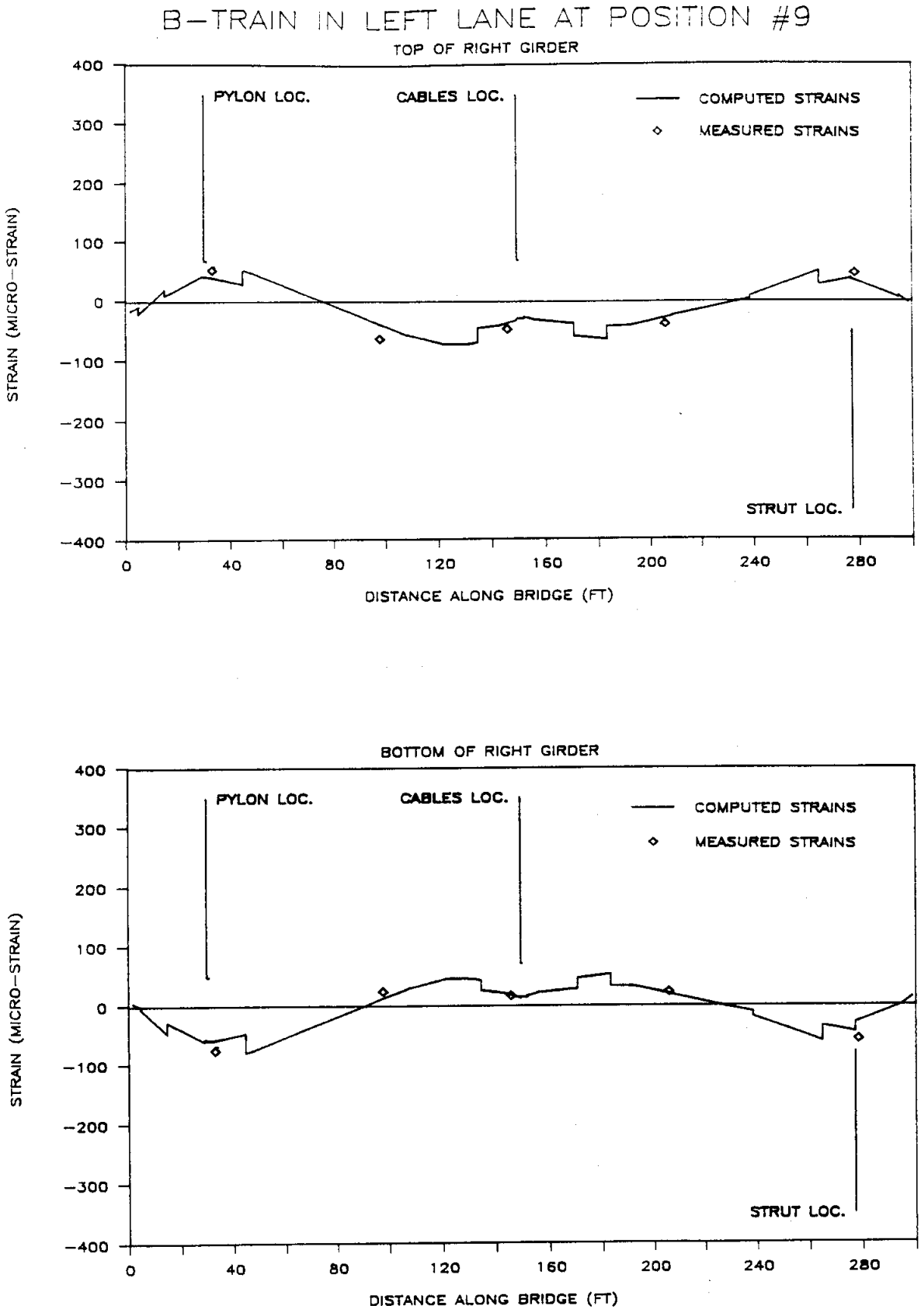

Fig. 4.14 Strain in the Right Girder for B-Train #207 in Left Lane at position #9

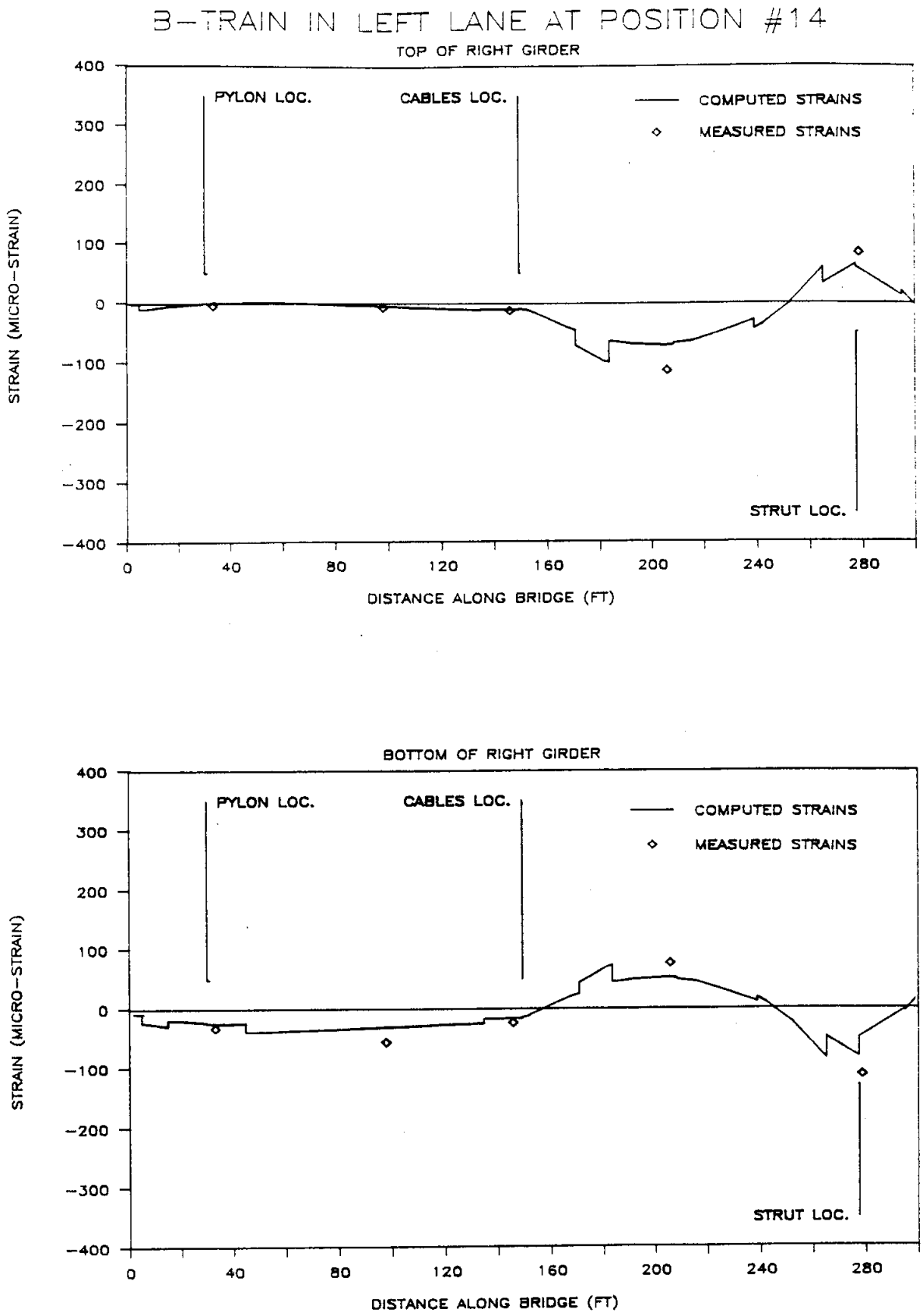

Fig. 4.15 Strain in the Right Girder for B-Train #207 in Left Lane at position #14

Table 4.3. Maximum Strains and Stresses for Tests #SLD0B06 (155.07 kip B-Train truck in the left lane)

Description	Load position	Strains (micro) Meas.	Strains (micro) Calc.	Stresses (ksi) Exper.	Stresses (ksi) Calc.
Left Side					
Top of Girder (98′)	#4	-218	-275	-6.3	-8.0
Bot of Girder (33.25′)	#4	-206	-295(b)	-6.0	-8.6
(278.50′)	#14	-210(a)	-172	-6.1	-5.0
Left Pylon (upsta. face)	#4	-132	-192	-3.8	-5.6
Left Strut (downsta. face)	#14	26	23	0.8	0.7
Right Side					
Top of Girder (33.25′)	#4	101	74(b)	2.9	2.1
(206′)	#14	-113(a)	-70	-3.3	-2.0
Bot of Girder (33.25′)	#4	-105	-81(b)	-3.0	-2.3
(278.5′)	#14	-112(a)	-46	-3.2	-1.3
Right Pylon (upsta. face)	#4	-56	-42	-1.6	-1.2

a) Maximum measured strain
b) Maximum calculated strain

Tests SLD0B08. This series of tests involved the same type of loading conditions as the previous test series, except a different B-Train truck (#216) was used to conduct the test.

This truck weighed 157.379 kips. It was positioned in the left lane in the observable wheel path, facing downstation. The truck was statically located between 50 and 52.5 in. from the guardrail at positions #4, 9, and 14. The calculated load distribution for this test series is presented in Appendix A, Table A.2.

The experimental and calculated strains for each test in this series are presented in Appendix C, Tables C.2a and C.2b. The strains along the left girder are shown in Figures 4.16 through 4.18 and the strains along the right girder are shown in Figures 4.19 through 4.21.

Table 4.4 summarizes the maximum strains for this test series and gives the resulting stresses. Although a different truck and axle loading was used, a comparison between the results shows consistent behavior with the previous series of tests (approximately the same loading situation). The maximum experimental stresses were -6.5 ksi and the maximum calculated were -8.6 ksi.

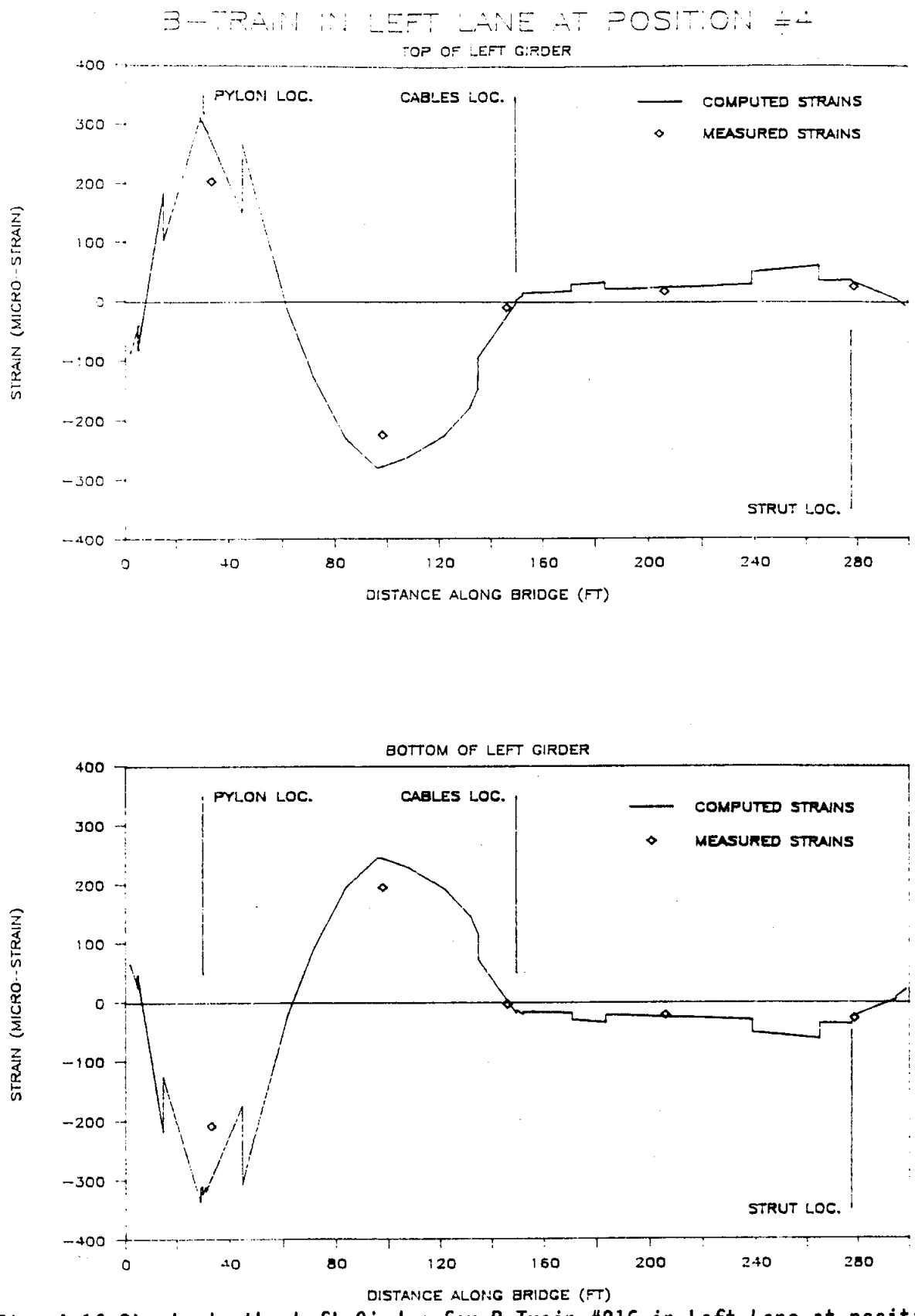

Fig. 4.16 Strain in the Left Girder for B-Train #216 in Left Lane at position #4

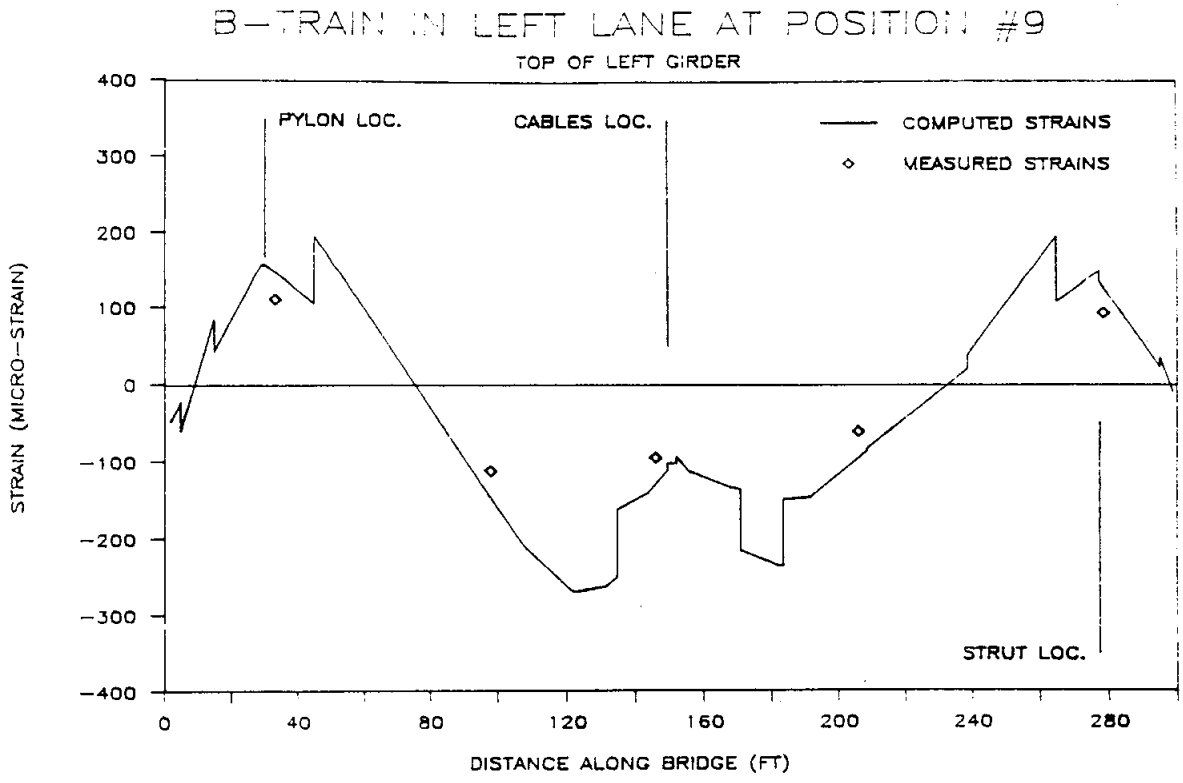

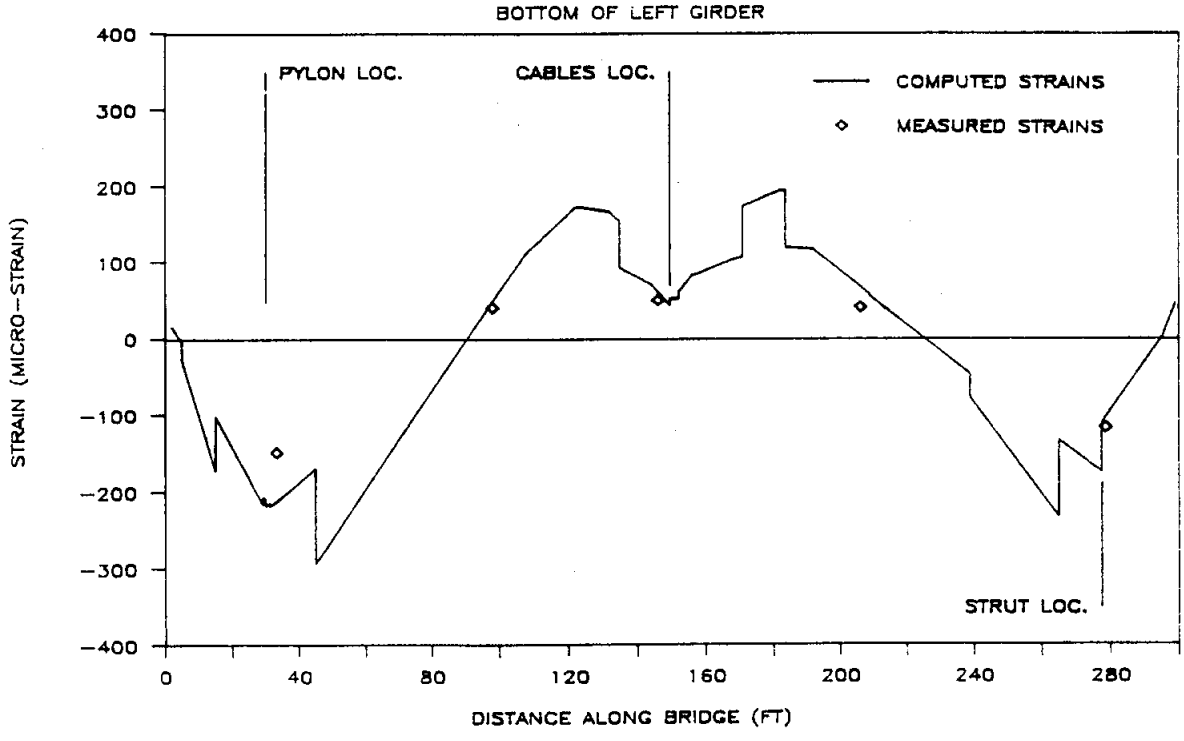

Fig. 4.17 Strain in the Left Girder for B-Train #216 in Left Lane at position #9

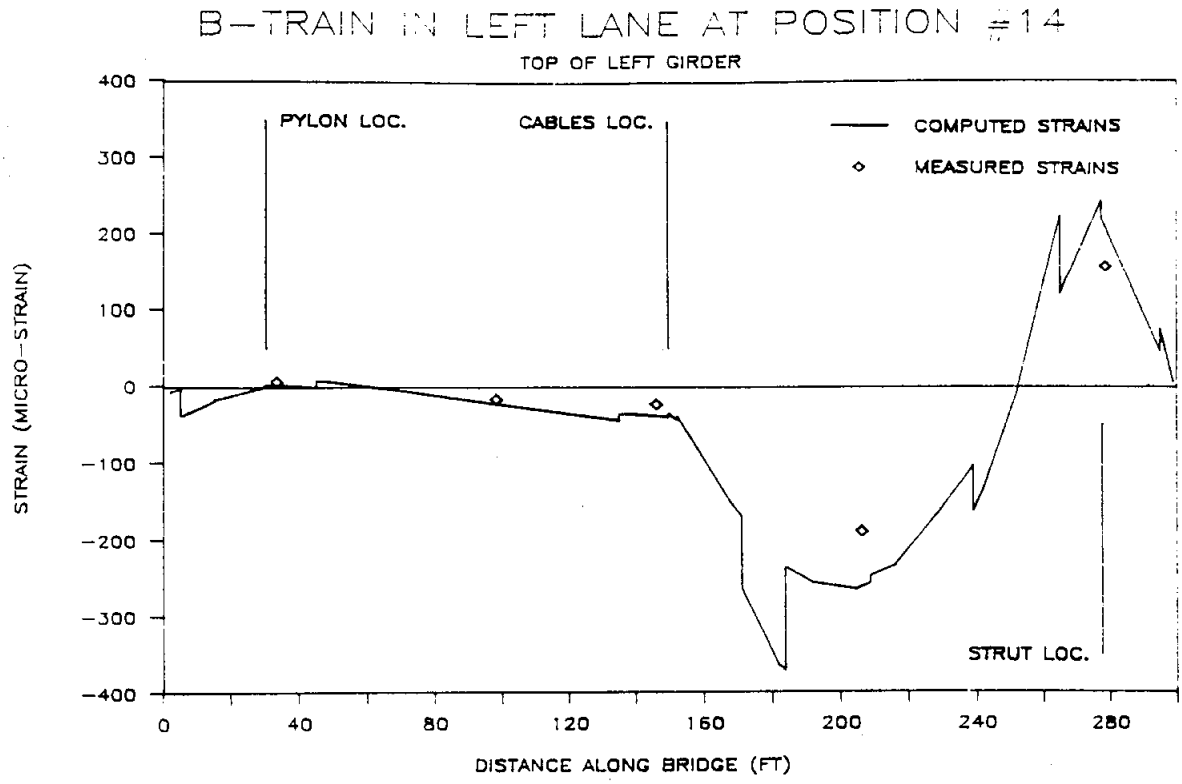

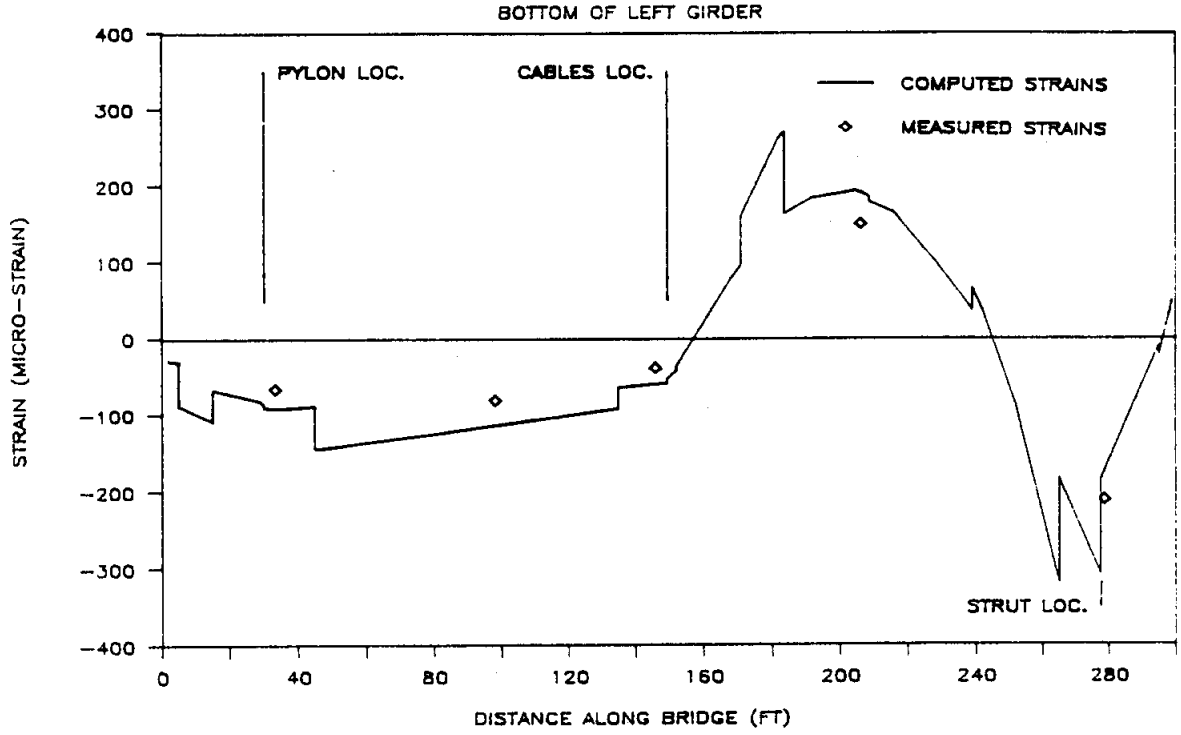

Fig. 4.18 Strain in the Left Girder for B-Train #216 in Left Lane at position #14

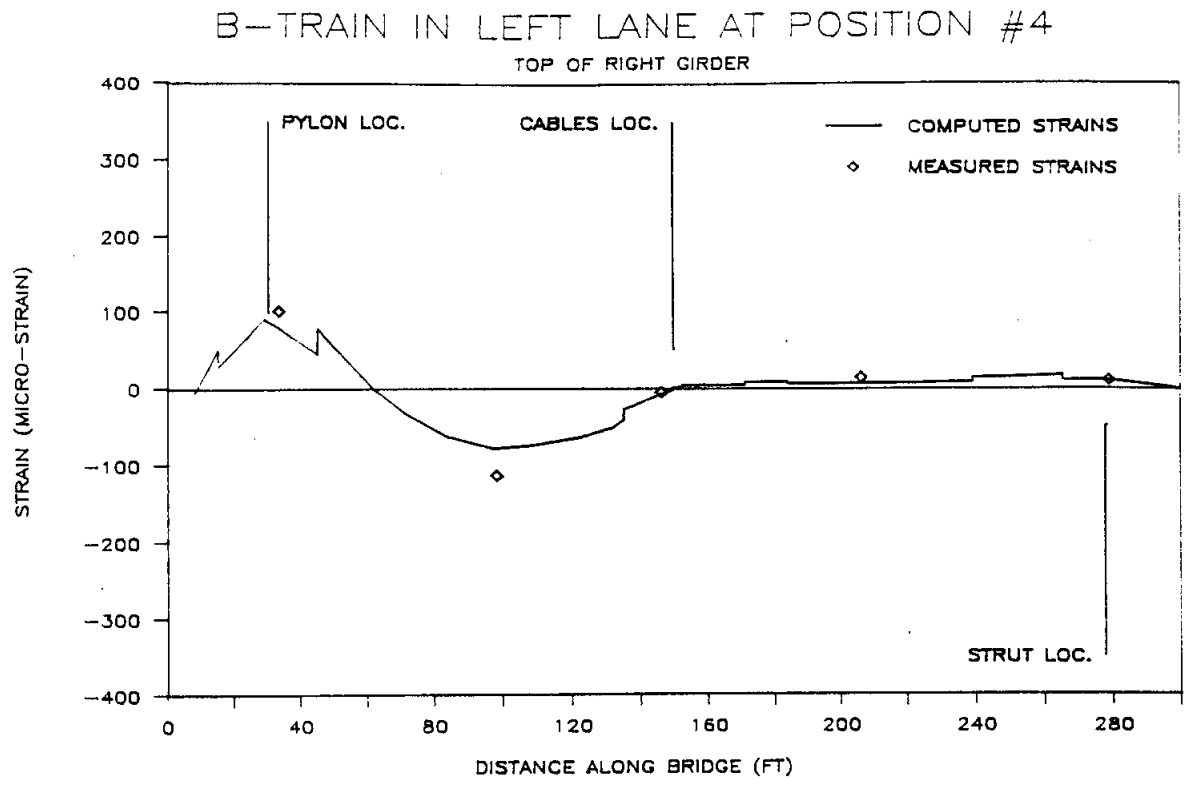

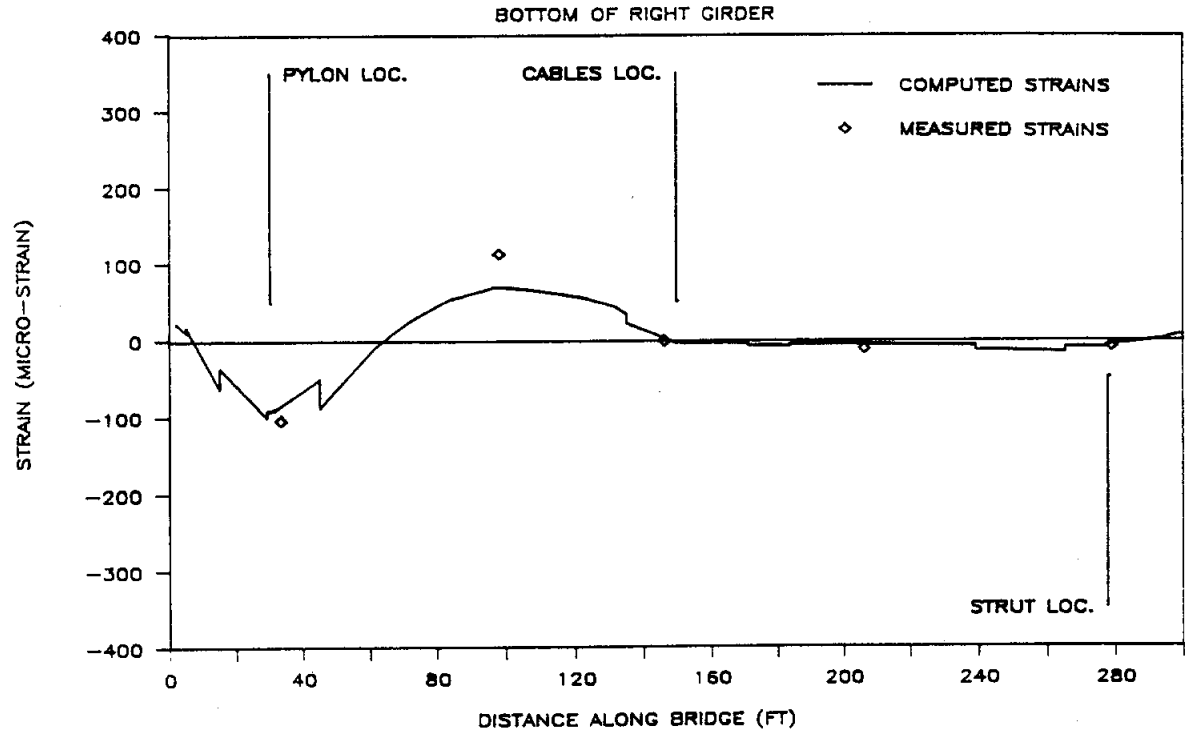

Fig. 4.19 Strain in the Right Girder for B-Train #216 in Left Lane at position #4

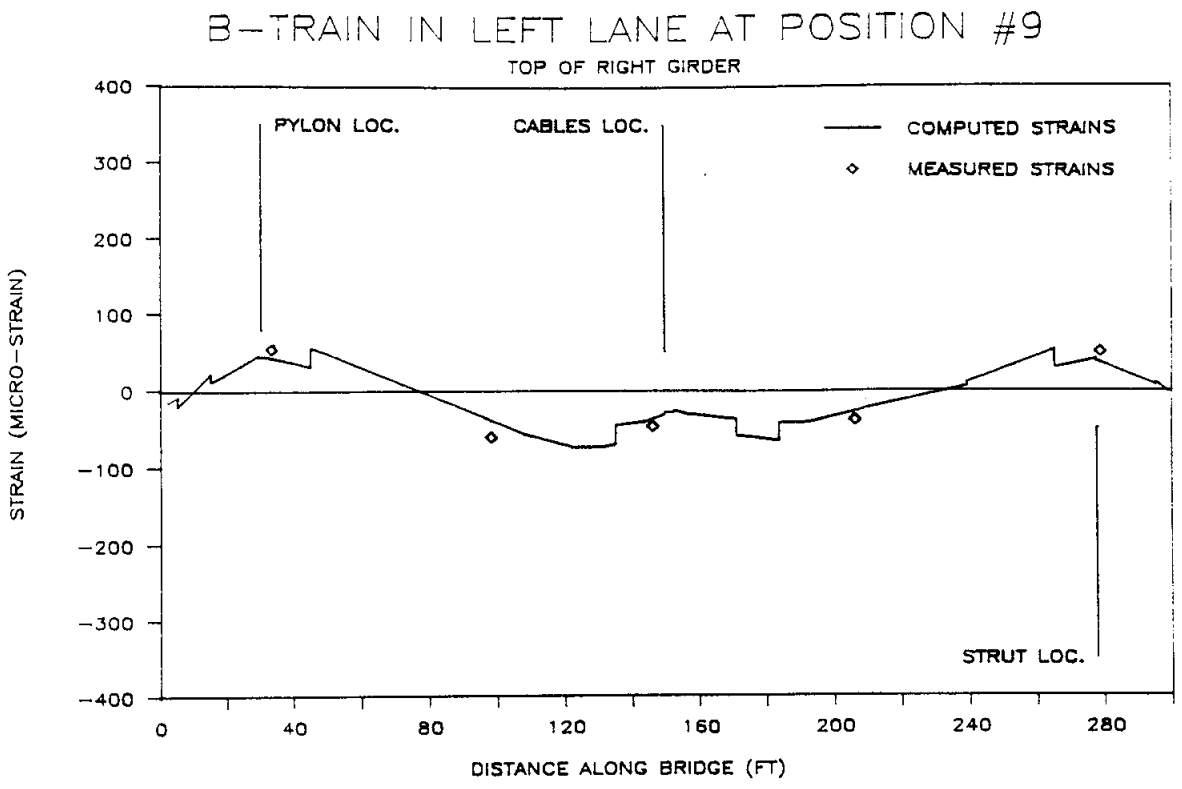

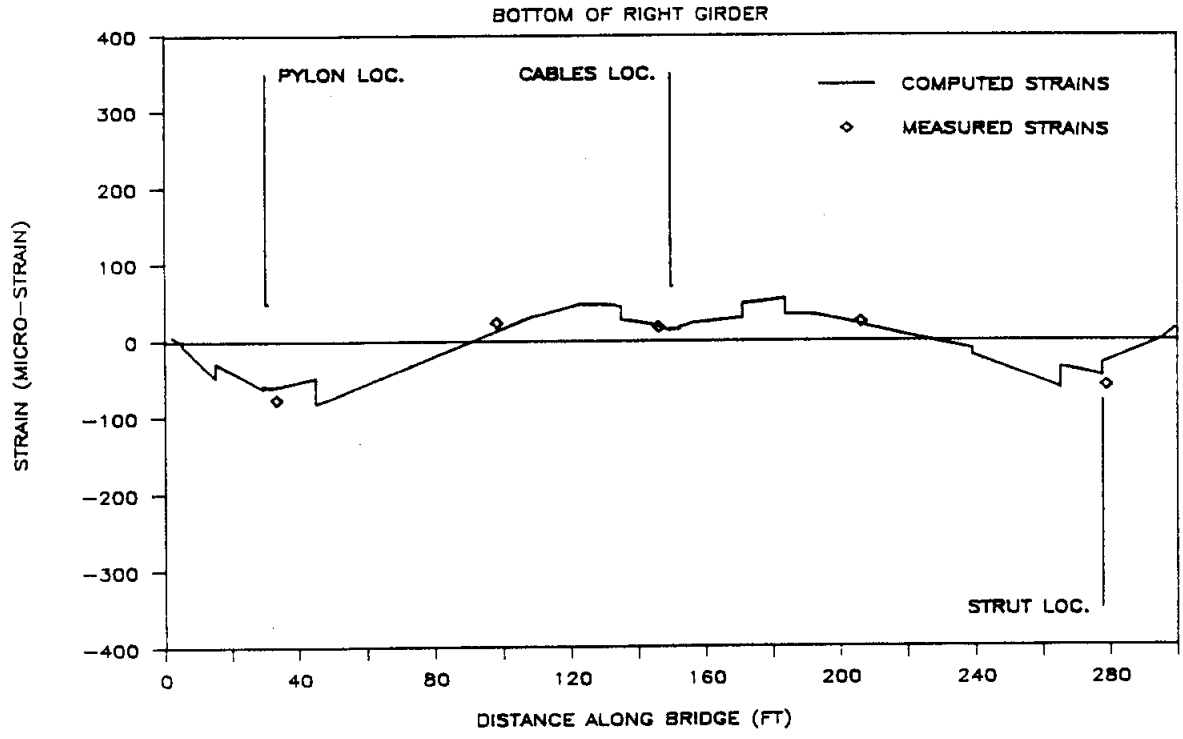

Fig. 4.20 Strain in the Right Girder for B-Train #216 in Left Lane at position #9

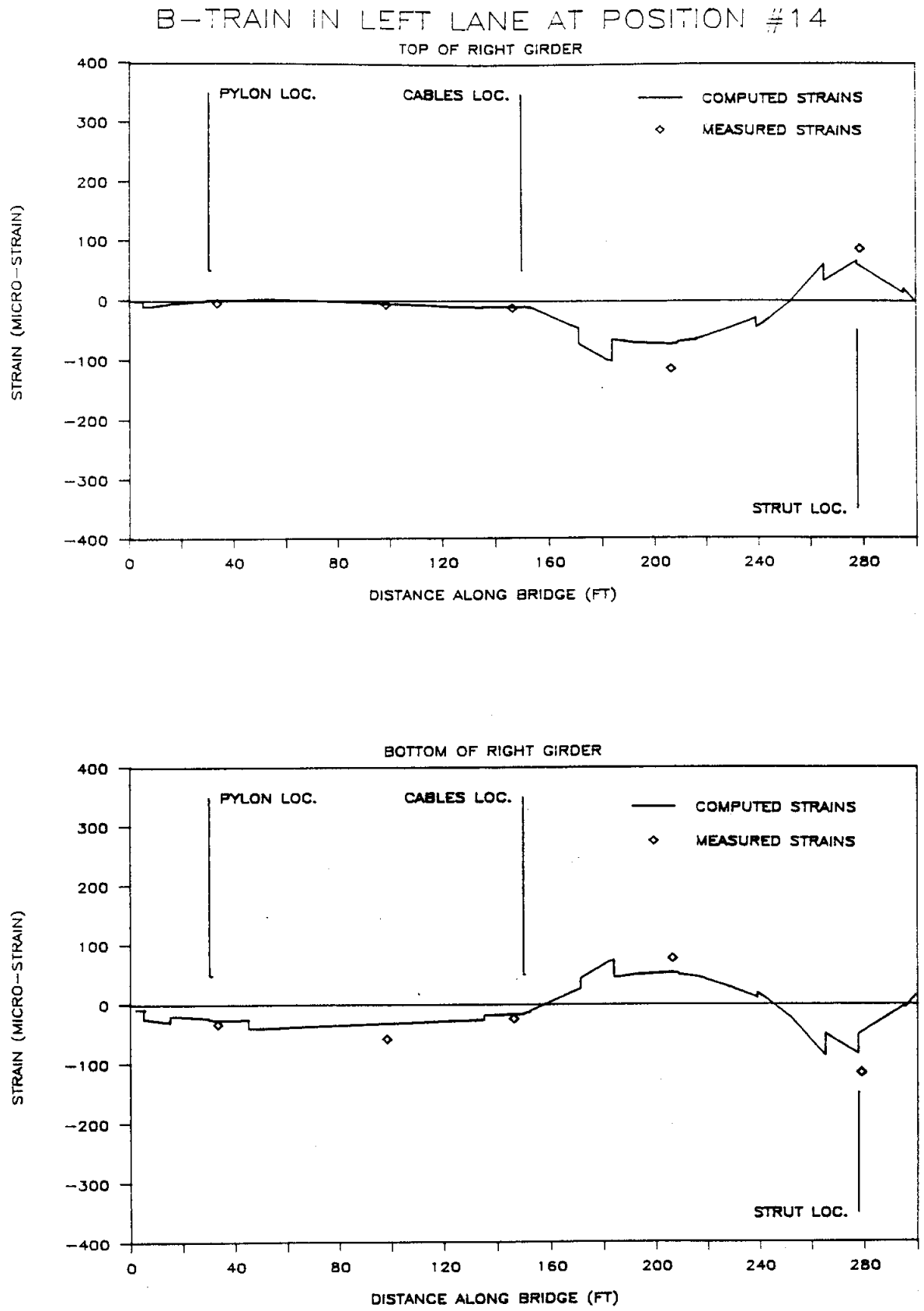

Fig. 4.21 Strain in the Right Girder for B-Train #216 in Left Lane at position #14

The maximum difference between measured and computed strains along the left side of the bridge occurred at the bottom of the girder near the pylon with the truck at position #4. The 2-D model overpredicted the strain at this location by 89 micro-strains. Along the right side of the bridge, the maximum difference occurred in the vicinity of the upstation strut, along the bottom of the girder, with the truck at position #14. The 2-D model underpredicted this strain by 68 micro-strains.

Tests SCDOB10. This series of tests involved static loads for a B-Train (#204) facing downstation centered on the bridge center line. The B-Train weighed 157.556 kips.

The portion of load carried by each girder is given in Table A.3, Appendix A. With the B-Train centered on the bridge center line (symmetric loading), the comparison between experimental and analytical values was substantially better. This observation was also noted for the comparison of deflections.

Table 4.4. Maximum Strains and Stresses for Tests #SLDOB08 (157.379 kip B-Train truck in the left lane)

Description	Load Position	Strains (micro) Meas.	Calc.	Stresses (ksi) Exper.	Calc.
Left Side:					
Top of Girder (98′)	#4	-224	-276	-6.5	-8.0
Bot of Girder (33.25′)	#4	-208	-297(b)	-6.0	-8.6
(278.50′)	#14	-211(a)	-174	-6.1	-5.0
Left Pylon (upsta. face)	#4	-134	-193	-3.9	-5.6
Left Strut (downsta. face)	#14	25	23	0.7	0.7
Right Side:					
Top of Girder (33.25′)	#4	101	78(b)	2.9	2.3
(206′)	#14	-114(a)	-72	-3.3	-2.1
Bot of Girder (33.25′)	#4	-104	-85(b)	-3.0	-2.5
(278.5′)	#14	-116(a)	-48	-3.4	-1.4
Right Pylon (upsta. face)	#4	-57	-45	-1.6	-1.3

a) Maximum measured strain.
b) Maximum calculated strain.

Appendix C, Table C.3a provides a detailed strain comparison for the left side of the bridge. Figures 4.22 through 4.24 show strains along the left girder and Figures 4.25 through 4.27 show the strains along the right girder.

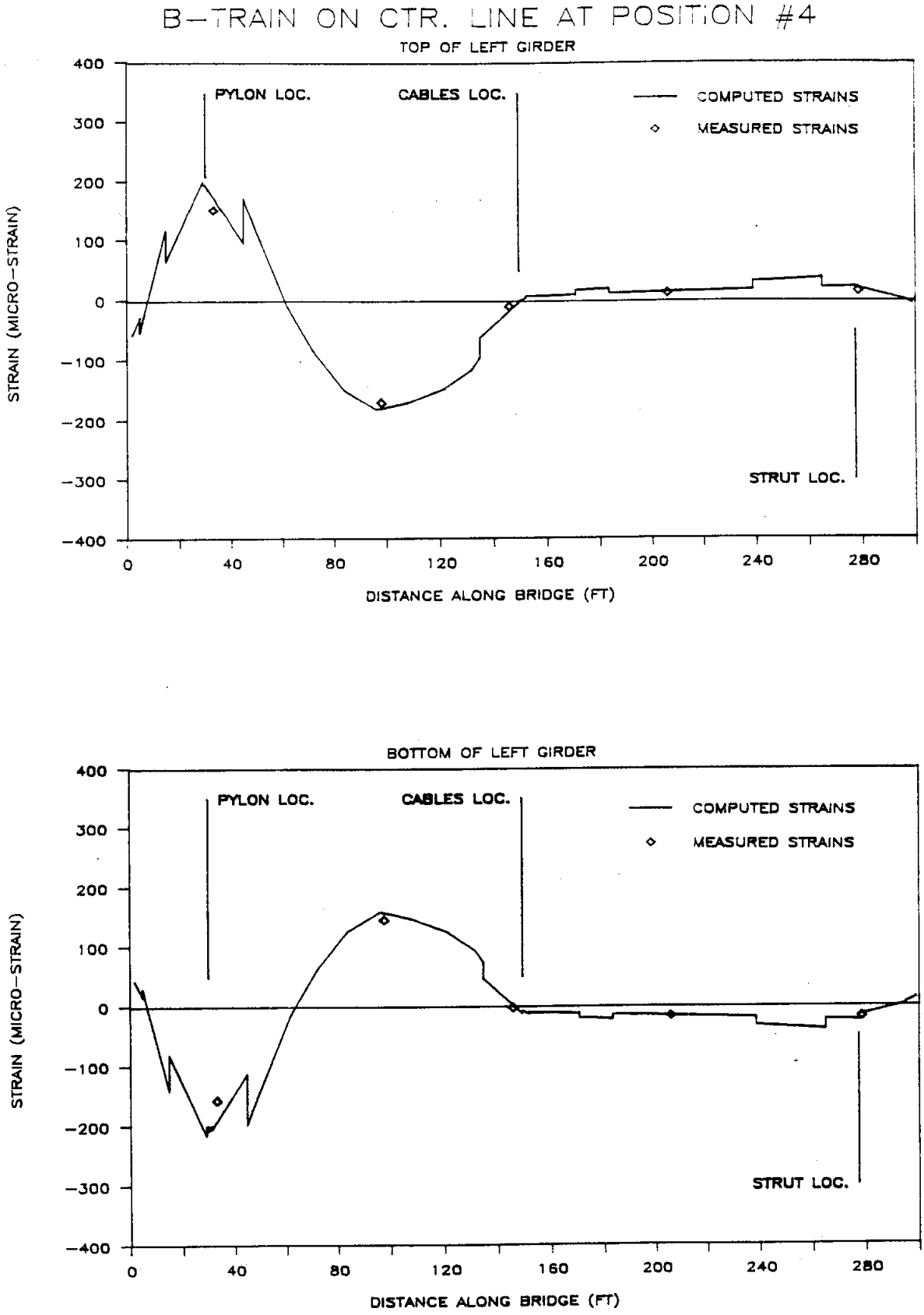

Fig. 4.22 Strain in the Left Girder for B-Train #204 on Center Line at position #4

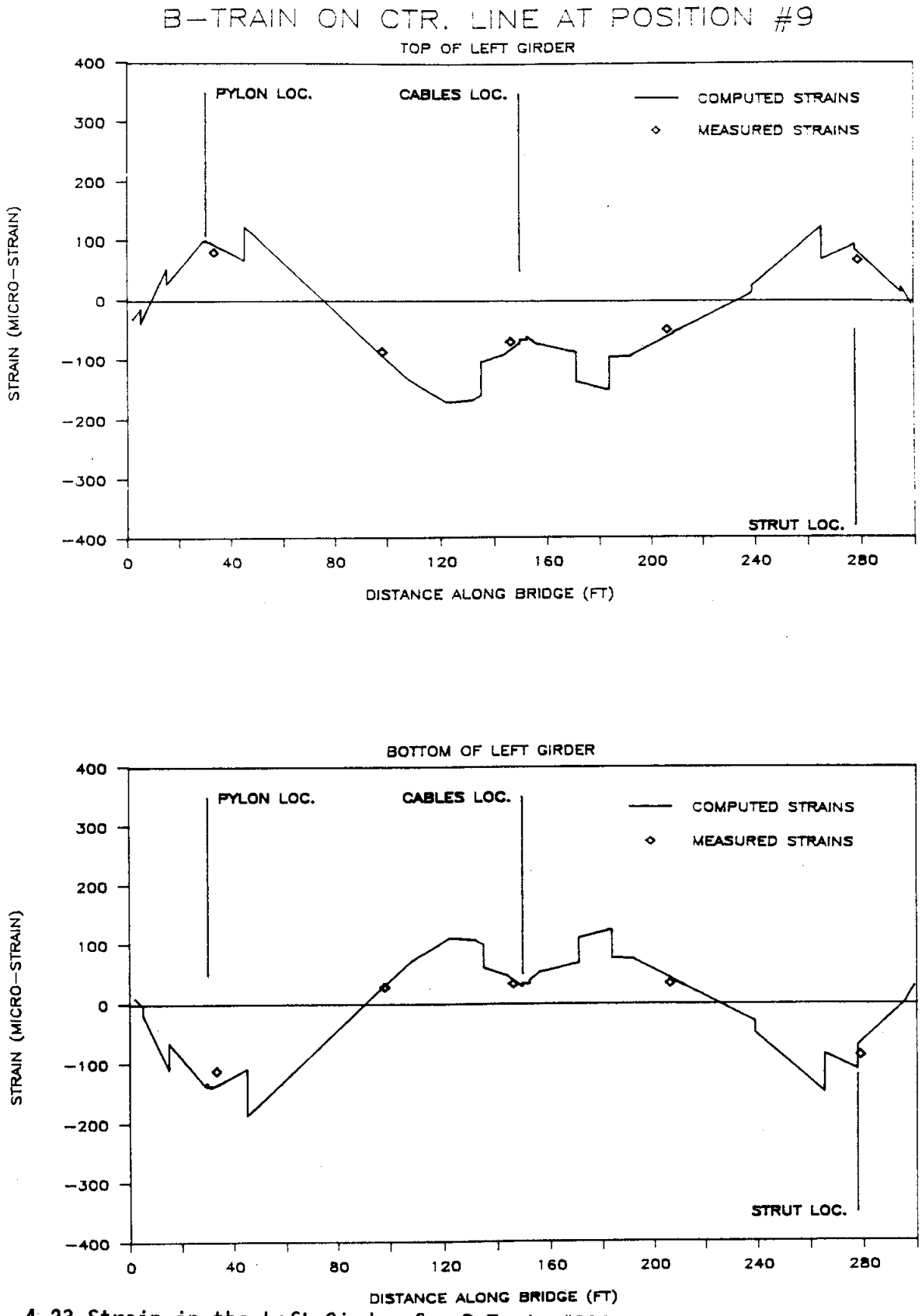

Fig. 4.23 Strain in the Left Girder for B-Train #204 on Center Line at position #9

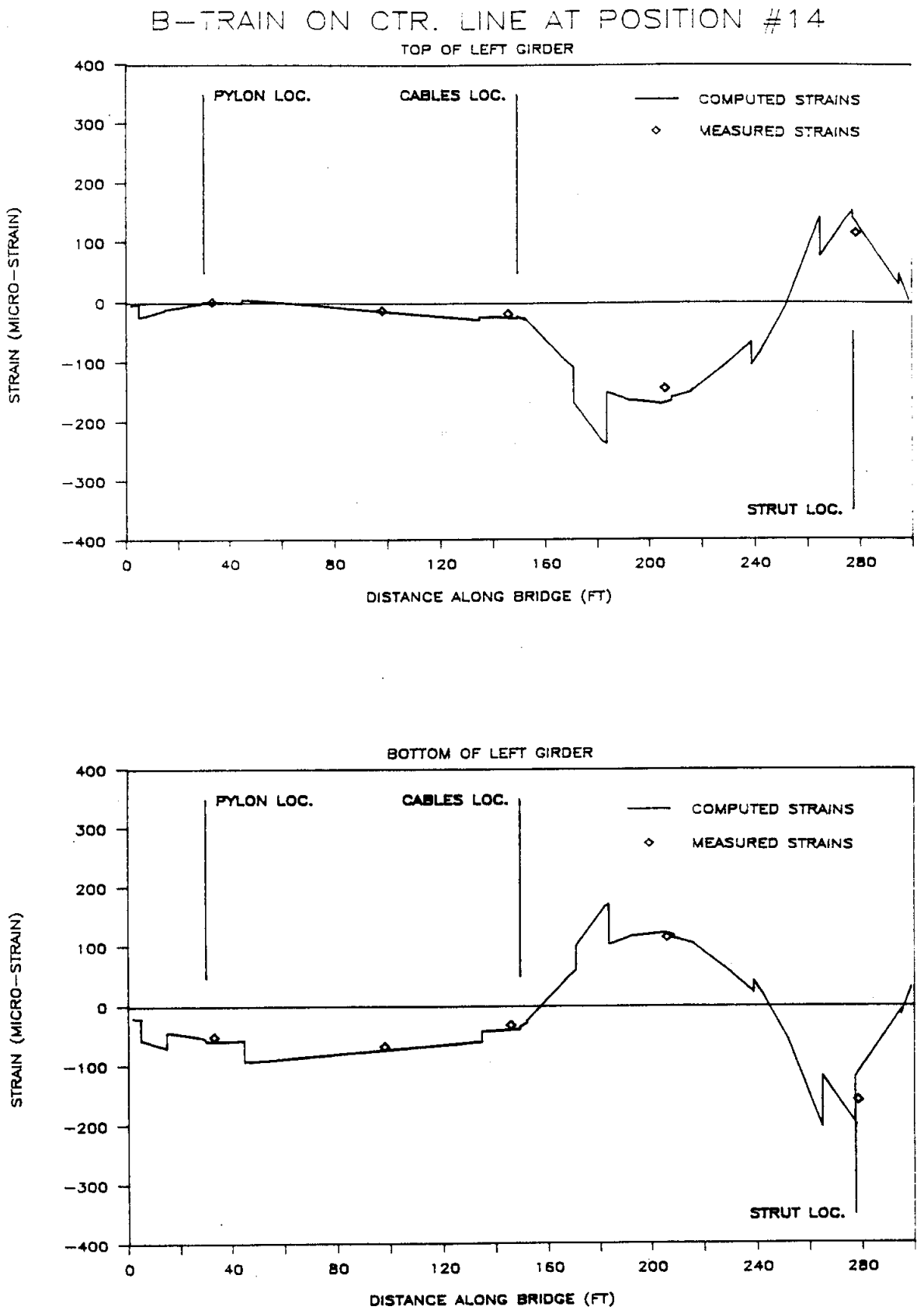

Fig. 4.24 Strain in the Left Girder for B-Train #204 on Center Line at position #14

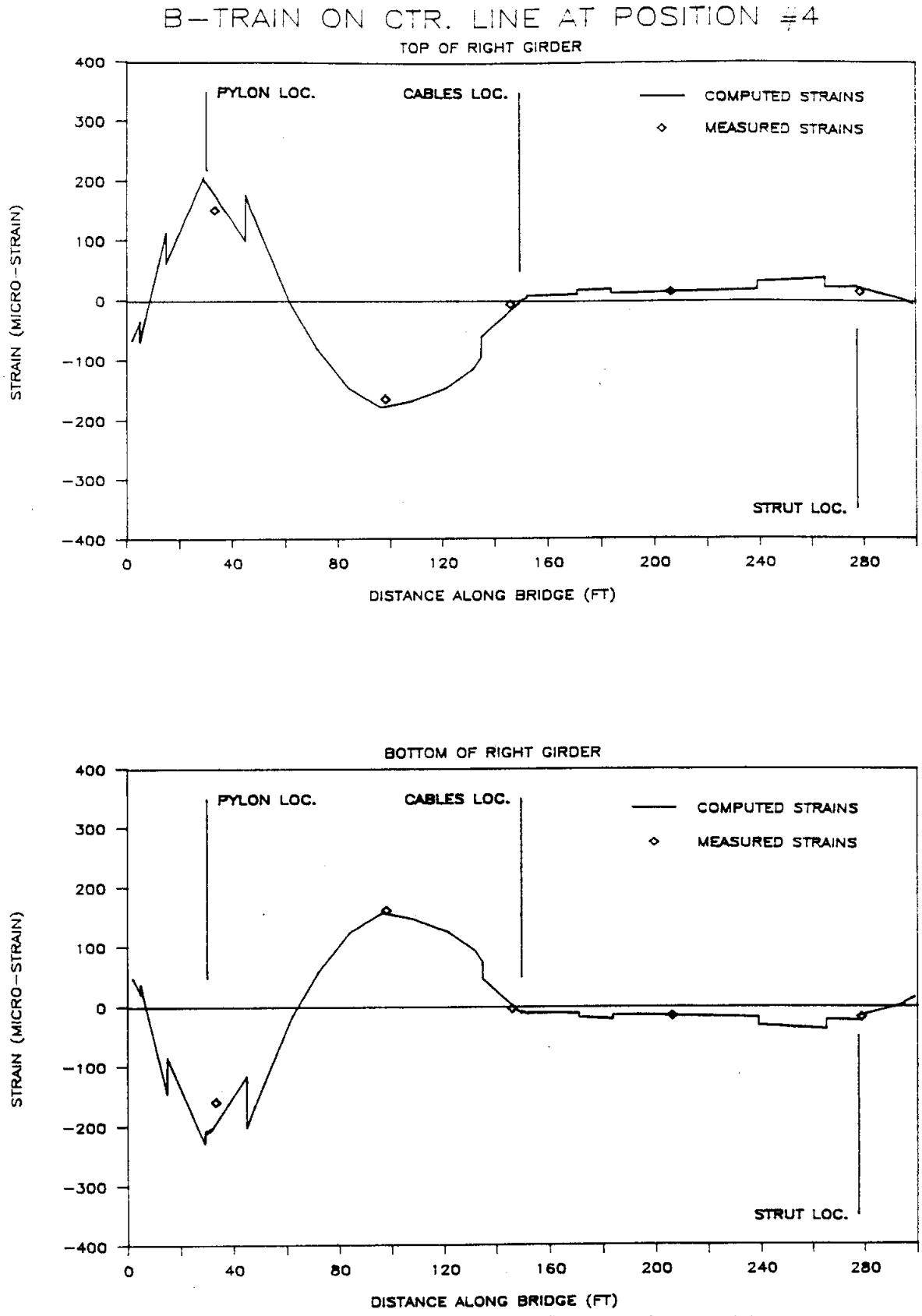

Fig. 4.25 Strain in the Right Girder for B-Train #204 on Center Line at position #4

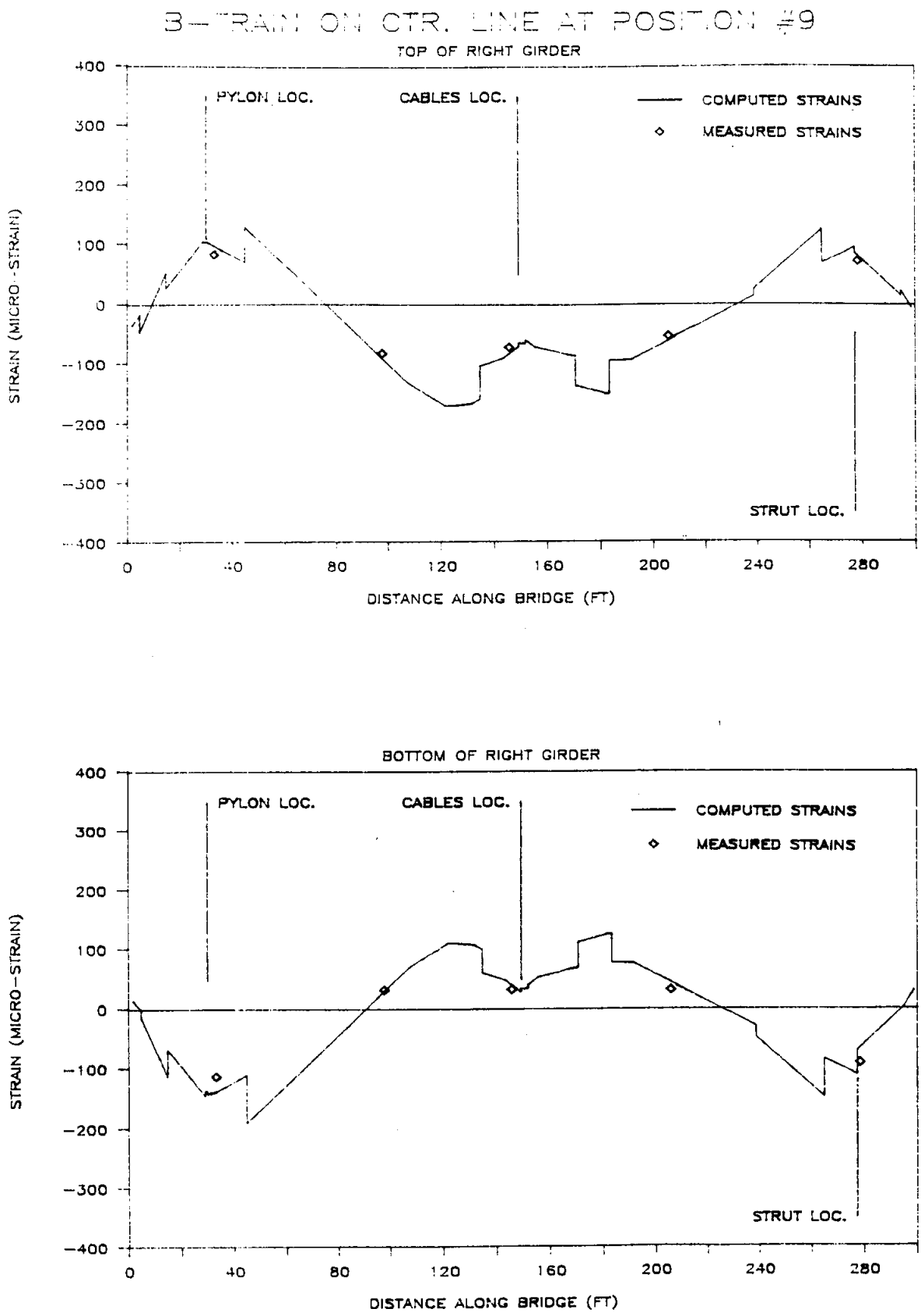

Fig. 4.26 Strain in the Right Girder for B-Train #204 on Center Line at position #9

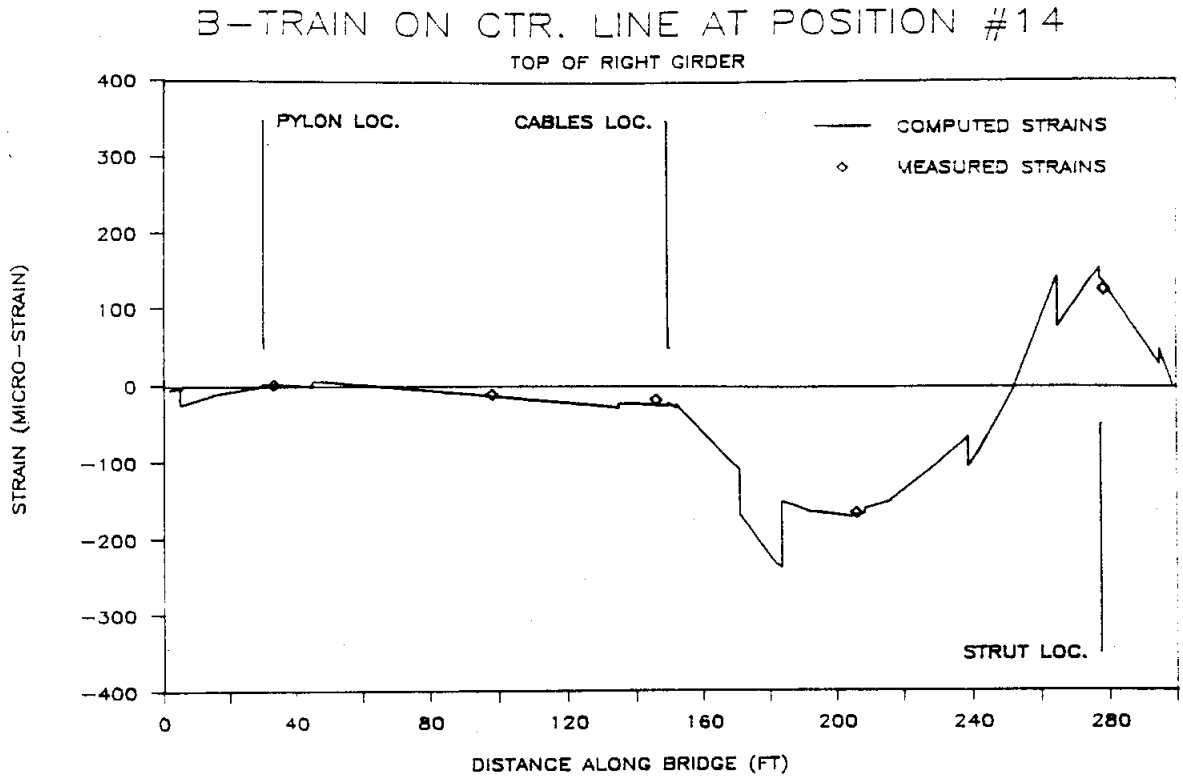

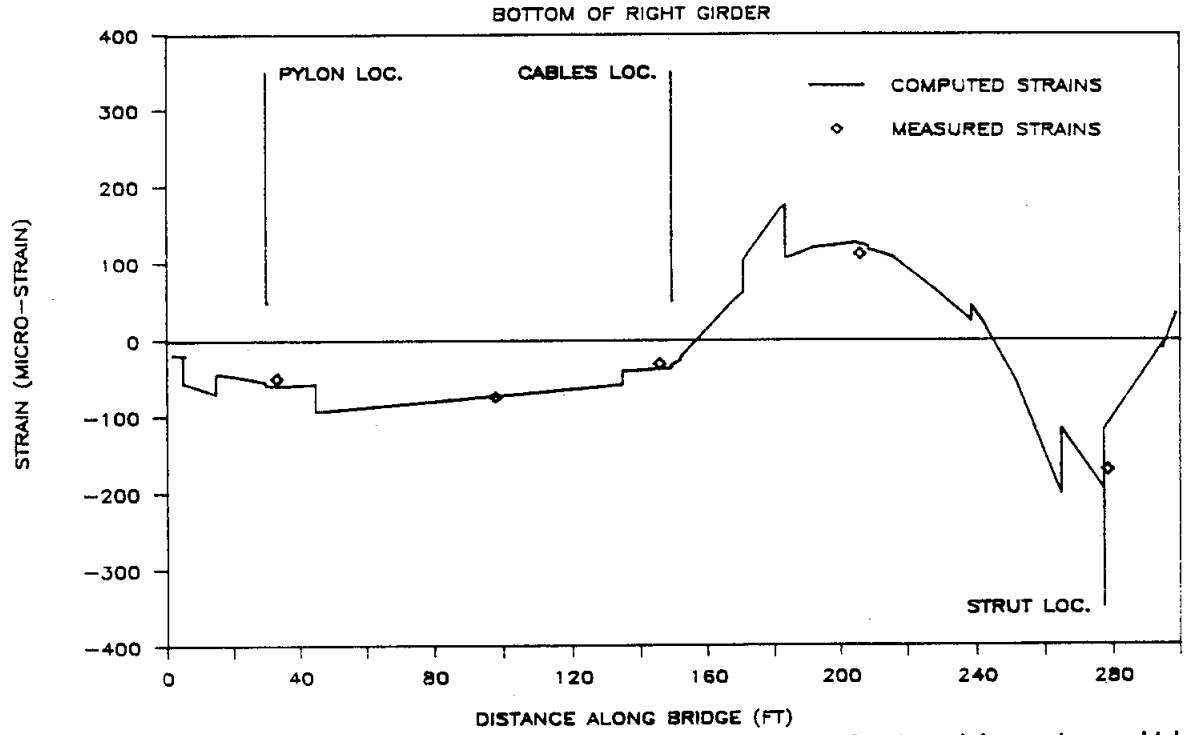

Fig. 4.27 Strain in the Right Girder for B-Train #204 on Center Line at position #14

The maximum difference between experimental and computed strains on the left side of the bridge was approximately 47 micro-strains, occurring in the vicinity of the upstation strut, along the bottom of the girder, with the truck at position #14.

Appendix C, Table C.3b presents the experimental and computed strains for the right side of the bridge. With two exceptions, all calculated strains were within 26 micro-strains of the measured. One exception occurred when the truck was at position #4 and the other at #14. The maximum differences of 35 and 60 micro-strains, respectively, occurred in the vicinity of the pylon and the upstation strut along the bottom of the girder.

Table 4.5 shows the maximum strains and stresses for this test series. The maximum experimental stress was -5.0 ksi. This stress occurred at the bottom of the right girder, 278.5 ft from the downstation end when the truck was at position #14. The maximum calculated stress was -5.6 ksi, and this stress occurred at the bottom of the right girder, 33.25 ft from the downstation end when the truck was at position #4.

Based on the results, a 2-D model provides a satisfactory solution for symmetric loading conditions.

Table 4.5. Maximum Strains and Stresses for Tests #SCDOB10
(157.556 kip B-Train truck (#204) in the left lane)

Description	Load Position	Strains (micro) Meas.	Strains (micro) Calc.	Stresses (ksi) Exper.	Stresses (ksi) Calc.
Left Side					
Top of Girder (98′)	#4	-169	-178	-4.9	-5.2
Bot of Girder (33.25′)	#4	-157	-191(b)	-4.6	-5.5
(278.50′)	#14	-158(a)	-111	-4.6	-3.2
Left Pylon (upsta. face)	#4	-99	-124	-2.9	-3.6
Left Strut (downsta. face)	#14	22	15	0.6	0.4
Right Side					
Top of Girder (98′)	#4	-164	-176(b)	-4.8	-5.1
Bot of Girder (33.25′)	#4	-158	-193(b)	-4.6	-5.6
(278.5′)	#14	-171(a)	-111	-5.0	-3.2
Right Pylon (upsta. face)	#4	-82	-102	-2.4	-3.0

a) Maximum measured strain.
b) Maximum calculated strain.

Tests #SRDOB11. The final test was conducted with the B-Train (#305) in the center of the right lane, facing downstation, and situated at positions #4, 9, and 14. The truck used in this test weighed 157.093 kips, and the calculated load distribution is provided in Table A.4, Appendix A.

A strain comparison on the right loaded side indicated a maximum difference of 74 micro-strains between the measured and calculated. This occurred along the bottom of the girder, in the vicinity of the upstation strut, when the truck was at position #4. Appendix C, Table C.4b provides a tabulated comparison of the results for these tests, and Figures 4.28 through 4.30 show the graphic comparison between measured girder strains and the computed strains for the entire right girder.

On the left side, the maximum discrepancy was 49 micro-strains on the bottom of the girder in the vicinity of the pylon, with the truck at position #14. Appendix C, Table C.4a shows a detailed numerical strain comparison. Figures 4.31 through 4.33 provide a graphical comparison of the strains.

As with the previous eccentric load conditions, the girder carrying the greater load appeared stiffer, and the side carrying the smaller load appeared more flexible than was predicted by the 2-D model (see Table 4.6).

Table 4.6. Maximum Stains and Stresses for Tests #SRDOB11 (157.093 kip B-Train truck (#305) in the right lane)

Description	Load Position	Strains (micro) Meas.	Calc.	Stresses (ksi) Exper.	Calc.
Left Side					
Top of Girder (98′)	#4	-128	-105	-3.7	-3.0
Bot of Girder (33.25′)	#4	-114	-113(b)	-3.3	-3.3
(278.50′)	#14	-115(a)	-66	-3.3	-1.9
Left Pylon (upsta. face)	#4	-69	-74	-2.0	-2.1
Left Strut (downsta. face)	#14	17	9	0.5	0.3
Right Side					
Top of Girder (33.25′)	#4	191	-249(b)	-5.5	-7.2
(98′)	#4	-207(a)	-246	-6.0	-7.1
Bot of Girder (33.25′)	#4	-197	-271(b)	-5.7	-7.9
(278.5′)	#14	-215(a)	-155	-6.2	-4.5
Right Pylon (upsta. face)	#4	-103	-144	-3.0	-4.1

a) Maximum measured strain.
b) Maximum calculated strain.

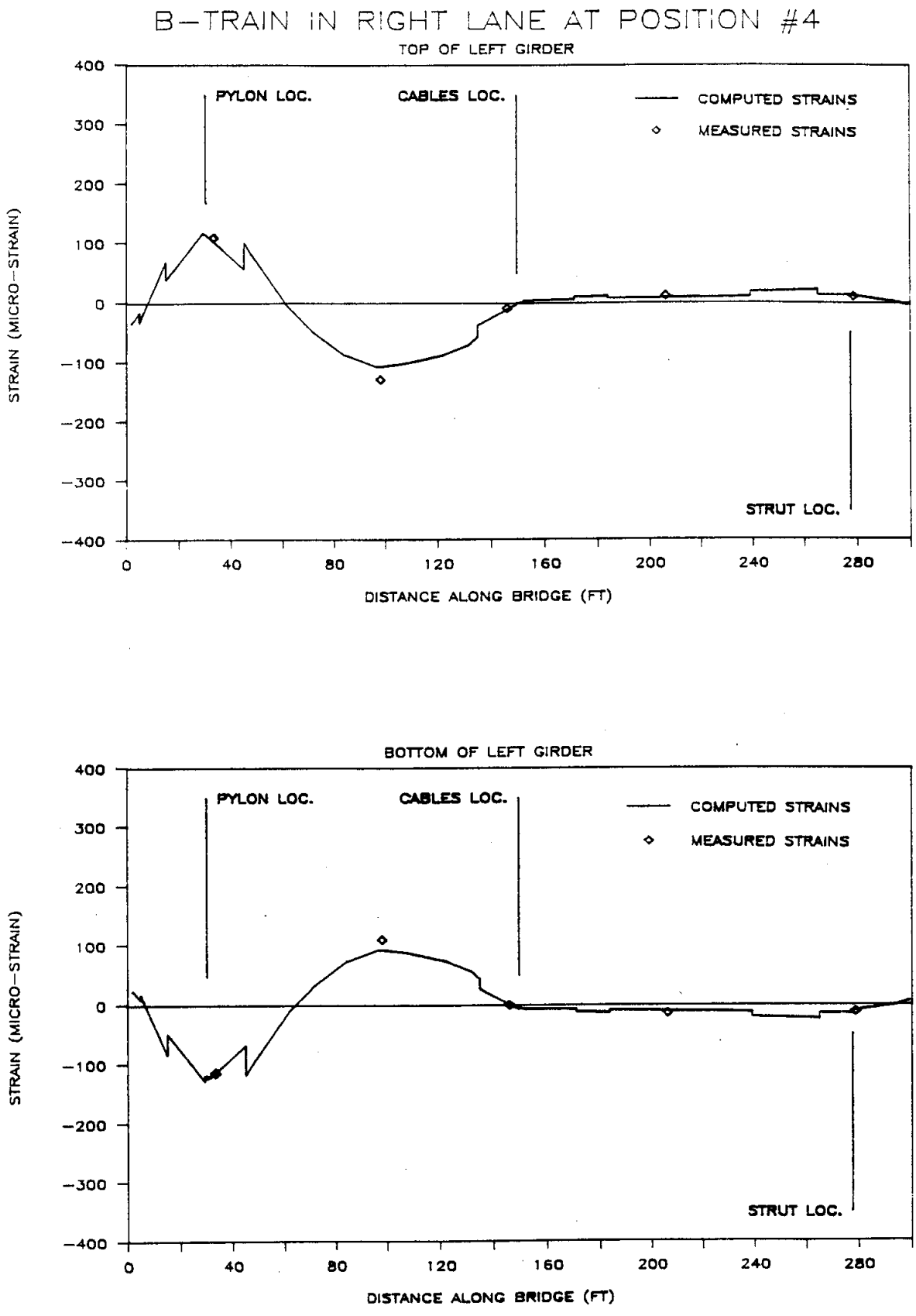

Fig. 4.28 Strain in the Left Girder for B-Train #305 in Right Lane at position #4

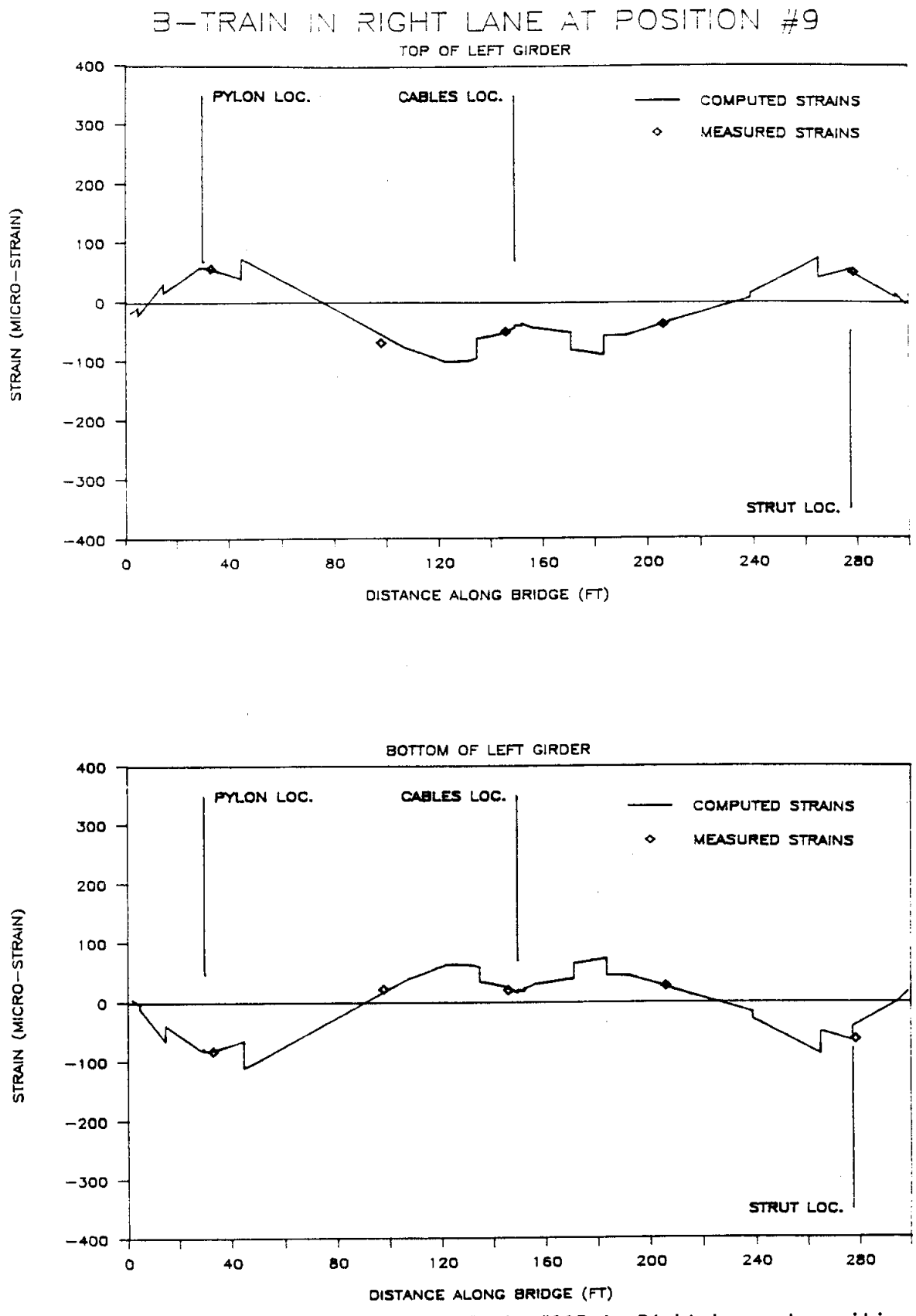

Fig. 4.29 Strain in the Left Girder for B-Train #305 in Right Lane at position #9

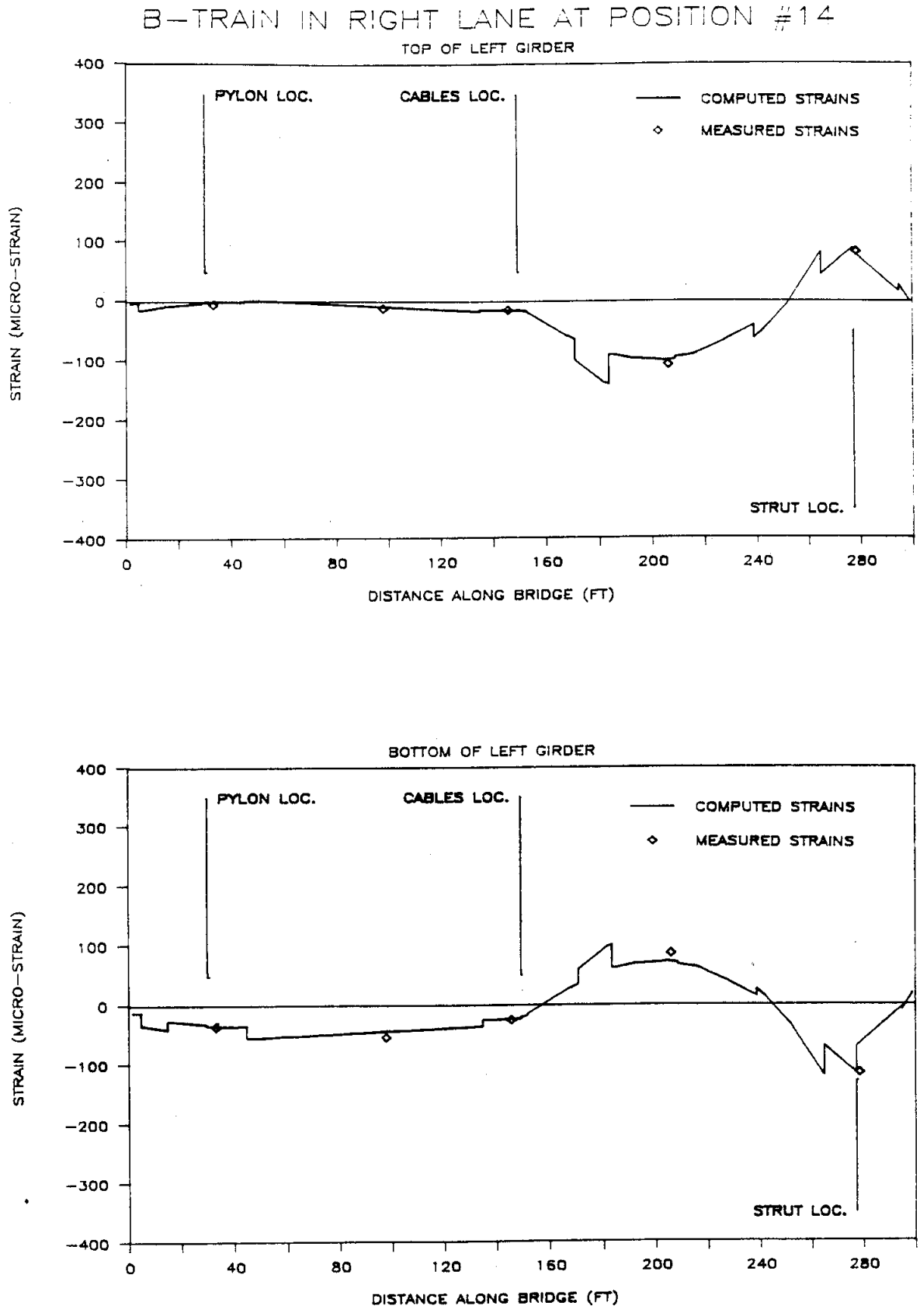

Fig. 4.30 Strain in the Left Girder for B-Train #305 in Right Lane at position #14

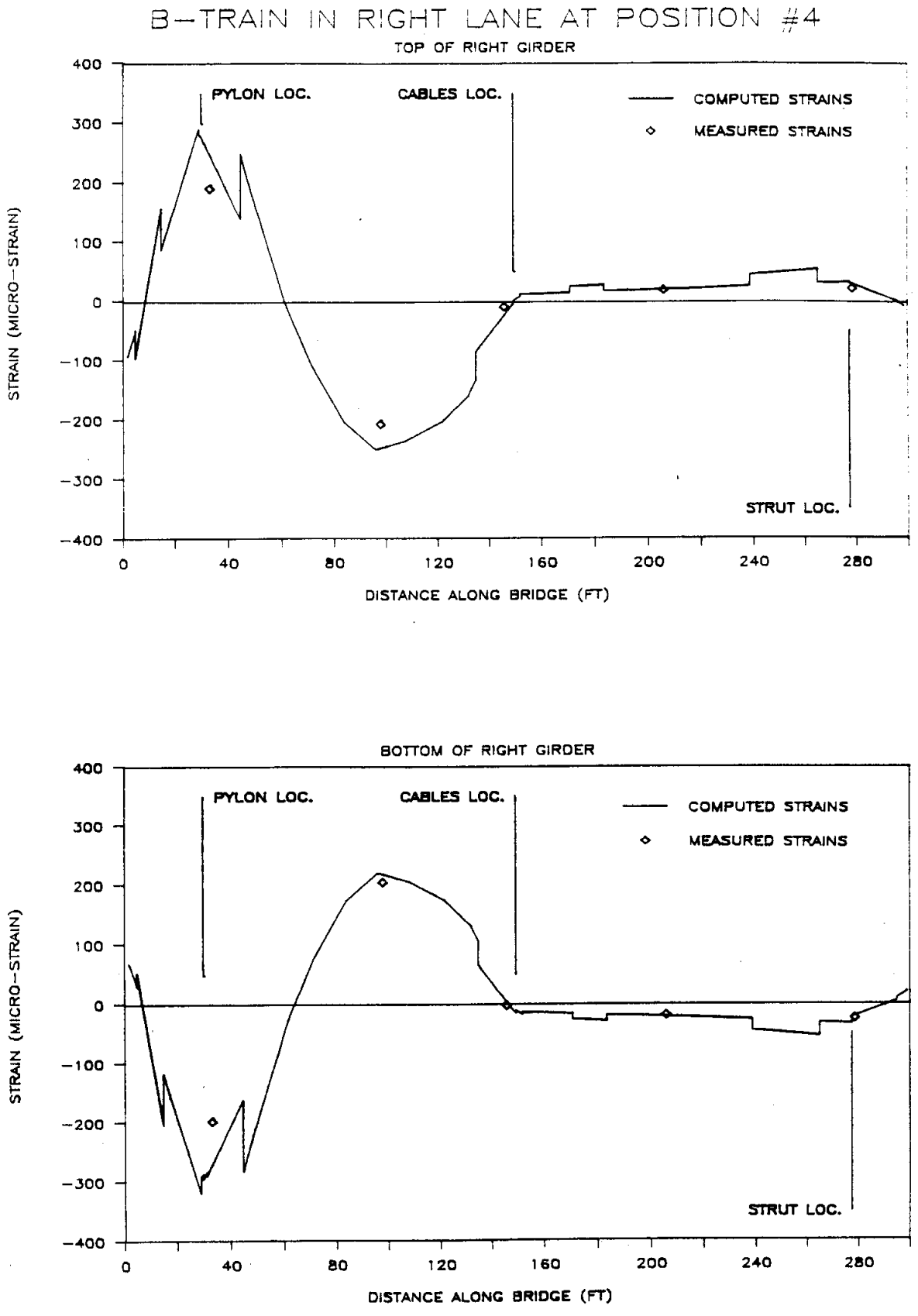

Fig. 4.31 Strain in the Left Girder for B-Train #305 in Right Lane at position #4

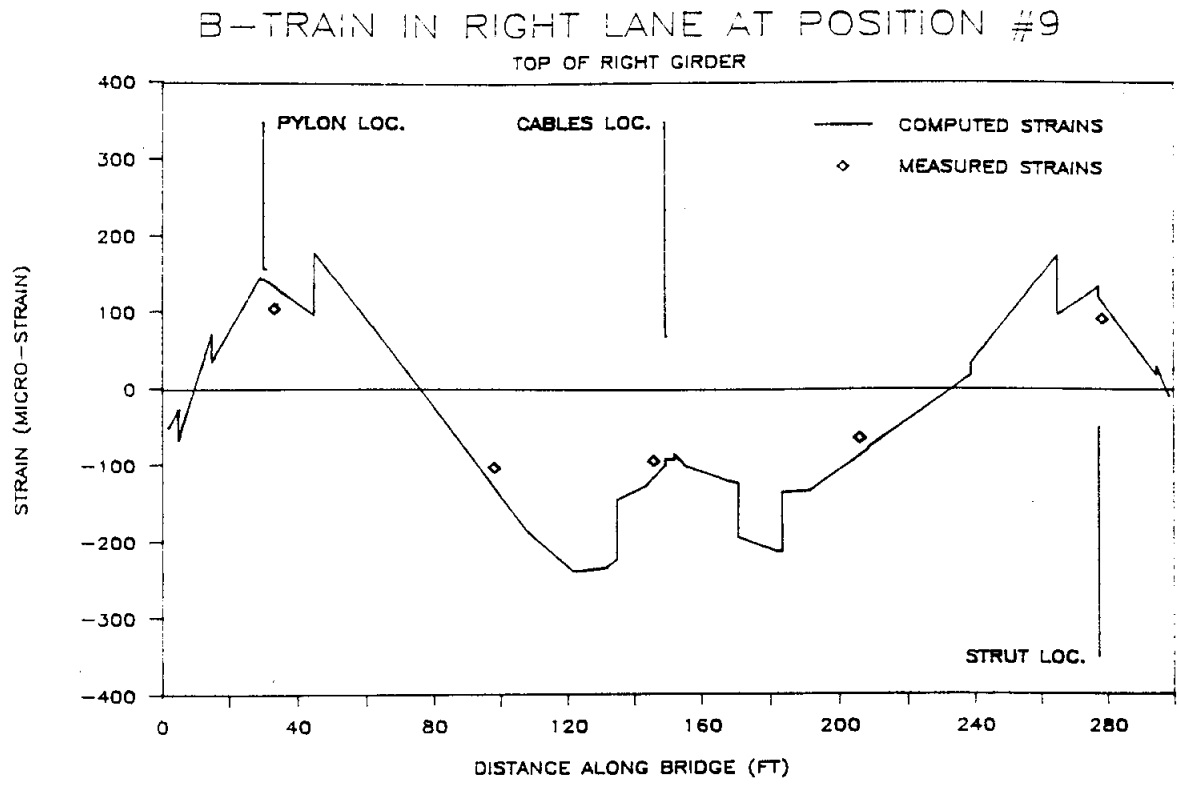

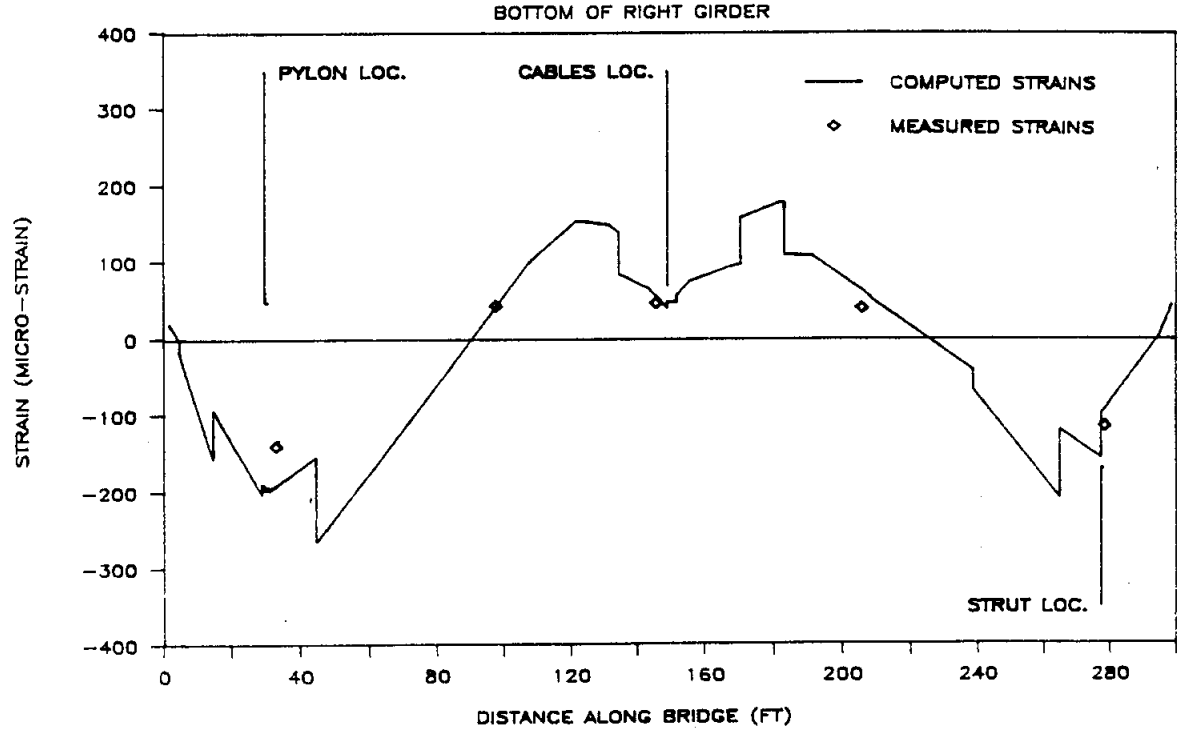

Fig. 4.32 Strain in the Left Girder for B-Train #305 in Right Lane at position #9

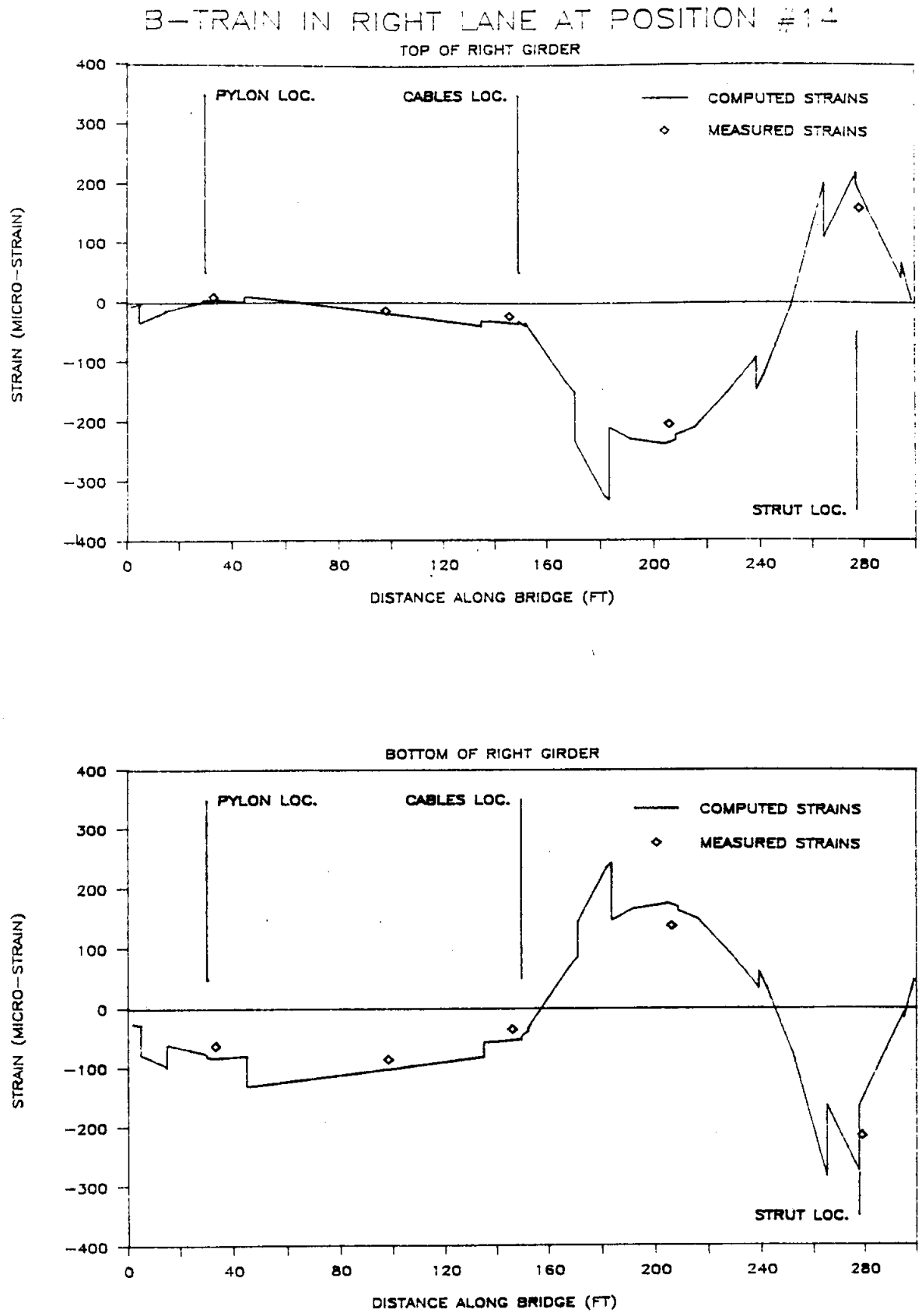

Fig. 4.33 Strain in the Left Girder for B-Train #305 in Right Lane at position #14

5. SUMMARY

5.1 Snooper Truck Loads

Experimental strains were compared with a two-dimensional finite element model for nine Snooper truck tests. These tests were conducted with the truck on the bridge centerline and the left and right lanes. The load positions were 48 ft, 108 ft, and 168 ft from the downstation end. Comparisons between calculated and experimental strains and stresses were generally good. The Snooper truck was used as a control vehicle and provided a means to evaluate the relative magnitude of strains imposed by the B-Trains.

5.2 B-Train Loads

There were four series of static load tests conducted on the Captain William Moore Creek Bridge in the summer of 1988. Each series of tests consisted of measurements at the same three load positions, giving a total of 12 static tests. There were six static tests with a B-Train in the left lane, three on the bridge center line, and three in the right lane. All tests were conducted with trucks facing downstation towards Skagway, Alaska. The weights of the B-Train trucks varied from 155.07 kips to 157.556 kips.

Experimental strains and girder deflections were compared with results from a 2-D finite element linear elastic model defined to have beam and truss type elements.

A comparison between experimental and computed data for the 12 tests showed that the 2-D model provided accurate results for a truck on the bridge center line (symmetric loads). When a truck was in a lane, the 2-D model overpredicted deflections and strains for the girder on the loaded side and underpredicted them for the girder on the empty side.

The results suggest that asymmetrical loads produce 3-dimensional behavior. Thus, predictions due to lane loads will required a 3-D analysis. The structure's behavior due to symmetrical loads may be satisfactorily predicted with a 2-D model.

Girder Deflections

Deflections were recorded for 2 series of tests. These were with a B-Train in the left lane and a B-Train on the center line. The results of these tests produced a maximum measured left girder deflection of 2.76 in (3.40 in calculated) for the truck in the left lane. The maximum measured right girder deflection was 2.16 in (2.18 in calculated) for the truck on the bridge center line.

Bridge Strains and Stresses

The results of these tests show that the maximum measured girder strain was -224 micro-strains (-6.5 ksi) and the maximum calculated girder strain was -297 micro-strains (-8.6 ksi). The maximum measured strain near the pylon base was -134 micro-strains (-3.9 ksi). The maximum calculated pylon base strain was -193 micro-strains (-5.6 ksi). The maximum measured strain in the upstation strut was 26 micro-strains (0.8 ksi) and the maximum calculated strain was 23 micro-strains (0.7 ksi).

6. CONCLUSIONS

The Captain William Moore Creek Bridge near Skagway, Alaska was instrumented in the summer of 1988 with strain gages, thermistors, an extensiometer, and environmental sensors and statically tested for two types of trucks. During the testing period, girder deflection measurements were recorded for selected tests.

Two types of trucks were used to load the bridge. These were a Snooper truck and a series of 160,000 lb. ore trucks (B-Trains). They were placed at positions previously determined to be critical to the overall performance of the bridge. The loads were positioned in the left lane, bridge centerline, and right lane.

The bridge structure was analyzed for the test load cases with a 2-D elastic model using the finite element method with beam elements. The computed strains and girder displacements were compared with the experimental results.

Based on parametric studies and a comparison of calculated results with experimental, the following conclusions were evident:

a) The bridge behavior is significantly influenced by the support conditions. For example, supports with prestressed anchors behaved as fixed supports and supports without prestressed rock anchors behaved as pinned supports.

b) The bridge behavior is significantly influenced by the interaction between the curved steel plate and the elastomeric bearing pad at the girder pylon interface. The results are influenced by the deformation of the neoprene pad.

c) The bridge behavior can be accurately approximated with a 2-D model for symmetric loads.

d) Accurate prediction of the behavior produced by lane loads (asymmetric loads) will require a 3-D model.

7. RECOMMENDATIONS FOR FURTHER STUDY

The study presented was limited to static loads. In order to develop a thorough understanding of the behavior of this structure, further research is recommended.

7.1 Experimental

The strain gages and monitoring cables were left in place at the bridge site. Due to the fact that the Captain William Moore Creek Bridge is a fracture-critical bridge with unusually heavy loads and subjected to a harsh environment, the following experimental studies are recommended:

a) Subject the bridge to static loads and monitor all the cables for the strains due to these loads.

b) Subject the bridge to moving B-Train traffic to assess the dynamic behavior of the structure. When these tests are conducted, the B-Train weights should be recorded, the speed of the vehicle should be measured, and the strains induced in the structure should be monitored.

7.2 Analytical

A 3-D finite element model with nonlinear cable elements, provision for stiffness reductions due to bearing deformations, and beam-to-girder rotational restraints should be developed. Using this model, both a static and dynamic analysis should be conducted. Following these studies, the effects of temperature, stresses induced by the construction sequence, and strengthening conditions should be examined.

8. REFERENCES

1) M.S. Trotski, "Cable-Stayed Bridges, An Approach To Modern Bridge Design", Van Nostrand Reinhold company, New York, 1988.

2) B.E. Lazar, "Stiffness Analysis of Cable-Stayed Bridges", Proc. ASCE Journal of the Structural Division, Vol. 98, No. ST7, pp. 1605-1612, July, 1972.

3) M.C. Tang, "Analysis of Cable-Stayed Girder Bridges", Proc. ASCE Journal of the Structural Division, Vol. 97, No. ST5, pp. 1481-1495, May, 1971.

4) Y.C. Loo and S. Srivanich, "A Simplified Analysis of Cable-Stayed Box Bridges", Inter. Journal of Structures, Paper No. 35, Vol. 3, pp. 93-103, July, 1983.

5) M. Como, A. Grimaldi, and F. Maceri, "Static Behavior of Long-Span Cable-Stayed Bridges", Inter. Journal Solids and Structures, Vol. 21, No. 8, pp. 831-850, 1985.

6) C. Crawford and P. Loris, "Brooklyn Bridge Computer Model", Computing in Civil Engineering: Proceedings of the Third Conference/New York, ASCE, pp. 540-549, 1984.

7) H. Nakai, T. Kitada, R. Ohminami, and T. Nishimura, "Elasto-Plastic and Finite Displacement Analysis of Cable-Stayed Bridges", Memoirs of the Faculty of Engineering, Osaka City University, Vol. 26, pp. 251-271, 1985.

8) T.H. Kayser and J. Binkhorst, "Computer Calculations of a Complex Steel Bridge Verified by Model Investigations (Applied at the Steel Bridge Spanning the River Waal Near Ewijk)", Ministry of Transport, Netherlands, Rijkswaterstaat, The Hague, Netherlands, No. 23, 1975.

9) M. Koizumi, A. Senpaku, H. Araki, Y. Kosugi, R. Yonehara, and S. Kawanobe, "Construction of 'Mieko-Nishi' Bridge", Nippon Kokan Technical Report, Overseas No. 45, pp. 2-12, 1985.

10) M.S. Troitsky and B.E. Lazar, "Model Analysis and Design of Cable-Stayed Bridges", Inst. of Civil Engineers Proc., London, Proc. Vol. 48, Paper 7375, pp. 439-464, Mar., 1971.

11) R.S. Das, "Design of Stiffening Girder of a Cable-Stayed Bridge", Journal of the Inst. of Engineering (India) Part CI, Vol. 56, pp. 240-246, May, 1976.

12) N. Gimsing, "Multi-Span Cable-Stayed Girder Bridges", Proc. ASCE Journal of the Structural Division, Vol. 102, No. ST10, pp. 1989-2003, Oct., 1976.

13) O.C. Zienkiewicz, "The Finite Element Method", McGraw-Hill Book Co., London, 1981.

14) "Design of Neoprene Bridge Bearing Pads", Elastomer Chemicals Despartment, E. I. duPont deNemours and Co. (Inc.), Wilmington 98, Delaware.

APPENDIX A

LOAD DISTRIBUTION TO THE BRIDGE DECK

Table A.1a Test No. SLDOB06, B-Train #207 In Left Lane

Description		Weight (kips)
Front Axle	-	12.291
1st Tandum	-	40.464
Lone Axle	-	21.873
2nd Tandum	-	40.287
3rd Tandum	-	40.155
Total		155.070

Table A.1b Load Distribution for the 2-D FEM models

Case #1 Position #4, B = 49"			Case #2 Position #9, B = 49"			Case #3 Position #14, B = 49"		
Node #	Girder Loads (kips) Left	Right	Node #	Girder Loads (kips) Left	Right	Node #	Girder Loads (kips) Left	Right
25	-9.678	-2.612	32	-9.678	-2.612	42	-9.678	-2.612
27	-20.975	-5.662	34	-20.975	-5.662	45	-20.975	-5.662
28	-12.790	-3.452	35	-12.790	-3.452	47	-12.790	-3.452
29	-19.171	-5.175	37	-19.171	-5.175	48	-19.171	-5.175
30	-23.793	-6.423	41	-23.793	-6.423	51	-23.793	-6.423
32	-4.075	-1.100	42	-4.075	-1.100	52	-4.075	-1.100
34	-9.486	-2.561	45	-9.486	-2.561	55	-9.486	-2.561
35	-22.134	-5.975	47	-22.134	-5.975	56	-22.134	-5.975
Total	-122.102	-32.960	Total	-122.1020	-32.960	Total	-122.102	-32.960

Notes:
1) 'B' distance was measured from the face of the guardrail to the center of the truck
2) Loads for the left girder were used for the left 2-D model.
3) Loads for the right girder were used for the right 2-D model.
4) The left and right totals sum to -155.062 kips (should be -155.070 kips).

Table A.2a Test No. SLD0B08, B-Train #216 In Left Lane

Description		Weight (kips)
Front Axle	-	12.225
1st Tandum	-	41.563
Lone Axle	-	21.322
2nd Tandum	-	41.344
3rd Tandum	-	40.925
Total		157.379

Table A.2b Load Distribution for the 2-D FEM models

Case #1 Position #4, B = 52.5"			Case #2 Position #9, B = 50.5"			Case #3 Position #14, B = 50"		
Node #	Girder Loads (kips) Left	Right	Node #	Girder Loads (kips) Left	Right	Node #	Girder Loads (kips) Left	Right
25	-9.523	-2.702	32	-9.582	-2.643	42	-9.597	-2.628
27	-21.314	-6.047	34	-21.446	-5.915	45	-21.479	-5.882
28	-12.897	-3.659	35	-12.977	-3.579	47	-12.997	-3.559
29	-18.684	-5.301	37	-18.800	-5.185	48	-18.829	-5.156
30	-24.155	-6.853	41	-24.305	-6.703	51	-24.342	-6.666
32	-4.137	-1.174	42	-4.163	-1.148	52	-4.169	-1.142
34	-9.564	-2.714	45	-9.623	-2.654	55	-9.638	-2.639
35	-22.316	-6.332	47	-22.454	-6.193	56	-22.489	-6.158
Total	-122.590	-34.782	Total	-123.350	-34.020	Total	-123.540	-33.830

Notes:
1) 'B' distance was measured from the face of the guardrail to the center of the truck
2) Loads for the left girder were used for the left 2-D model.
3) Loads for the right girder were used for the right 2-D model.
4) The distributed loads sum to -157.372; -157.370; and -157.370 for Cases 1,2 and 3, respectively. These should be (-157.379)

Table A.3a Test No. SCDOB10, B-Train #204 on Bridge Center Line

Description		Weight (kips)
Front Axle	-	12.071
1st Tandum	-	41.256
Lone Axle	-	21.982
2nd Tandum	-	41.652
3rd Tandum	-	40.595
Total		157.556

Table A.3b Load Distribution for the 2-D FEM models

Case #1 Position #4, B = 168"		Case #2 Position #9, B = 168"		Case #3 Position #14, B = 168"	
Node #	Girder Loads (kips) Left and Right	Node #	Girder Loads (kips) Left and Right	Node #	Girder Loads (kips) Left and Right
25	-6.036	32	-6.036	42	-6.036
27	-13.579	34	-13.579	45	-13.579
28	-8.262	35	-8.262	47	-8.262
29	-12.305	37	-12.305	48	-12.305
30	-15.620	41	-15.620	51	-15.620
32	-2.675	42	-2.675	52	-2.675
34	-6.089	45	-6.089	55	-6.089
35	-14.208	47	-14.208	56	-14.208
Total	-78.774	Total	-78.774	Total	-78.774

Notes:
1) 'B' distance was measured from the face of the guardrail to the center of the truck.
2) Loads for the left girder were used for the left 2-D model.
3) Loads for the right girder were used for the right 2-D model.
4) The sum of the distributed loads for the left and right girders is -157.548 kips (should be -157.556)

Table A.4a Test No. SCDOB11, B-Train #305 In Right Lane

Description		Weight (kips)
Front Axle	-	12.159
1st Tandum	-	40.837
Lone Axle	-	21.542
2nd Tandum	-	41.520
3rd Tandum	-	41.035
Total		157.093

Table A.4b Load Distribution for the 2-D FEM models

Case #1 Position #4, B = 252"			Case #2 Position #9, B = 252"			Case #3 Position #14, B = 252"		
Node #	Girder Loads (kips) Left	Right	Node #	Girder Loads (kips) Left	Right	Node #	Girder Loads (kips) Left	Right
25	-3.613	-8.547	32	-3.613	-8.547	42	-3.613	-8.547
27	-7.987	-18.896	34	-7.987	-18.896	45	-7.987	-18.896
28	-4.852	-11.480	35	-4.852	-11.480	47	-4.852	-11.480
29	-7.190	-17.012	37	-7.190	-17.012	48	-7.190	-17.012
30	-9.252	-21.888	41	-9.252	-21.888	51	-9.252	-21.888
32	-1.585	-3.749	42	-1.585	-3.749	52	-1.585	-3.749
34	-3.657	-8.653	45	-3.657	-8.653	55	-3.657	-8.653
35	-8.534	-20.190	47	-8.534	-20.190	56	-8.534	-20.190
Total	-46.670	-110.415	Total	-46.670	-110.415	Total	-46.670	-110.415

Notes:
1) 'B' distance was measured from the face of the guardrail to the center of the truck
2) Loads for the left girder were used for the left 2-D model.
3) Loads for the right girder were used for the right 2-D model.
4) The sum of the distributed loads for the left and right girders is -157.085 kips (should be -157.093)

APPENDIX B

GIRDER DEFLECTIONS FOR B-TRAIN LOADS

Table B.1 Left Girder Deflections for a 157.379 kip B-Train, Test Series #SLD0B08

Node No.	Position #4 Deflections (in) Measured	Computed	Diff.	Position #9 Deflections (in) Measured	Computed	Diff.	Position #14 Deflections (in) Measured	Computed	Diff.
3	0.00	0.00	0.00	0.00	0.00	0.00	0.00	0.00	0.00
25	-0.36	-0.59	0.23	-0.24	-0.38	0.14	0.00	-0.12	0.12
30	-1.80	-2.44	0.64	-2.40	-2.29	-0.11	-0.72	-0.84	0.12
37	-1.44	-2.15	0.71	-2.76	-3.40	0.64	-1.44	-2.08	0.64
51	-0.36	-0.69	0.33	-1.56	-2.11	0.55	-2.04	-2.66	0.62
65	0.00	0.00	0.00	0.00	0.00	0.00	0.00	0.01	-0.01
Maximum difference		(0.71)			(0.64)			(0.64)	

Note: Difference = measured - computed

Table B.2 Right Girder Deflections for a 157.379 kip B-Train, Test Series #SLD0B08

Node No.	Position #4 Deflections (in)			Position #9 Deflections (in)			Position #14 Deflections (in)		
	Measured	Computed	Diff.	Measured	Computed	Diff.	Measured	Computed	Diff.
3	0.00	0.00	0.00	0.00	0.00	0.00	0.00	0.00	0.00
25	-0.12	-0.15	0.03	-0.12	-0.10	-0.02	0.00	-0.03	0.03
30	-1.20	-0.68	-0.52	-0.96	-0.63	-0.33	-0.36	-0.23	-0.13
37	-1.08	-0.60	-0.48	-1.68	-0.94	-0.74	-0.96	-0.58	-0.38
51	-0.36	-0.20	-0.16	-0.96	-0.59	-0.37	-1.20	-0.74	-0.46
65	0.00	0.00	0.00	0.00	0.00	0.00	0.00	0.00	0.00
Maximum difference		(-0.52)			(-0.74)			(-0.46)	

Note: Difference = measured - computed

Table B.3 Left Girder Deflections for a 157.556 kip B-Train, Test Series #SCD0B10

Node No.	Position #4 Deflections (in)			Position #9 Deflections (in)			Position #14 Deflections (in)		
	Measured	Computed	Diff.	Measured	Computed	Diff.	Measured	Computed	Diff.
3	0.00	0.00	0.00	0.00	0.00	0.00	0.00	0.00	0.00
25	0.12	-0.38	0.50	0.24	-0.24	0.48	0.24	-0.07	0.31
30	-1.20	-1.57	0.37	-1.08	-1.46	0.38	-0.48	-0.54	0.06
37	-1.08	-1.38	0.30	-1.92	-2.17	0.25	-1.08	-1.33	0.25
51	-0.36	-0.44	0.08	-1.08	-1.34	0.26	-1.44	-1.70	0.26
65	0.00	0.00	0.00	0.00	0.00	0.00	0.00	0.00	0.00
Maximum difference		(0.50)			(0.48)			(0.31)	

Note: Difference = measured - computed

Table B.4 Right Girder Deflections for a 157.556 kip B-Train, Test Series #SCDOB10

Node No.	Position #4 Deflections (in)			Position #9 Deflections (in)			Position #14 Deflections (in)		
	Measured	Computed	Diff.	Measured	Computed	Diff.	Measured	Computed	Diff.
3	0.00	0.00	0.00	0.00	0.00	0.00	0.00	0.00	0.00
25	----	-0.35	----	-0.12	-0.22	0.10	-0.24	-0.07	-0.17
30	----	-1.54	----	-1.44	-1.45	0.01	-0.60	-0.54	-0.06
37	----	-1.37	----	-2.16	-2.18	0.02	-1.56	-1.34	-0.22
51	0.36	-0.45	0.09	-1.44	-1.36	-0.08	-2.04	-1.72	-0.32
65	0.00	0.00	0.00	0.00	0.00	0.00	0.00	0.00	0.00
Maximum difference		(----)			(0.10)			(-0.32)	

Note: Difference = measured - computed

APPENDIX C

STRAINS PRODUCED BY B-TRAIN LOADS

Table C.1a Left Side Bridge Strains for Test Series #SLD0B06
(155.07 kip B-Train (#207) in the Left Lane)

Strain Gage Information					Test Truck Location					
					Position #4		Position #9		Position #14	
					Micro-Strains		Micro-Strains		Micro-Strains	
Member	Gage Location	Cable No.	Node No.	Distance (ft)	Measured	Computed	Measured	Computed	Measured	Computed
Girder:	top(a)	18	22	33.25	202	271	114	146	8	2
	bottom(b)	20			-206	-295	-149	-208	-67	-90
	top (a)	6	31	98.00	-218	-275	-111	-144	-16	-23
	bottom(b)	8			189	242	42	50	-82	-111
	top(a)	14	38	146.00	-9	-24	-92	-126	-23	-38
	bottom(b)	17			-5	3	50	61	-38	-58
	top(a)	12	49	206.00	17	25	-59	-93	-189	-258
	bottom(b)	10			-21	-26	41	67	151	189
	top(a)	2	61	278.50	24	32	92	125	156	208
	bottom(b)	4			-28	-23	-115	-101	-210	-172
Pylon:	downsta.(c)	22	11	30.84	51	78	24	25	1	-10
	upsta.(c)	24			-132	-193	-100	-121	-41	-32
Strut:	downsta.(c)	25	66	298.76	8	6	20	19	26	23
Maximum strain difference = (meas. - comptd.)					(89)		(59)		(69)	

a) gage at inner surface of top plate

b) gage at inner surface of bottom plate

c) gage at the extreme fiber (surface of the member)

Table C.1b Right Side Bridge Strains for Test Series #SLD0B06
(155.07 kip B-Train (#207) in the Left Lane)

Strain Gage Information					Test Truck Location					
					Position #4		Position #9		Position #14	
					Micro-Strains		Micro-Strains		Micro-Strains	
Member	Gage Location	Cable No.	Node No.	Distance (ft)	Measured	Computed	Measured	Computed	Measured	Computed
Girder:	top(a)	16	22	33.25	101	74	54	41	-4	1
	bottom(b)	19			-105	-81	-76	-57	-33	-25
	top (a)	1	31	98.00	-112	-73	-62	-38	-7	-6
	bottom(b)	3			110	65	24	13	-56	-30
	top(a)	13	38	146.00	-4	-7	-45	-34	-12	-10
	bottom(b)	15			-3	1	16	17	-24	-15
	top(a)	9	49	206.00	13	7	-37	-26	-113	-70
	bottom(b)	11			-12	-6	23	19	76	52
	top(a)	7	61	278.50	8	9	47	34	85	56
	bottom(b)	5			-9	-6	-58	-27	-112	-46
Pylon:	downsta.(c)	21	11	29.06	11	12	1	6	-4	-1
	upsta.(c)	23			-56	-43	-49	-32	-22	-11
Maximum strain difference = (meas. - comptd.)					(45)		(-31)		(-66)	

a) gage at inner surface of top plate

b) gage at inner surface of bottom plate

c) gage at the extreme fiber (surface of the member)

Table C.2a Left Side Bridge Strains for Test Series #SLD0B08
(157.379 kip B-Train (#216) in the Left Lane)

Strain Gage Information					Test Truck Location					
					Position #4		Position #9		Position #14	
					Micro-Strains		Micro-Strains		Micro-Strains	
Member	Gage Location	Cable No.	Node No.	Distance (ft)	Measured	Computed	Measured	Computed	Measured	Computed
Girder:	top(a)	18	22	33.25	204	272	112	148	7	2
	bottom(b)	20			208	-297	-148	-211	-66	-91
	top (a)	6	31	98.00	-224	-276	-111	-146	-16	-23
	bottom(b)	8			196	243	42	50	-81	-112
	top(a)	14	38	146.00	-10	-25	-94	-128	-23	-39
	bottom(b)	17			-3	3	51	62	-38	-59
	top(a)	12	49	206.00	17	25	-60	-94	-189	-260
	bottom(b)	10			-22	-26	41	68	150	190
	top(a)	2	61	278.50	25	32	94	127	157	210
	bottom(b)	4			-28	-23	-116	-102	-211	-174
Pylon:	downsta.(c)	22	11	30.84	54	78	24	25	1	-10
	upsta.(c)	24			-134	-193	-100	-122	-40	-32
Strut:	downsta.(c)	25	66	298.76	6	6	19	19	25	23
Maximum strain difference = (meas. - comptd.)					(89)		(63)		(71)	

a) gage at inner surface of top plate

b) gage at inner surface of bottom plate

c) gage at the extreme fiber (surface of the member)

Table C.2b Right Side Bridge Strains for Test Series #SLD0B08
(157.379 kip B-Train (#216) in the Left Lane)

Strain Gage Information					Test Truck Location					
					Position #4		Position #9		Position #14	
					Micro-Strains		Micro-Strains		Micro-Strains	
Member	Gage Location	Cable No.	Node No.	Distance (ft)	Measured	Computed	Measured	Computed	Measured	Computed
Girder:	top(a)	16	22	33.25	101	78	54	42	-4	1
	bottom(b)	19			-105	-85	-76	-59	-33	-25
	top (a)	1	31	98.00	-113	-77	-60	-40	-7	-6
	bottom(b)	3			113	69	24	14	-57	-31
	top(a)	13	38	146.00	-5	-7	-46	-35	-12	-11
	bottom(b)	15			-2	1	17	17	-24	-16
	top(a)	9	49	206.00	14	7	-39	-26	-114	-72
	bottom(b)	11			-12	-7	24	19	77	53
	top(a)	7	61	278.50	10	9	50	35	87	58
	bottom(b)	5			-9	-6	-60	-28	-116	-48
Pylon:	downsta.(c)	21	11	29.06	12	13	2	6	-3	-1
	upsta.(c)	23			-57	-45	-50	-33	-21	-12
Maximum strain difference = (meas. - comptd.)					(44)		(-32)		(-68)	

a) gage at inner surface of top plate

b) gage at inner surface of bottom plate

c) gage at the extreme fiber (surface of the member)

Table C.3a Left Side Bridge Strains for Test Series #SCD0B10
(157.556 kip B-Train (#204) on the Bridge Centerline)

Strain Gage Information					Test Truck Location					
					Position #4		Position #9		Position #14	
					Micro-Strains		Micro-Strains		Micro-Strains	
Member	Gage Location	Cable No.	Node No.	Distance (ft)	Measured	Computed	Measured	Computed	Measured	Computed
Girder:	top(a)	18	22	33.25	153	175	82	94	1	2
	bottom(b)	20			-157	-191	-112	-134	-50	-58
	top (a)	6	31	98.00	-169	-178	-86	-93	-13	-15
	bottom(b)	8			146	157	29	32	-67	-72
	top(a)	14	38	146.00	-8	-16	-69	-82	-18	-24
	bottom(b)	17			-3	2	34	40	-31	-38
	top(a)	12	49	206.00	14	16	-48	-60	-144	-167
	bottom(b)	10			-17	-17	34	43	116	122
	top(a)	2	61	278.50	16	21	68	81	117	134
	bottom(b)	4			-19	-15	-87	-65	-158	-111
Pylon:	downsta.(c)	22	11	30.84	40	50	17	16	-1	-7
	upsta.(c)	24			-99	-124	-72	-78	-28	-21
Strut:	downsta.(c)	25	66	298.76	8	4	17	12	22	15
Maximum strain difference = (meas. - comptd.)					(34)		(22)		(-47)	

a) gage at inner surface of top plate

b) gage at inner surface of bottom plate

c) gage at the extreme fiber (surface of the member)

Table C.3b Right Side Bridge Strains for Test Series #SCD0B10
(157.556 kip B-Train (#204) on the Bridge Centerline)

Strain Gage Information					Test Truck Location					
					Position #4		Position #9		Position #14	
					Micro-Strains		Micro-Strains		Micro-Strains	
Member	Gage Location	Cable No.	Node No.	Distance (ft)	Measured	Computed	Measured	Computed	Measured	Computed
Girder:	top(a)	16	22	33.25	152	178	83	97	2	3
	bottom(b)	19			158	193	-112	-136	-49	-59
	top (a)	1	31	98.00	-164	-176	-82	-91	-11	-14
	bottom(b)	3			163	156	33	31	-74	-72
	top(a)	13	38	146.00	-6	-16	-72	-82	-17	-25
	bottom(b)	15			-3	3	33	41	-31	-37
	top(a)	9	49	206.00	15	16	-53	-61	-165	-168
	bottom(b)	11			-15	-15	33	45	111	124
	top(a)	7	61	278.50	15	21	72	82	127	135
	bottom(b)	5			-18	-14	-91	-65	-171	-111
Pylon:	downsta.(c)	21	11	29.06	21	30	10	13	1	-1
	upsta.(c)	23			-82	-102	-69	-76	-30	-27
Maximum strain difference = (meas. - comptd.)					(35)		(-26)		(-60)	

a) gage at inner surface of top plate

b) gage at inner surface of bottom plate

c) gage at the extreme fiber (surface of the member)

Table C.4a Left Side Bridge Strains for Test Series #SRD0B11
(157.093 kip B-Train (#305) in the Right Lane)

Strain Gage Information					Test Truck Location					
					Position #4		Position #9		Position #14	
					Micro-Strains		Micro-Strains		Micro-Strains	
Member	Gage Location	Cable No.	Node No.	Distance (ft)	Measured	Computed	Measured	Computed	Measured	Computed
Girder:	top(a)	18	22	33.25	111	103	57	56	-4	1
	bottom(b)	20			-114	-113	-82	-79	-35	-34
	top (a)	6	31	98.00	-128	-105	-69	-55	-11	-9
	bottom(b)	8			111	93	23	19	-54	-42
	top(a)	14	38	146.00	-8	-9	-49	-48	-13	-15
	bottom(b)	17			-0	1	21	23	-25	-22
	top(a)	12	49	206.00	12	10	-37	-36	-106	-98
	bottom(b)	10			-14	-10	28	26	87	72
	top(a)	2	61	278.50	11	12	51	48	85	80
	bottom(b)	4			-11	-9	-63	-39	-115	-66
Pylon:	downsta.(c)	22	11	30.84	26	30	9	10	-4	-4
	upsta.(c)	24			-69	-74	-50	-46	-16	-12
Strut:	downsta.(c)	25	66	298.76	5	2	13	7	17	9
Maximum strain difference = (meas. - comptd.)					(-23)		(-24)		(-49)	

a) gage at inner surface of top plate

b) gage at inner surface of bottom plate

c) gage at the extreme fiber (surface of the member)

Table C.4b Right Side Bridge Strains for Test Series #SRD011
(157.093 kip B-Train (#305) in the Right Lane)

Strain Gage Information					Test Truck Location					
					Position #4		Position #9		Position #14	
					Micro-Strains		Micro-Strains		Micro-Strains	
Member	Gage Location	Cable No.	Node No.	Distance (ft)	Measured	Computed	Measured	Computed	Measured	Computed
Girder:	top(a)	16	22	33.25	191	249	106	135	8	3
	bottom(b)	19	22	33.25	197	-271	-139	-190	-62	-82
	top (a)	1	31	98.00	-207	-246	-102	-128	-14	-20
	bottom(b)	3	31	98.00	205	219	44	43	-85	-100
	top(a)	13	38	146.00	-8	-22	-93	-115	-22	-34
	bottom(b)	15	38	146.00	-2	4	47	56	-35	-52
	top(a)	9	49	206.00	20	22	-63	-86	-204	-234
	bottom(b)	11	49	206.00	-18	-22	40	64	138	173
	top(a)	7	61	278.50	22	29	92	115	160	189
	bottom(b)	5	61	278.50	-24	-19	-114	-91	-215	-155
Pylon:	downsta.(c)	21	11	29.06	26	42	16	19	3	-2
	upsta.(c)	23	11	29.06	-103	-143	-86	-106	-39	-38
Maximum strain difference = (meas. - comptd.)					(74)		(51)		(-60)	

a) gage at inner surface of top plate

b) gage at inner surface of bottom plate

c) gage at the extreme fiber (surface of the member)

APPENDIX D

STRAINS AND DEFLECTIONS FOR THE SNOOPER

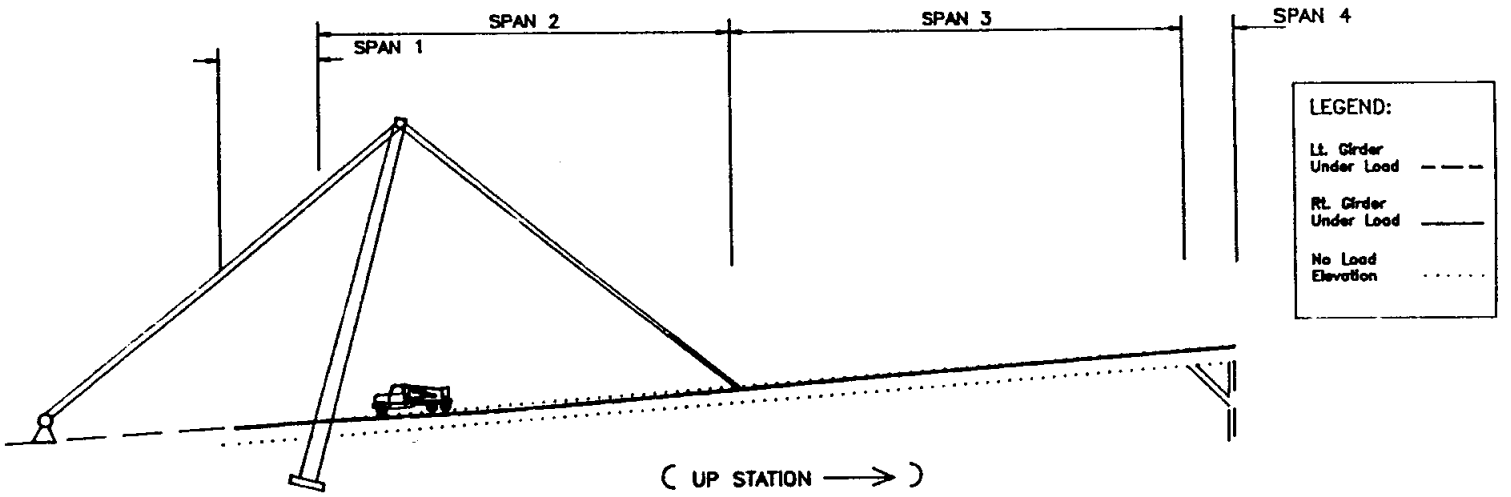

BRIDGE PROFILE WITH SNOOPER TRUCK AT POSITION #4

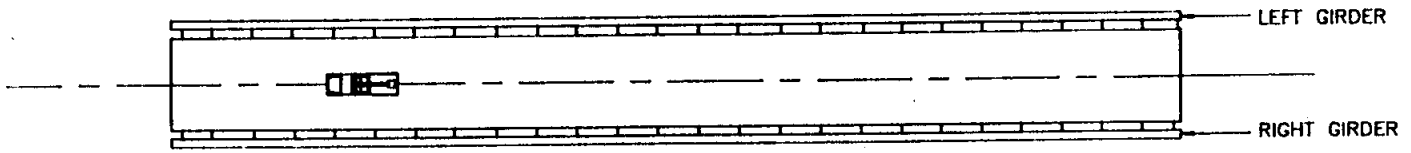

BRIDGE PLAN WITH SNOOPER TRUCK AT POSITION #4

Fig. D.1 Calculated Girder Deflections for Snooper on Centerline at position #4.

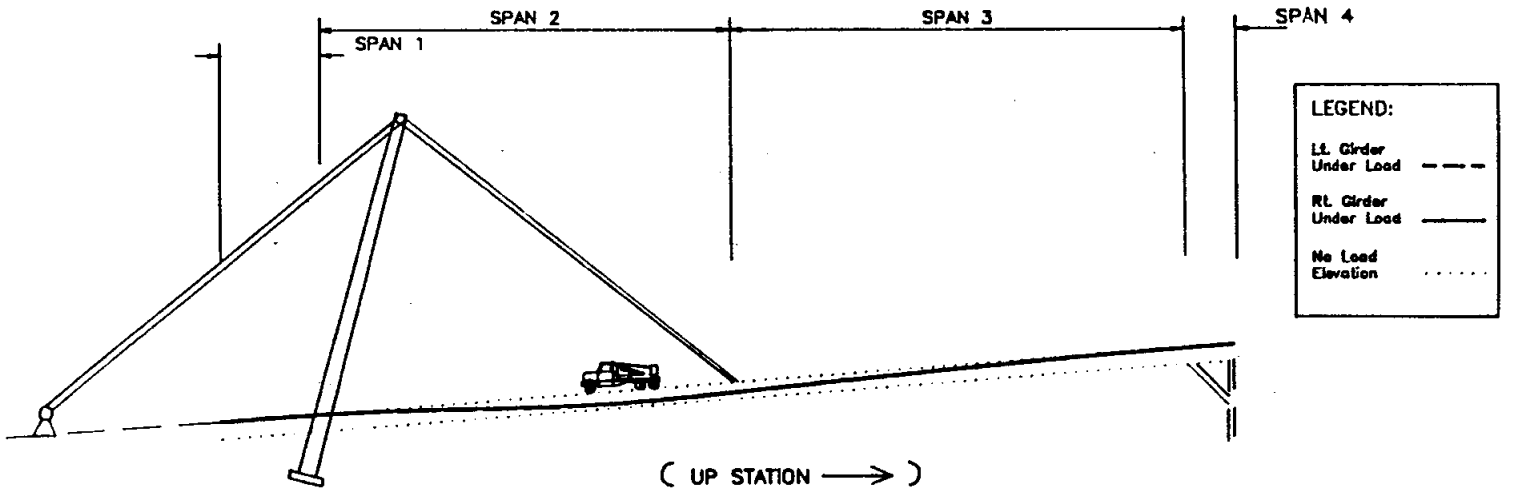

BRIDGE PROFILE WITH SNOOPER TRUCK AT POSITION #9

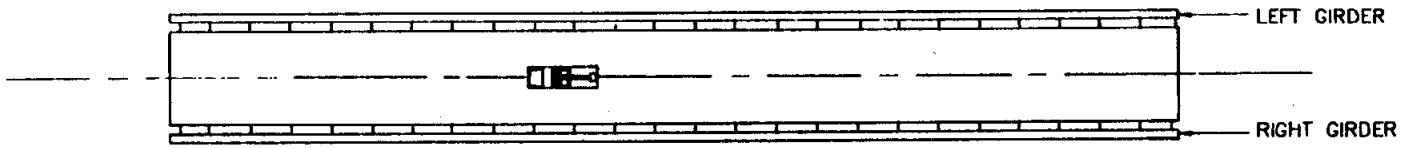

BRIDGE PLAN WITH SNOOPER TRUCK AT POSITION #9

Fig. D.2 Calculated Girder Deflections for Snooper on Centerline at Position #9.

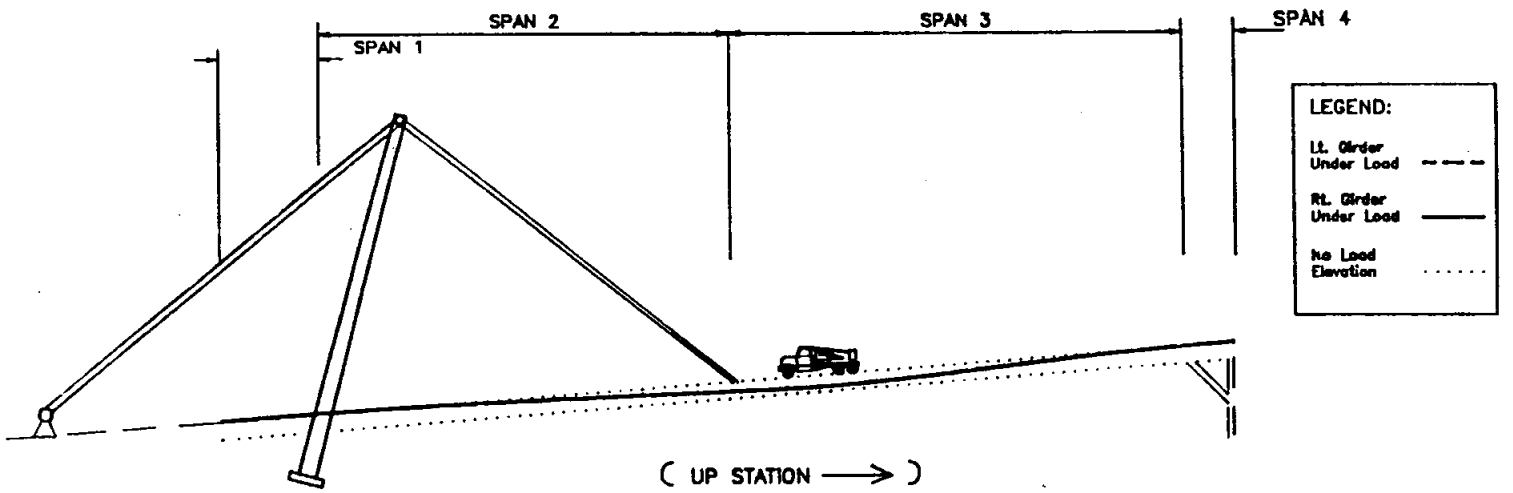

BRIDGE PROFILE WITH SNOOPER TRUCK AT POSITION #14

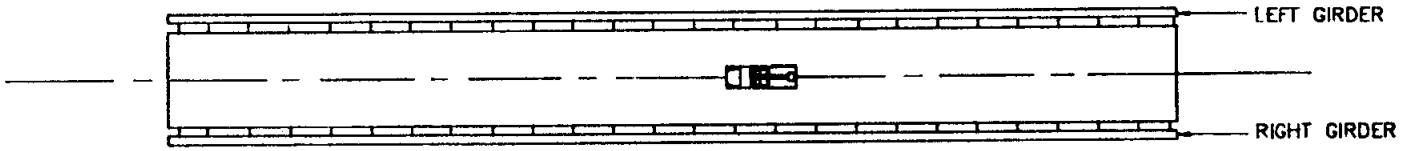

BRIDGE PLAN WITH SNOOPER TRUCK AT POSITION #14

Fig. D.3 Calculated Girder Deflections for Snooper on Centerline at position #14.

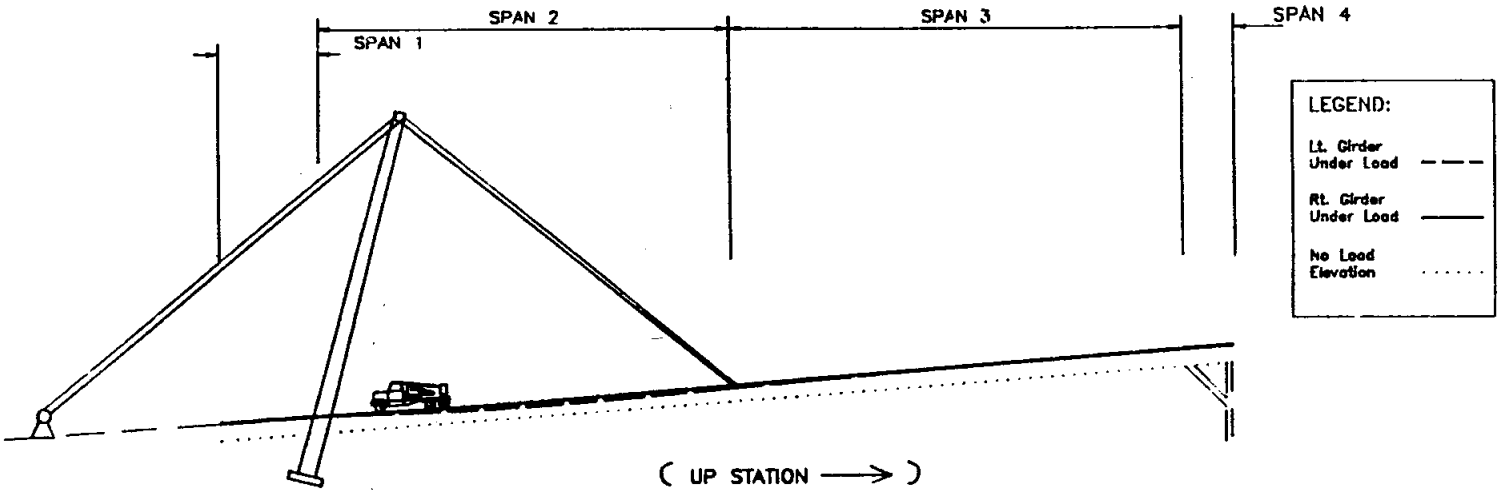

BRIDGE PROFILE WITH SNOOPER TRUCK AT POSITION #4

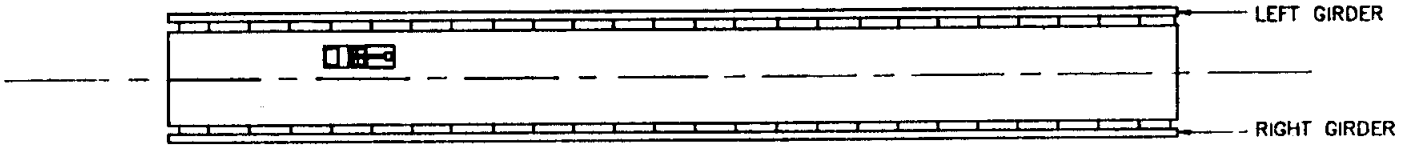

BRIDGE PLAN WITH SNOOPER TRUCK AT POSITION #4

Fig. D.4 Calculated Girder Deflections for Snooper in Left Lane at position #4.

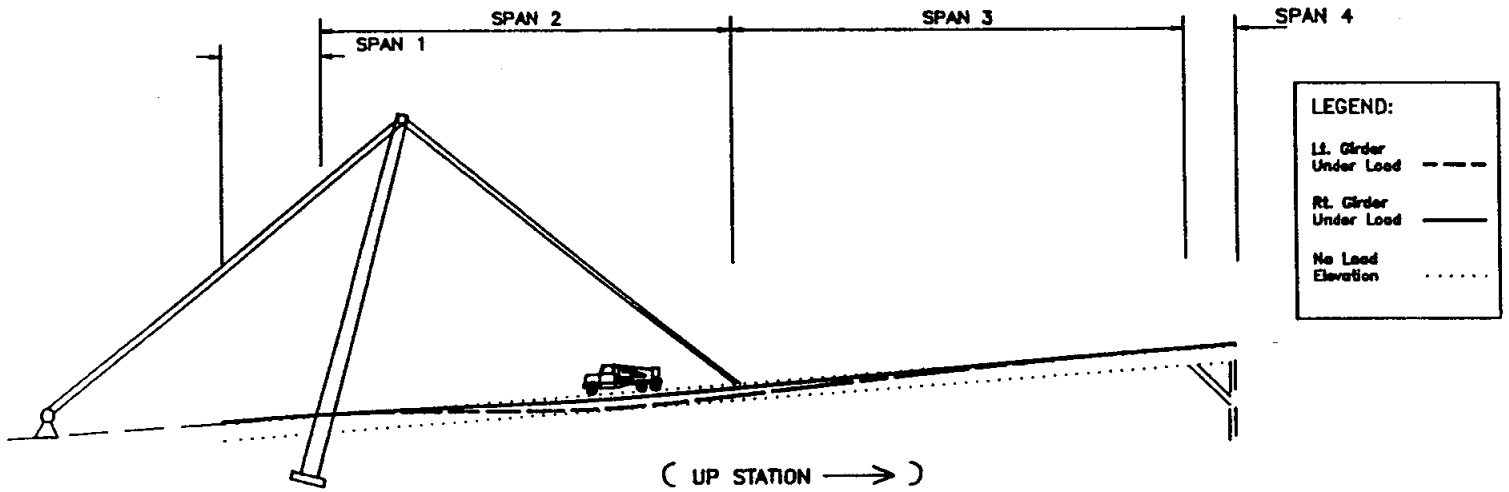

BRIDGE PROFILE WITH SNOOPER TRUCK AT POSITION #9

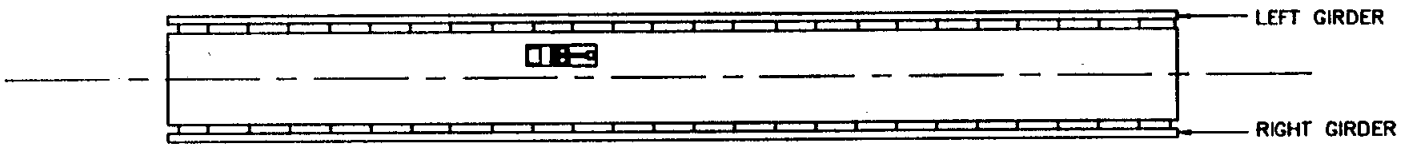

BRIDGE PLAN WITH SNOOPER TRUCK AT POSITION #9

Fig. D.5 Calculated Girder Deflections for Snooper in Left Lane at position #9.

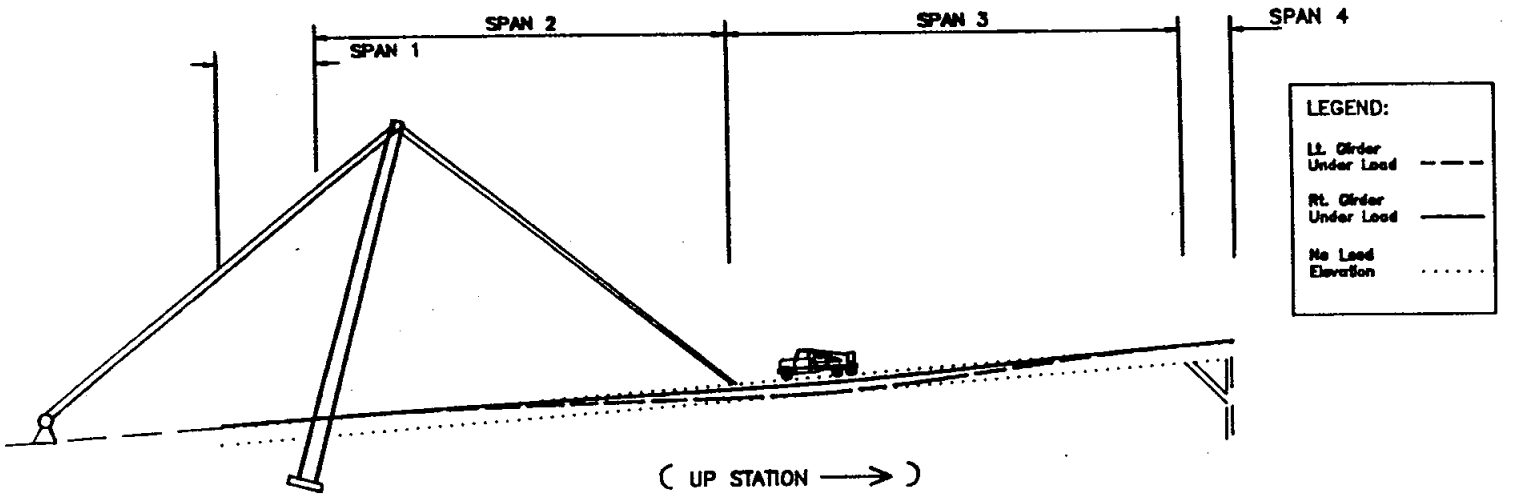

BRIDGE PROFILE WITH SNOOPER TRUCK AT POSITION #14

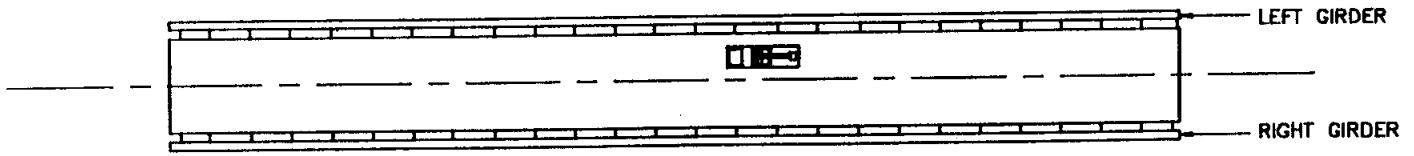

BRIDGE PLAN WITH SNOOPER TRUCK AT POSITION #14

Fig. D.6 Calculated Girder Deflections for Snooper in Left Lane at position #14.

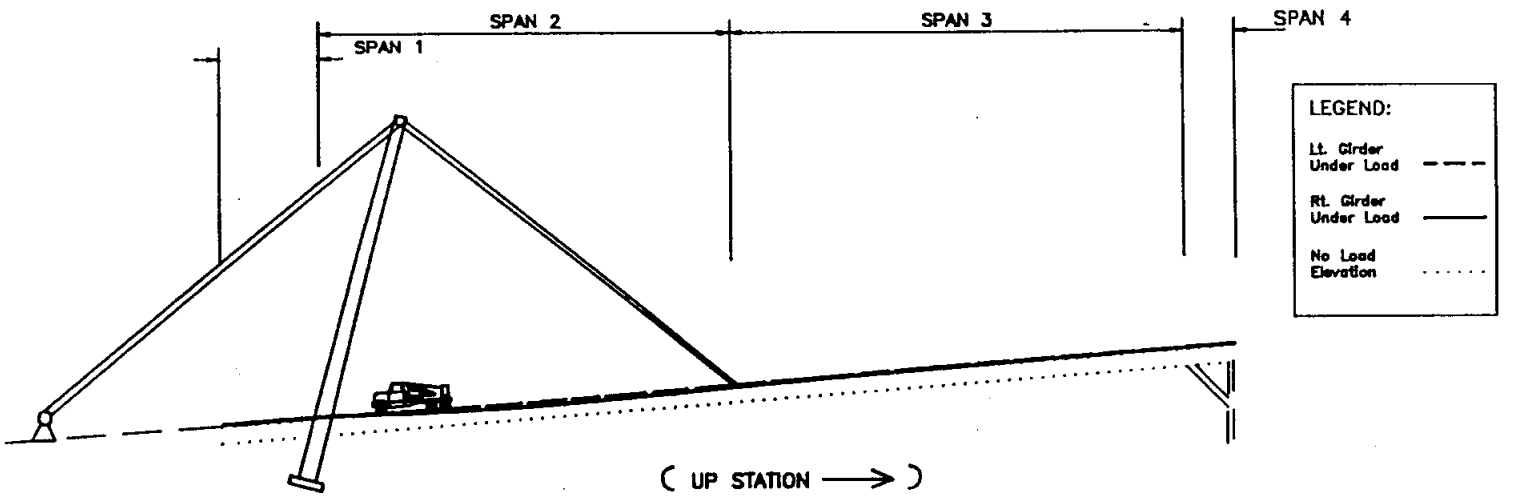

BRIDGE PROFILE WITH SNOOPER TRUCK AT POSITION #4

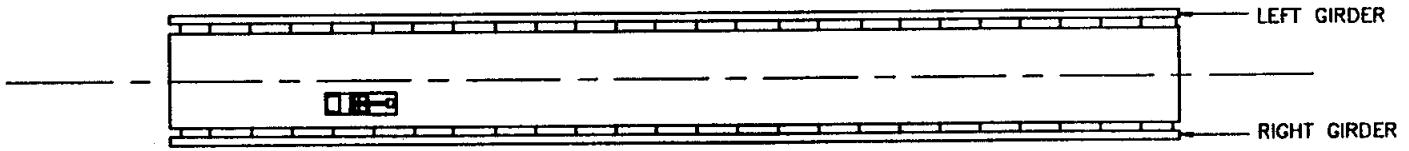

BRIDGE PLAN WITH SNOOPER TRUCK AT POSITION #4

Fig. D.7 Calculated Girder Deflections for Snooper in Right Lane at position #4.

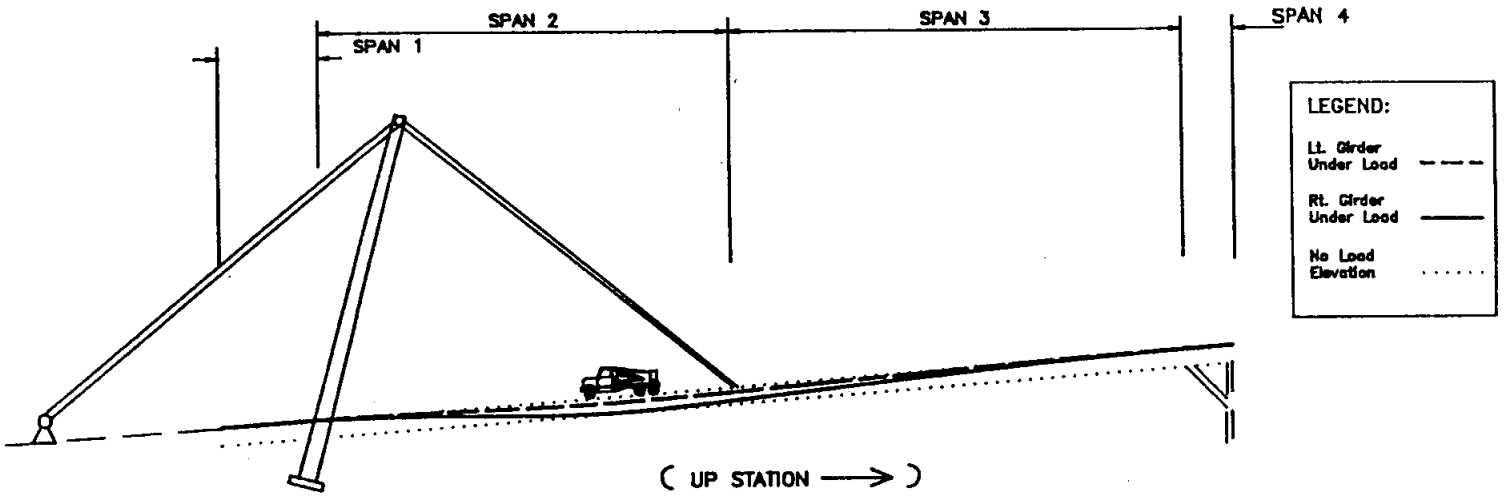

BRIDGE PROFILE WITH SNOOPER TRUCK AT POSITION #9

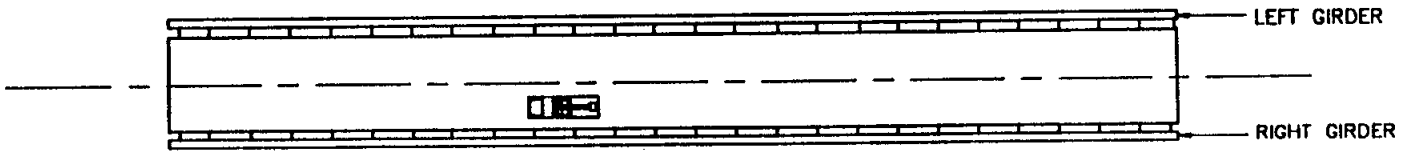

BRIDGE PLAN WITH SNOOPER TRUCK AT POSITION #9

Fig. D.8 Calculated Girder Deflections for Snooper in Right Lane at position #9.

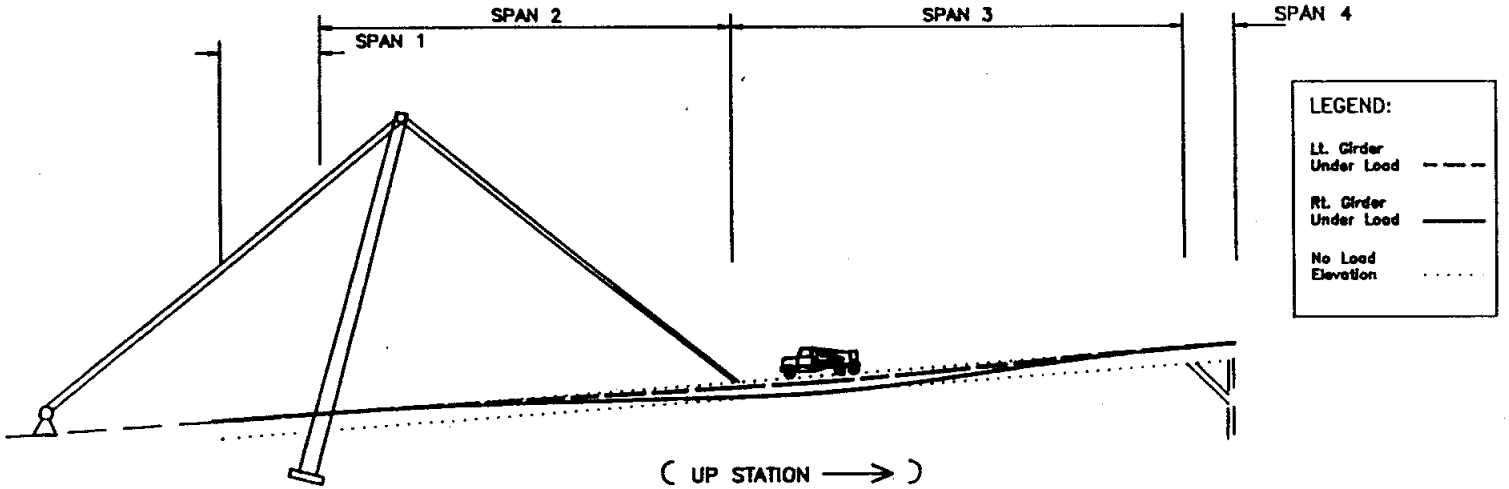

BRIDGE PROFILE WITH SNOOPER TRUCK AT POSITION #14

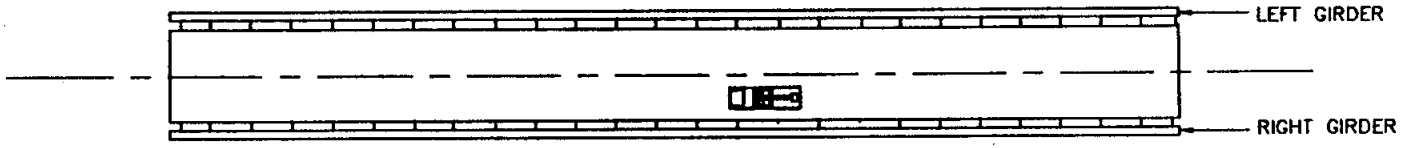

BRIDGE PLAN WITH SNOOPER TRUCK AT POSITION #14

Fig. D.9 Calculated Girder Deflections for Snooper in Right Lane at position #14.

Table D.1a Left Side Bridge Strains for Test Series #SCD0S04
(Snooper Truck on Bridge Centerline, T4_2SCL)

Strain Gage Information					Test Truck Location					
					Position #4		Position #9		Position #14	
					Micro-Strains		Micro-Strains		Micro Strains	
Member	Gage Location	Cable No.	Node No.	Distance (ft)	Measured	Computed	Measured	Computed	Measured	Computed
Girder:	top(a)	18	22	33.25	38	41	41	44	9	8
	bottom(b)	20			-30	-43	-41	-51	-18	-22
	top (a)	6	31	98.00	-2	-20	-24	-50	5	-4
	bottom(b)	8			15	19	25	40	-18	-17
	top(a)	14	38	146.00	12	3	1	-13	-4	-12
	bottom(b)	17			-4	-4	-3	7	-5	-2
	top(a)	12	49	206.00	14	3	9	4	-27	-37
	bottom(b)	10			-3	-3	-10	-5	22	29
	top(a)	2	61	278.50	15	1	12	10	30	33
	bottom(b)	4			1	0	-9	-8	-35	-27
Pylon:	downsta.(c)	22	11	30.84	15	15	13	9	6	0
	upsta.(c)	24			-18	-32	-32	-29	-17	-11
Strut:	down sta.(c)	25	66	298.76	-2	0	3	2	4	4
Maximum strain difference = (meas. - cmptd.)					(18)		(26)		(10)	

a) gage at inner surface of top plate

b) gage at inner surface of bottom plate

c) gage at the extreme fiber (surface of the member)

Table D.1b Right Side Bridge Strains for Test Series #SCD0S04
(Snooper Truck on Bridge Centerline, T4_2SCR)

Strain Gage Information					Test Truck Location					
					Position #4		Position #9		Position #14	
					Micro-Strains		Micro-Strains		Micro Strains	
Member	Gage Location	Cable No.	Node No.	Distance (ft)	Measured	Computed	Measured	Computed	Measured	Computed
Girder:	top(a)	16	22	33.25	41	42	39	45	8	9
	bottom(b)	19			-36	-44	-41	-51	-17	-22
	top (a)	1	31	98.00	-0	-20	-23	-50	6	-3
	bottom(b)	3			8	19	26	40	-19	-17
	top(a)	13	38	146.00	17	3	2	-14	-5	-13
	bottom(b)	15			-11	-4	-4	7	-6	-2
	top(a)	9	49	206.00	12	3	9	4	-29	-38
	bottom(b)	11			-8	-3	-9	-5	19	30
	top(a)	7	61	278.50	4	1	10	10	28	33
	bottom(b)	5			-0	-0	-9	-8	-34	-27
Pylon:	downsta.(c)	21	11	29.06	9	8	12	6	5	1
	upsta.(c)	23			-26	-24	-30	-25	-18	-13
Maximum strain difference = (meas. - cmptd.)					(20)		(27)		(-11)	

a) gage at inner surface of top plate

b) gage at inner surface of bottom plate

c) gage at the extreme fiber (surface of the member)

Table D.2a Left Side Bridge Strains for Test Series #SCD0S05
(Snooper Truck in the Left Lane, T5_2SLL)

Strain Gage Information					Test Truck Location: Position #4 Micro-Strains		Position #9 Micro-Strains		Position #14 Micro-Strains	
Member	Gage Location	Cable No.	Node No.	Distance (ft)	Measured	Computed	Measured	Computed	Measured	Computed
Girder:	top(a)	18	22	33.25	53	64	55	62	15	12
	bottom(b)	20			-51	-66	-58	-71	-28	-31
	top (a)	6	31	98.00	-16	-32	-55	-71	2	-5
	bottom(b)	8			14	31	43	57	-23	-24
	top(a)	14	38	146.00	8	5	-11	-19	-10	-18
	bottom(b)	17			-11	-6	4	10	-4	-3
	top(a)	12	49	206.00	6	5	6	6	-37	-52
	bottom(b)	10			-4	-5	-6	-7	33	41
	top(a)	2	61	278.50	-3	2	10	14	36	46
	bottom(b)	4			4	-1	-12	-11	-46	-38
Pylon:	downsta.(c)	22	11	30.84	10	23	7	13	-1	0
	upsta.(c)	24			-39	-49	-38	-40	-22	-16
Strut:	down sta.(c)	25	66	298.76	8	0	8	2	10	6
Maximum strain difference = (meas. - cmptd.)					(-17)		(16)		(15)	

a) gage at inner surface of top plate

b) gage at inner surface of bottom plate

c) gage at the extreme fiber (surface of the member)

Table D.2b Right Side Bridge Strains for Test Series #SCD0SL5
(Snooper Truck in the Left Lane, T5_2SLR)

Strain Gage Information					Test Truck Location					
					Position #4		Position #9		Position #14	
					Micro-Strains		Micro-Strains		Micro-Strains	
Member	Gage Location	Cable No.	Node No.	Distance (ft)	Measured	Computed	Measured	Computed	Measured	Computed
Girder:	top(a)	16	22	33.25	18	25	21	27	3	5
	bottom(b)	19			-20	-26	-23	-30	-11	-13
	top (a)	1	31	98.00	-6	-12	-22	-30	2	-2
	bottom(b)	3			5	11	20	24	-13	-10
	top(a)	13	38	146.00	7	2	-2	-8	-3	-8
	bottom(b)	15			-8	-2	-1	4	-5	-1
	top(a)	9	49	206.00	1	2	2	2	-20	-22
	bottom(b)	11			-1	-2	-2	-3	15	18
	top(a)	7	61	278.50	-6	1	1	6	14	20
	bottom(b)	5			5	-0	-1	-4	-18	-16
Pylon:	downsta.(c)	21	11	29.06	0	5	-1	4	-3	1
	upsta.(c)	23			-12	-14	-14	-15	-9	-8
Maximum strain difference = (meas. - cmptd.)					(-7)		(8)		(-6)	

a) gage at inner surface of top plate

b) gage at inner surface of bottom plate

c) gage at the extreme fiber (surface of the member)

Table D.3a Left Side Bridge Strains for Test Series #SCD0SR5
(Snooper Truck in the Right Lane, T5_2SRL)

Strain Gage Information					Test Truck Location: Position #4 — Micro-Strains		Position #9 — Micro-Strains		Position #14 — Micro-Strains	
Member	Gage Location	Cable No.	Node No.	Distance (ft)	Measured	Computed	Measured	Computed	Measured	Computed
Girder:	top(a)	18	22	33.25	21	25	24	26	6	5
	bottom(b)	20			-19	-26	-26	-30	-12	-13
	top (a)	6	31	98.00	-9	-12	-25	-30	2	-2
	bottom(b)	8			10	11	18	24	-15	-10
	top(a)	14	38	146.00	4	2	-4	-8	-3	-7
	bottom(b)	17			-3	-2	1	4	-6	-1
	top(a)	12	49	206.00	4	2	4	2	-17	-22
	bottom(b)	10			-3	-2	-4	-3	16	17
	top(a)	2	61	278.50	0	1	3	6	14	19
	bottom(b)	4			1	-0	-3	-5	-18	-16
Pylon:	downsta.(c)	22	11	30.84	6	9	2	5	-3	-0
	upsta.(c)	24			-14	-19	-16	-17	-9	-7
Strut:	downsta.(c)	25	66	298.76	1	0	4	1	8	2
Maximum strain difference = (meas. - cmptd.)					(7)		(-6)		(6)	

a) gage at inner surface of top plate

b) gage at inner surface of bottom plate

c) gage at the extreme fiber (surface of the member)

Table D.3b Right Side Bridge Strains for Test Series #SCD0SR5
(Snooper Truck in the Right Lane, T5_2SRR)

Strain Gage Information					Test Truck Location					
					Position #4		Position #9		Position #14	
					Micro-Strains		Micro-Strains		Micro-Strains	
Member	Gage Location	Cable No.	Node No.	Distance (ft)	Measured	Computed	Measured	Computed	Measured	Computed
Girder:	top(a)	16	22	33.25	45	65	48	63	13	12
	bottom(b)	19			-44	-67	-53	-72	-26	-31
	top (a)	1	31	98.00	-19	-32	-53	-70	0	-5
	bottom(b)	3			21	30	47	56	-22	-24
	top(a)	13	38	146.00	6	5	-11	-19	-10	-18
	bottom(b)	15			-5	-6	6	10	-4	-3
	top(a)	9	49	206.00	5	5	4	6	-43	-53
	bottom(b)	11			-3	-4	-5	-6	30	42
	top(a)	7	61	278.50	1	2	11	14	36	46
	bottom(b)	5			0	0	-13	-11	-46	-38
Pylon:	downsta.(c)	21	11	29.06	7	13	6	8	2	1
	upsta.(c)	23			-26	-37	-30	-36	-19	-18
Maximum strain difference = (meas. - cmptd.)					(23)		(19)		(-12)	

a) gage at inner surface of top plate
b) gage at inner surface of bottom plate
c) gage at the extreme fiber (surface of the member)